



UNIVERSITY OF
BIRMINGHAM

Isolation Enhancement in a Dual Port Antenna

By

Donya Jasteh

A thesis submitted to

The University of Birmingham

For the degree of

Master of Philosophy (MPhil)

School of Electronic, Electrical and Computer Engineering

The University of Birmingham

October 2011

UNIVERSITY OF
BIRMINGHAM

University of Birmingham Research Archive

e-theses repository

This unpublished thesis/dissertation is copyright of the author and/or third parties. The intellectual property rights of the author or third parties in respect of this work are as defined by The Copyright Designs and Patents Act 1988 or as modified by any successor legislation.

Any use made of information contained in this thesis/dissertation must be in accordance with that legislation and must be properly acknowledged. Further distribution or reproduction in any format is prohibited without the permission of the copyright holder.

Abstract

Nowadays multiple antennas are very popular. However embedding many antennas closely in a compact printed circuit board will raise the issue of mutual coupling between them, which will decrease their performance.

The research described in this thesis, concerns enhancing the isolation in a dual port antenna. The general approach is to design a four-port feed network to be connected to the antenna to fulfil this task. The sample antenna that the approaches were applied to is an already designed by a member of Antenna and Applied Electromagnetics Laboratory.

The feed-network that has been designed consists of a coupler and a phase shifter. Different kinds of couplers have been designed and implemented. The simulation and measurement results are compared and the conclusions are drawn.

Acknowledgment

First and foremost, I would like to thank my supervisors Professor Peter S. Hall and Dr Peter Gardner, whose support, assurance and invaluable guidance has contributed enormously to the existence of this thesis.

I am hugely grateful to my family for their generous support throughout my studies, and indeed the whole of my life. Their wisdom, kindness and excellent advice have made me who I am today and I hope that I have made them proud.

Contents

1	Introduction.....	1
1.1	Background	1
1.2	Motivation	2
1.3	Project Objectives	4
1.4	Layout of Thesis.....	5
2	Literature Review.....	7
2.1	Antenna Theory.....	7
2.1.1	Printed Antennas	8
2.2	VSWR & Return Loss.....	8
2.3	Ultra Wideband Technology	9
2.3.1	UWB benefits and Applications	10
2.4	Cognitive Radio.....	11
2.4.1	Cognitive Radio Main functions.....	12
2.4.2	Spectrum Sensing and Allocation.....	12
2.5	Multi Element Antennas.....	13
2.5.1	MIMO Antennas	14
2.6	A review of techniques of improving the isolation in multi-port antennas.....	14
2.6.1	Isolation Techniques in multiport antennas	15
2.7	Directional Couplers	24
3	Isolation Using a Hybrid Coupler	27
3.1	Antenna Description.....	27
3.1.1	Ground Plane Width (Wg).....	28
3.1.2	Narrowband antenna feed line	30
3.1.3	Electric current distributions on the antenna	32
3.2	Coupler Design.....	34
3.3	Results	42
3.4	Discussion	49
4	Isolation Using a Branch-line Coupler	51
4.1	Branch-line Coupler Design.....	51

4.2	Results	62
4.3	Discussion	68
5	Investigation into use of filters in a branch-line Coupler	69
5.1	Investigation of the Filtering Action	69
5.2	Filter Design.....	77
5.3	Discussion	84
6	Conclusions and Future Work	85
6.1	Conclusions	85
6.1.1	Challenges.....	86
6.2	Future Work	87
7	References.....	89
Appendix A	The Scattering Matrix.....	96
Appendix B	Touchstone Files.....	97

List of Figures

Figure 1.1: Simulated S-parameters of dual port UWB-narrowband antenna.....	5
Figure 2.1: Antenna as a transition device. (Balanis, 1997)	7
Figure 2.2: This layout shows 15 different two-antenna configurations located on the same finite ground plane. The matchsticks symbolize the PIFA's, and the dot on the matchstick denotes the location of the shorting pin. (Jakobsen and Thaysen, 2007)	16
Figure 2.3: Left: Two-port antenna without coupling cancellation. Right: Cancellation of path A by a second path B (Esser et al., 2006).	17
Figure 2.4: Schematic diagram of MIMO antennas with slits in the ground plane, (a) (Kokkinos et al., 2008), (b) (Karaboikis et al., 2004), (c) (Chiu et al., 2007).	18
Figure 2.5: Schematic diagram of the MIMO antennas with stub (a), (b) (Chiu et al., 2007).	20
Figure 2.6: Schematic diagram of the PIFAs with (a) split ring resonator (Lihao et al., 2010) (b) parasitic decoupling element (Mak et al., 2008) (c) suspended transmission line (Diallo et al., 2006).	21
Figure 2.7: Schematic diagram of the antenna with combination of decoupling techniques (Park and Jung., 2010).	22
Figure 2.8: The function blocks of the decoupling structure proposed in (Chen et al., 2008).	22
Figure 2.9: Schematic diagram of the LTE antenna with a branchline decoupling feed network (Bhatti et al., 2009).	23
Figure 2.10: Commonly used symbol for directional couplers. (Pozar, 1998).....	24
Figure 3.1: Geometry of the proposed antenna. (a) UWB antenna (b) Narrowband antenna (Ebrahimi and Hall, 2009)	28
Figure 3.2: Simulated reflection coefficient curves for different Wg , wideband antenna (Ebrahimi, 2011).....	29
Figure 3.3: Simulated reflection coefficient curves for different Lg , wideband antenna (Ebrahimi, 2011).....	29
Figure 3.4: Simulated reflection coefficient curves for different h (a) wideband antenna, (b) narrowband antenna (Ebrahimi, 2011)	31
Figure 3.5: Current distributions when the wideband antenna is excited and the narrowband antenna is terminated to a 50Ω load at 5 GHz.	32
Figure 3.6: Current distributions when the narrowband antenna is excited and the wideband antenna is terminated to a 50Ω load at 5 GHz. (a) Top view, (b) Bottom view.	33

Figure 3.7: Representation of a 180° hybrid: (a) As a power divider with port 1 as input; (b) as a power divider with port 4 as input; (c) as a power combiner with ports 2 and 3 as input. (Simons, 2001).....	35
Figure 3.8: The ring hybrid or rat-race coupler (Gardner, 2010).....	36
Figure 3.9: The ring hybrid or rat-race coupler	36
Figure 3.10: Simulated Rat-race coupler S-parameters	38
Figure 3.11: S-parameters of the antenna and feed network, phase shifter value is equal to 55 °	39
Figure 3.12: S-parameters of the antenna and feed network, phase shifter value is equal to 84 °	39
Figure 3.13: S-parameters of the antenna and feed network, phase shifter value is equal to 110 °	40
Figure 3.14: Prototype of the retrace coupler+ phase shifter	40
Figure 3.15: Geometry of the final structure in CST design environment. (a) microstrip (b) CPW and ground plane	41
Figure 3.16: Prototype of the designed structure (a) Top view (b) Bottom view	42
Figure 3.17: Coupling between the composite network ports (before and after adding the feed network).....	42
Figure 3.18: Measured and simulated return loss for port 1(with and without feed network).43	
Figure 3.19: Measured and simulated return losses for port 2 (S22).....	44
Figure 3.20: Current distributions when the port1 is excited and the port 2 is terminated to a 50 Ω load at 5 GHz. (a) Top View (b) Bottom View.	45
Figure 3.21: Current distributions when port 2 is excited and the port1 is terminated to a 50 Ω load at 5 GHz. (a) Top View (b) Bottom View.	46
Figure 3.22 : Simulated 3D radiation pattern of the structure when port 1 is excited.	47
Figure 3.23: Simulated 3D radiation pattern of the structure when port 2 is excited.	48
Figure 3.24: Composite Structure consists of coupler and antenna.....	49
Figure 4.1: Geometry of a branch-line Coupler. (Pozar, 1998).....	51
Figure 4.2: Schematic of a 12 dB Branch-line coupler Schematic in Microwave Office.	55
Figure 4.3: S-parameters of the 12 dB Branch-cline coupler designed at 5.2 GHz.....	56
Figure 4.4: Schematic of the branch-line coupler + phase shifter + antenna in Microwave Office	57
Figure 4.5: Simulated S-parameters of the composite network after adding the feed network to the antenna (Feed network consists of a 12 dB coupler).	58

Figure 4.6 : Simulated S-parameters of the composite network after adding the feed network to the antenna (Feed network consists of a 5 dB coupler).	58
Figure 4.7 : Simulated S-parameters of the composite network after adding the feed network to the antenna (Feed network consists of a 16 dB coupler).	59
Figure 4.8: Geometry of the final structure in CST Microwave Studio. (a) microstrip (b) CPW and ground plane.....	60
Figure 4.9: Simulation S-parameters results of the composite structure by CST	61
Figure 4.10: PCB of the designed structure (a) Microstrip (NB Antenna+ phase-shifter + branch-line coupler) (b) CPW + ground plane (UWB antenna+ ground)	61
Figure 4.11: Measured transmission coefficient of the composite structure	62
Figure 4.12: Reflection Coefficient of port 1 of the composite structure: represents UWB antenna	63
Figure 4.13: Reflection coefficient of port 2 of the composite structure: represents narrowband antenna	64
Figure 4.14 : Current distributions when the port1 is excited and the port 2 is terminated to a 50 Ω load at 5 GHz. (a) Top View (b) Bottom View.	65
Figure 4.15 : Current distributions when the port1 is excited and the port 2 is terminated to a 50 Ω load at 5 GHz. (a) Top View (b) Bottom View.	67
Figure 5.1: Simulated S-parameters of the 4 port feed-network.....	71
Figure 5.2: 4-port feed network connected to the antenna with a 144° phase-shift at both antennas ports.....	72
Figure 5.3: Simulated s-parameters of the composite structure.....	73
Figure 5.4: Schematic of a 12 dB branch-line coupler ; the shunt line is replaced by a 2 port network	74
Figure 5.5: simulated s-parameters of the Branch-line coupler with embedded 2-port networks instead of shunt lines	75
Figure 5.6: Schematic of the ideal branch-line coupler connected to the antenna via phase shifter	76
Figure 5.7: Simulated S-parameters of the composite network.....	77
Figure 5.8: Schematic of the lumped element band-pass filter.....	78
Figure 5.9: Sub-circuit overview of the lumped element band-pass filter in Fig 5.8	78
Figure 5.10: Simulated S-parameters of the lumped element band -pass filter	79
Figure 5.11: Schematic of the 12 dB branch-line Coupler with emended filters	80
Figure 5.12: Simulated S-parameters of the branch-line coupler with embedded filters.	81

Figure 5.13: Schematic of the branch-line coupler with embedded BPF connected to the antenna82

Figure 5.14: Simulated S-parameters of the antenna connected to the branch-line coupler....83

Figure 6.1: Branch-line coupler with an embedded YIG tuned filter.....87

List of Abbreviations

BPF	Band Pass Filter
CPW	CoPlanar Waveguide
CR	Cognitive Radio
DR	Dielectric Resonator
FCC	Federal Communication Commission
ISM	Industrial Scientific Medical
IR	Impulse Radio
MIMO	Multiple Input Multiple Output
PCB	Printed Circuit Board
PIFA	Planar Inverted F Antenna
RF	Radio Frequency
SDR	Software Defined Radio
U-NII	Unlicensed National Information Infrastructure
UWB	Ultra Wide Band
VSWR	Voltage Standing Wave Ratio
WLAN	Wireless Local Area Network
YIG	Yttrium Iron Garnet

Chapter 1

Introduction

1.1 Background

Peak wireless spectral efficiency has hitherto been doubling every 30 months. User demand for bandwidth, however, does so at a much faster rate – every 11 months. Mobile broadband traffic is on the increase, driven by factors like improved mobile networks performance, the availability of devices like smart-phones and tablets, and mobile applications introducing new uses of mobile devices and services. There is clearly a demand for high data-rate services in the mobile environment. (Bennett, 2010)

In general, there are four approaches to managing the spectrum access (Berlemann, 2009).

- 1) *Licensed spectrum for exclusive usage*, whereby the licensee has exclusive usage rights for a specific spectrum.
- 2) *Licensed spectrum for shared usage*, which restricts the licensed spectrum for shared usage to a specific technology – e.g., the spectrum used for public safety services.
- 3) *Unlicensed spectrum* is available to all radio systems operating according to the regulated standards. The industrial, scientific and medical (ISM) 2.4 GHz band and the unlicensed national information infrastructure (U-NII) 5–6 GHz bands are examples of an unlicensed or license-exempt spectrum.
- 4) *Open spectrum*, which allows everyone to access any range of the spectrum without restriction. However, in order to maintain the quality of service and avoid interference and complexity, a minimum set of rules should be respected.

The licensed spectrum approach often allows spectrum resources to be wasted. For instance, the spectrum allocated to a communication system is sometimes more than required.

Therefore, only part of the allocated spectrum is used by the service and other portions of the spectrum become idle. Similarly, if a service with an allocated spectrum is not commercially successful, the licensed spectrum might remain unused. Large parts of the spectrum are thus currently used inefficiently. Paradoxically, 90-95% of the licensed radio spectrum is not in use anywhere at any given time (Berlemann, 2009). The current radio regulatory regime is too complex to handle the increasingly dynamic nature of emerging wireless applications. Furthermore, the number of wireless services collocated in a limited range of frequency and the demand for additional higher data rate spectrum are growing fast. Hence, the regulatory bodies are motivated to employ new strategies to resolve spectrum scarcity in some bands and inefficient spectrums use others.

An effective way of improving reliability and increasing channel capacity is to use Multi-Element antennas, such as Multiple-Input Multiple-Output (MIMO) antenna systems. MIMO technology has attracted attention in wireless communications because it offers significant increases in data throughput and link range without additional bandwidth or transmit power. MIMO antennas make use of multiple antennas at both the transmitter and receiver to exploit the spatial channel for capacity increase. It is one of several forms of smart antenna technology.

With a view to relaxing spectrum crowding, the Federal Communication Commission (FCC) authorized in 2002 the unlicensed use of ultra wideband (UWB) technology. Since then, UWB technology has been of significant interest in industry and academia.

1.2 Motivation

The rapid increase of wireless communication standards has led to the development of multiband antennas for multimode handset terminals. As a result, the optimal integration of compact multiport antennas in cellular phones has presented antenna engineering with a new challenge (Li, Rahmat-samii, 2005). The design of well-matched collocated antennas on the same PCB might seem to be a practical task (Chim et al., 2004), but improving their isolation remains the greater challenge, especially at frequencies where the phone chassis and its surroundings contribute to the radiation mechanism (Kivekas et al., 2003). Moreover, even if a multimode radio front-end module already exhibits an acceptable isolation between its

outputs, decreasing the antenna's mutual coupling remains absolutely necessary to ensure that less power is lost in the other radiators. (Kildal, 2004).

Close antenna element spacing inevitably leads to mutual coupling. Generally speaking, this coupling means that current induced on one antenna produces a voltage at the terminals of nearby elements. (Wallace and Jensen, 2004).

It is well known that mutual coupling distorts antenna patterns and therefore modifies the correlation results. The change in input impedances of the antennas is another consequence of mutual coupling; it results in a greater mismatch between the antennas, their corresponding source and load impedances (Lau et al., 2006).

High antenna coupling (or low isolation) can cause signal leakage from one antenna to another, thus increasing the signal correlation between channels. It can also decrease antenna radiation efficiency, owing to the loss of the power dissipated in the coupled antenna port.

1.3 Project Objectives

The main goal of this project is to design and build a feed network capable of feeding to a dual-port antenna in order to enhance the isolation between its two ports. The most important application of a dual-port Ultra Wideband-Narrowband antenna would be Cognitive Radio (CR).

Several decoupling techniques have been reported in papers, some of which will be discussed briefly in the Literature Review section of this dissertation (Chapter 2). However, Ultra Wideband-Narrowband antenna decoupling has not been written about before.

Improving the isolation in multi-antenna systems is very important. Moreover, Cognitive Radio (CR) applications require an even higher level of isolation. For CR, the level of desired coupling may vary from one case to another. The UWB antenna scans the environment for potential far-off or close-by transmitters; if the mutual coupling power between the UWB and Narrowband antenna ports is higher than potential transmitter power, then the UWB antenna might not be able to detect the transmitter. This will lead to decreasing the performance of cognitive radio. Therefore, achieving a good level of isolation is essential in cognitive radio applications.

This project aims to design an external feed network for connection to an already designed dual-port antenna, without any changes to the antenna's structure having to be made. The purpose of the feed-network is to reduce the mutual coupling between the two ports of the antenna in order to enhance the isolation.

Another aim of this project is to maintain the narrowband antenna's resonating frequency, having added the decoupling feed network to the antenna. The UWB antennas reflection coefficient should also be maintained in the reasonable range (about -10 dB reflection coefficient).

This approach is applied to an already designed dual-port UWB-Narrowband antenna with a high level of coupling (-3 dB) at the resonating frequency of the Narrowband antenna (See Fig. 1.1). The antenna has been designed by a member of Antenna and Applied Electromagnetics Laboratory. The antenna would be suitable for Cognitive Radio applications. The UWB antenna has been designated to fulfil the spectrum sensing task; the

Narrowband antenna, to carry out the communication task. A more detailed description of the antenna structure and performance can be found in Chapter 3 of this thesis.

Fig. 1.1 represents the simulated S-parameters of the antenna. S_{11} and S_{22} represent the coupling between the two antenna ports. As can be seen it peaks at 5.2 GHz, which is in the operating band of the Narrowband antenna. S_{12} and S_{21} are the reflection coefficients of the UWB and Narrowband antennas respectively.

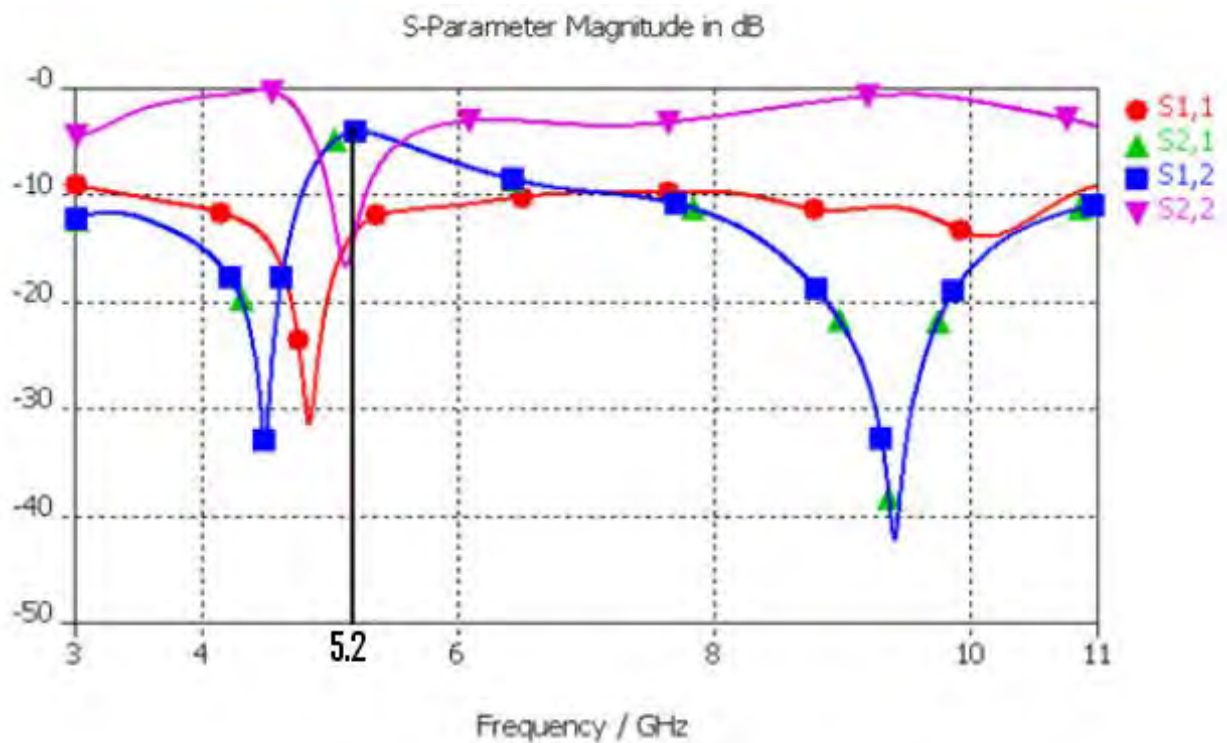


Figure 1.1: Simulated S-parameters of dual port UWB-narrowband antenna

1.4 Layout of Thesis

Chapter 2 is a review of some of the literature on the project's field. It also contains some concepts and definitions which clarify the subjects being discussed in this dissertation. Chapter 2 gives an overview of UWB antennas and their advantages. There is a brief description of Cognitive Radio principles and its main functions. The chapter also mentions Multi-antennas and reviews some of the literature on isolation enhancement techniques.

Chapter 3 starts with a brief description about the already designed antenna used to assess the isolation improvement approach. Chapter 3 concerns the initial approach to the design of the feed network for isolation enhancement. The design method of the 3 dB rat-race coupler, simulation results and measurement results are presented. The chapter ends with a discussion of the results in the context of the overall aim of the project.

Chapter 4 presents the design of a branch-line coupler with a coupling value C . The feed network consists of a branch-line coupler and a phase-shifter, to be connected to the antenna. Therefore the value of C is optimized to achieve the objectives of the project. The last section discusses the results, comparing them to the results of chapter 3. It also explains the motivations for further improvements of the results which are discussed in the next chapter.

Chapter 5 investigates the use of filters in a branch-line coupler. Initially the theoretical filtering action is investigated. To examine the theory, a lumped element band-pass filter is designed and then embedded into the branch-line coupler and simulated. The result of the ideal filter case is compared to the lumped element filter.

Finally *Chapter 6* draws conclusion to the work. The primary objectives are reviewed and the significant achievements are highlighted. Furthermore, this chapter suggests solutions which could lead to further improvements to the filtering action in PCB structures at 5 GHz.

Chapter 2

Literature Review

This section is concerned with relevant concepts and definitions that give a proper insight to the reader for better understanding of the project procedure and illustrations that is given through the report. It also consists of some useful background on the project's subject area.

2.1 Antenna Theory

An antenna is defined by IEEE Standard Definitions as “a means for radiating or receiving radio waves.” As can be seen in Fig. 2.1, antenna is the transitional structure between free-space and a guiding device. The guiding device or transmission line could be a coaxial line or a waveguide (hollow pipe), and it used to transport electromagnetic energy from the transmitting source to the antenna, or from the antenna to the receiver. In the former case we have a transmitting antenna and in the latter a receiving antenna. (Balanis, 1997)

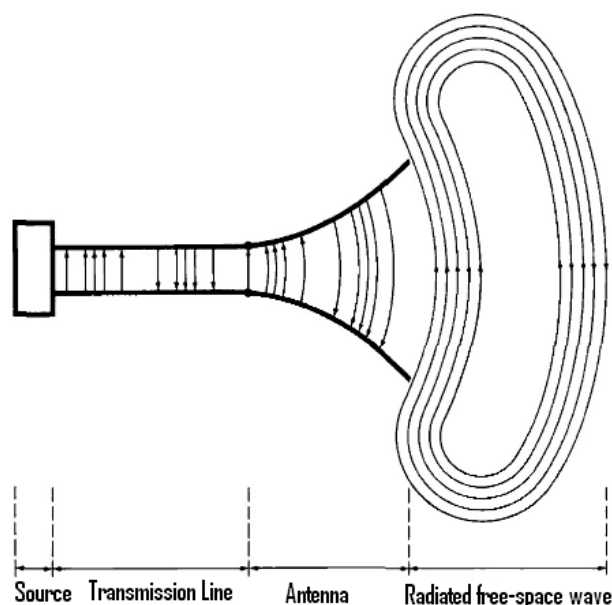


Figure 2.1: Antenna as a transition device. (Balanis, 1997)

Antennas are essential parts of a radio link that can be classified into various categories according to their radiation principle, physical structure, manufacturing technology and/or radiation characteristics.

2.1.1 Printed Antennas

Antennas can be made using printed circuit techniques. Various shapes and structures can be etched on a single- or double-sided copper-clad dielectric. Different classes of antennas can be manufactured using this method. Due to their many advantages patch antennas are very popular. They are low profile, conformable to different surfaces. A remarkable amount of work has been done on microstrip antennas over the past 25 years. (Wong, 2002)

2.2 VSWR & Return Loss

VSWR, or Voltage Standing Wave Ratio, is a measure of how well the components of the RF network are matched in impedance. A mismatch in impedances can cause, signal power loss, which results in weak transmissions, poor reception or both. In the case of large mismatches in the RF section of a wireless base station, it doesn't matter if the latest digital technology is being used; the system will be inferior. An extreme mismatch between a transmitter and an antenna can cause permanent damage to the transmitter.

Maximum power transfer between two system components occurs when their respective impedances are matched. If the impedances are not identical, some RF power will be reflected back, resulting in a reduction in the amount of power delivered to the load. (Rau, 1998) "VSWR is defined as the ratio of the maximum voltage to the minimum voltage in the standing wave." The larger the impedance mismatch, the larger the amplitude of the standing wave ratio. VSWR represents the ratio of the system's characteristic impedance to the impedance of the load (e.g. antenna). (Rau, 1998)

Although the concept of VSWR is easy to comprehend, it is extremely difficult to measure directly. Thus other parameters, such as return loss and reflection coefficient could be measured instead.

Return loss is the difference in power (expressed in dB) between the incident power and the power reflected back by the load due to a mismatch. A perfect match would result in no

reflected power (as it is all delivered to the load), so the return loss would be infinite. Conversely, an open circuit would reflect back all power, so the return loss would be zero. When dealing with return loss, the higher the value, the better the impedance match. “Reflection Coefficient” is the square root of the ratio between the incident and reflected power. Actually, it is the ratio between the incident and reflected voltage. The reflection coefficient is mathematically related to return loss. Return loss is simply equal to reflection coefficient expressed in dB. The reflection coefficient is a voltage ratio and must be squared to be used for power calculations. (Rau, 1998)

2.3 Ultra Wideband Technology

Since the adoption of Ultra wideband technology by the “Federal Communications Commission” (US-FCC) in 2002 there has been a great interest in ultra wideband (UWB) antennas. (Abbosh, 2007) Considering the regulated access to the spectrum and the limited bandwidth availability, responding to the demand for higher capacity and data rates requires innovative technologies that can coexist with devices operating at various frequency bands. UWB communication which is an underlay (or sometimes referred as shared unlicensed) system, coexists with licensed and unlicensed narrowband systems.

The “Federal Communications Commission” defines an Ultra Wideband device as any device that occupies either a fractional bandwidth greater than 20% or more than 500 MHz of absolute bandwidth of spectrum. The FCC has also permitted the UWB radio transmissions in the unlicensed frequency band from 3.1 GHz to 10.6 GHz. (FCC, 2002)

A UWB signal occupies extremely large bandwidth (i.e. more than 500MHz) where the Radio Frequency (RF) energy is spread over an enormous spectrum which is wider than any licensed narrowband wireless systems and invisible to them due to the low power emission. In spite of the low power transmission, UWB offers smart solutions in many wireless communication areas, such as wireless personal area networks, wireless telemetry and telemedicine, and wireless sensors networks. UWB can offer a capacity that is much higher than the current narrowband systems for short-range applications.

2.3.1 UWB benefits and Applications

UWB offers great flexibility of spectrum usage. This system is characterized in fact by a variety of parameters that can enable the design of adaptive transceivers and that can be used for optimizing system performance as a function of the required data rate, range, power, quality of- service, and user preference.

UWB technology provides high data rates over very short range. The data rate can, however, be traded-off for extension in range. Similarly, data rate and range can be traded-off for power, especially for low data rate and short range applications. Most importantly, the same device can be designed to provide service for multiple applications with a variety of requirements without the need for additional hardware. (Arslan et al., 2006).

Excellent time resolution is another key benefit of UWB signals for ranging applications. Due to the extremely short duration of transmitted pulses, sub decimetre ranging is possible. In IR-UWB systems, no up/down-conversion is required at the transceivers, with the potential benefit of reducing the cost and size of the devices. Other benefits of UWB include low power transmission and robustness against eavesdropping (since UWB signals look like noise) (Arslan et al., 2006). On the other hand, it is important to note that UWB receivers are a little bit difficult to build, due to the need to synchronise TX and RX.

UWB has several applications all the way from wireless communications to radar imaging, and vehicular radar. The ultra wide bandwidth and hence the wide variety of material penetration capabilities allows UWB to be used for radar imaging systems, including ground penetration radars, through-wall radar imaging, surveillance systems, and medical imaging. Images within or behind obstructed objects can be obtained with a high resolution using UWB.

Similarly, the excellent time resolution and accurate ranging capability of UWB can be used for vehicular radar systems for collision avoidance, guided parking, etc. Positioning location and relative positioning capabilities of UWB systems are other great applications that have received significant attention. Last but not least is the wireless communication application, which is arguably the reason why UWB became part of the wireless world, including wireless home networking, high-density use in office buildings and business cores, UWB wireless printer, keyboard, wireless speakers, wireless universal serial bus (USB), high-speed wireless

personal area networks, wireless body area networks, wireless sensors networks, wireless telemetry, and telemedicine (Arslan et al, 2006).

2.4 Cognitive Radio

As mentioned in the introduction the fourth approach for spectrum management is the evolution towards dynamic and open access spectrum which requires some level of intelligence in the networks and is not achievable by pure hardware-based radios.

In the early 1990s Joseph Mitola introduced the idea of combining the hardware and software in a radio system; Software Defined Radio (SDR) (Mitola, 1995). These radios typically have a RF front end with a software-controlled tuner. Baseband signals are passed into an analogue-to-digital converter. The quantized baseband is then demodulated in a reconfigurable device such as a field-programmable gate array, digital signal processor, or personal computer. The reconfigurability of the modulation scheme makes it a software-defined radio. In 2000, Mitola took the SDR concept one step further, coining the term cognitive radio. CRs are basically SDRs with artificial intelligence, capable of sensing and reacting to their environment. (Mitola, 2000)

Cognitive radio can be described as a Wireless communication system in which either a network or wireless node changes its transmission or reception parameters to communicate effectively avoiding interference with licensed or unlicensed users. The alteration of parameters is based on the active monitoring of several features in the external and internal radio environment, such as radio frequency spectrum, user behaviour and network status. (FCC, 2003)

In terms of spectrum use the above description can be translated as below:

CR system employs technology that allows the system to obtain knowledge about the spectrum usage in its surrounding environment, to dynamically and autonomously adjust the transmission channel (carrier frequency and bandwidth) according to the current spectrum usage and requirements and learn from the results obtained by focusing on most promising channels.

2.4.1 Cognitive Radio Main functions

The main functions of Cognitive Radios are: (Akyildiz, Ian F. et al., 2006)

Spectrum Sensing: Detecting the unemployed spectrum and sharing it without destructive interference with other users, it is a significant requirement of the Cognitive Radio network to sense spectrum gaps, detecting primary users is the most efficient way to detect spectrum holes.

Spectrum sensing techniques can be classified into three categories:

- Transmitter detection
- Cooperative detection
- Interference based detection

Spectrum Management: Capturing the best available spectrum to achieve user communication requirements. “Cognitive radios should decide on the best spectrum band to meet the Quality of service requirements over all available spectrum bands, therefore spectrum management functions are required for Cognitive radios.”

Spectrum Mobility: It is defined as the procedure when a cognitive radio user changes its frequency of operation. “Cognitive radio networks target to use the spectrum in a dynamic manner by allowing the radio terminals to operate in the best available frequency band, maintaining seamless communication requirements during the transition to better spectrum.”

Spectrum Sharing: It is providing the reasonable spectrum arrangement method, one of the main challenges in open spectrum usage is the spectrum sharing. (Akyildiz, Ian F. et al., 2006)

2.4.2 Spectrum Sensing and Allocation

In order to identify the spectrum holes, CR systems need to scan the spectrum and spot the vacant or idle parts of the spectrum which is known as spectrum sensing. Based on the information, CR knows about its own internal state and surrounding environment, it then determines the optimum frequency band and subsequently starts the communication. This procedure is referred to as communication. Two main approaches for spectrum sensing and communication are as follow:

- A. The continuous spectrum sensing is carried out in a process in parallel to the communication link.
- B. A single channel is used for both spectrum sensing and communication.

A two antenna system is proposed for approach (A) (Hur et al, 2006). One antenna is wideband and omni-directional, feeding a receiver capable of both coarse and fine spectrum sensing over a broad bandwidth. The second antenna is directional and feeds a frequency agile front end that can be tuned to the selected band. A single wideband antenna feeding both spectrum sensing module and the frequency agile front end can also be a solution for approach (A) (Laskar et al, 2006).

In approach (B), spectrum sensing and radio reconfiguration are performed when the communication link quality falls below defined thresholds. H. Harada used two thresholds (Harada, 2007). Link quality falling below the first threshold triggers spectrum sensing, so that a better system configuration can be identified that will meet the link quality requirements. When the quality degrades below a second lower threshold, the system is reconfigured.

Considering the system requirements discussed above a potential antenna solution for CR might be an antenna with multiple functionalities. The potential system might include an antenna with wideband frequency response and omni-directional radiation pattern for spectrum sensing together with reconfigurable narrowband functionality. Narrowband functionality can be achieved by supplementary filtering in the RF stage; however, this might add to the complexity of the RF front end circuitry. Filtering and reconfiguration can be included into the antenna in order to reduce the complexity of the filtering circuits in RF stage.

2.5 Multi Element Antennas

An alternative approach to design antennas suitable for multi standard radio applications is to employ several antennas. In its simplest case that multiple antennas are placed next to each other, this technique might not seem very promising for compact devices. However, together with an efficient integration concept this technique could be valuable.

2.5.1 MIMO Antennas

One of the effective ways of improving reliability and increasing the channel capacity is using multi-element antennas, such as multiple-input multiple-output (MIMO) antenna systems. It makes use of multiple antennas at both the transmitter and receiver to exploit the spatial channel for increasing the capacity. It is one of several forms of smart antenna technology. (Lau, 2006)

MIMO technology has attracted attention in wireless communications, because it offers significant increases in data throughput and link range without additional bandwidth or transmit power. It achieves this by higher spectral efficiency (more bits per second per hertz of bandwidth) and link reliability or diversity (reduced fading). Because of these properties, MIMO is an important part of modern wireless communication standards. (AWE Communications, 2010)

In MIMO systems, a transmitter sends multiple streams by multiple transmit antennas. The transmit streams go through a matrix channel which consists of all $N_t N_r$ paths between the N_t transmit antennas at the transmitter and N_r receive antennas at the receiver. Then, the receiver gets the received signal vectors by the multiple receive antennas and decodes the received signal vectors into the original information.

2.6 A review of techniques of improving the isolation in multi-port antennas

In multi standard radio systems with simultaneously operating antennas, excellent isolation between antenna ports is a requirement. It is a very difficult task to integrate multiple antennas closely in a small and compact mobile handset while maintaining good isolation between antenna elements because the antennas couple strongly to each other and to the ground plane by sharing the surface currents on them.

Printed antenna arrays suffer from relatively high level of mutual coupling between individual elements due to surface waves. This becomes progressively worse with increasing frequency, dielectric constant, and substrate thickness. (Yazdanbakhsh and Solbach, 2009)

High antenna coupling (or low isolation) would cause signal leakage from one antenna to another, so increasing the signal correlation between the channels. It will also decrease the antenna radiation efficiency due to the loss of the power dissipated in the coupled antenna port.

The change in input impedances of the antennas is another consequence of mutual coupling, and it results in larger mismatch between the antennas and their corresponding source and load impedances. (Lau, 2006) Various port decoupling techniques have been reported in literature.

2.6.1 Isolation Techniques in multiport antennas

Enhancement techniques for multiport antennas can be categorized into two main groups:

1. Isolation enhancement by changing the antennas structure (or redesigning)
2. Isolation enhancement by adding an external feed network to the antenna without making any changes to the already designed antenna's structure.

The first approach is more common in literature. However the second approach is the concern of this project. The second approach is more general as it can be applied to any similar antenna with slight changes in parameters such as the frequency of design and the port arrangement.

2.6.1.1 Isolation enhancement by changing the antennas structure

In the case that operating frequency bands are sufficiently widely separated, embedded or external filtering structures can be used to provide the required isolation. On the other hand, there are applications where bands have to be closely spaced or even have to occupy the same band such as multiple input multiple output system (MIMO), where in principle the demanded isolation cannot be achieved with microwave filters or where isolation provided by filters is not sufficient.

The signal correlation between two receiver antennas can be reduced by increasing the antenna spacing. Good isolation can be achieved by separating antennas by much more than half a wavelength. However, this spacing is usually limited (especially at low frequencies), particularly for a mobile terminal which has very restricted size for the antennas. To achieve

maximum separation for instance in a typical mobile phone or laptop the antennas are distributed around the periphery of the device. In some applications, due to the constraint of the spacing of the antenna elements, polarization diversity is preferred. (Andrews et al., 2001)

When multiple antennas are collocated on a single device, some factors such as the antenna positions relative to each other and to the ground plane influence the radiation. In addition, in applications such as mobile phones, the ground plane or device chassis is considered as part of the antenna and therefore contributes to the radiation. Therefore, it is important to find the appropriate configuration of antennas which can satisfy all the system requirements. (Jakobsen and Thaysen ,2007) related the antenna mutual orientations and locations to the mutual coupling between two identical antennas on an infinite ground plane. They investigated 15 symmetrical as well as asymmetrical coupling scenarios using two identical PIFAs located close to each other on the finite ground plane as shown in Fig. 2.2. They concluded that in MIMO application in addition to low mutual coupling, the bandwidth should also be maintained to achieve good MIMO performance. Taking into account bandwidth and mutual coupling configuration it was concluded that configuration B4 had the best performance although it is not the case with the largest spacing.

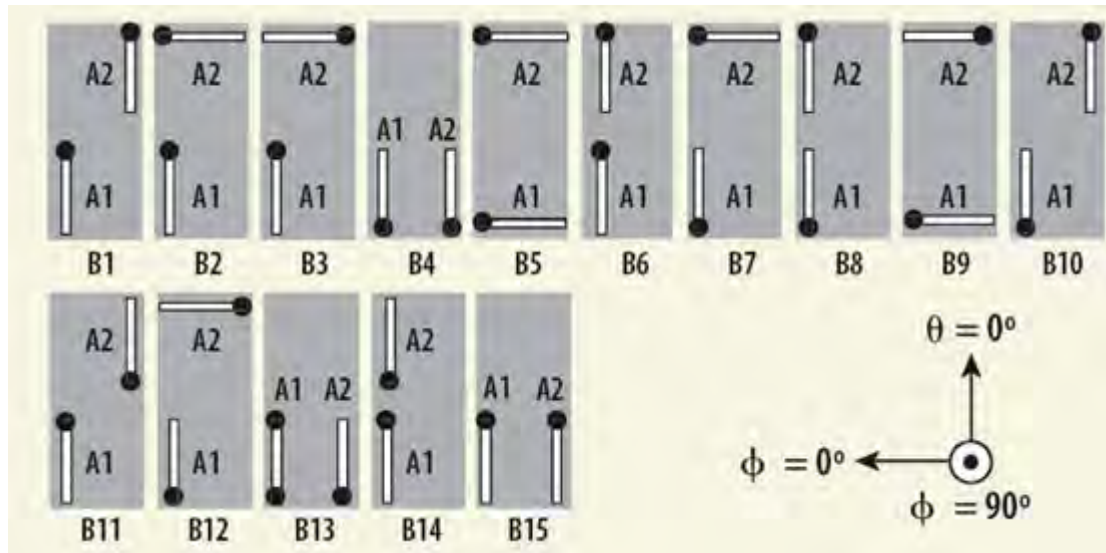


Figure 2.2: This layout shows 15 different two-antenna configurations located on the same finite ground plane. The matchsticks symbolize the PIFA's, and the dot on the matchstick denotes the location of the shorting pin. (Jakobsen and Thaysen, 2007)

The other way to decrease the correlation is using multiple antennas with different radiation patterns. It is better to have the patterns complementary to each other in space, so as to receive multipath signals from different directions.

In fact, isolation between the antenna ports can be enhanced by employing cancellation techniques (Esser et al., 2006). These techniques require a modification of the antenna structure such that in addition to the already existing “propagation path A” (Fig. 2.3, left) a second path B is created (Fig. 2.3, right) whose parameters can be adjusted to cancel the unwanted transmission via path A.

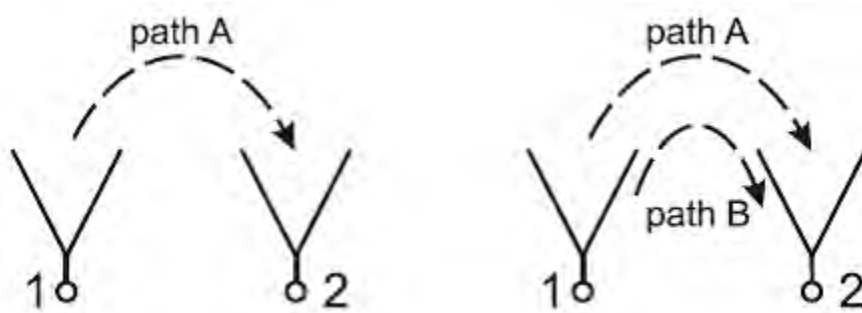


Figure 2.3: Left: Two-port antenna without coupling cancellation. Right: Cancellation of path A by a second path B (Esser et al., 2006).

A well-known practice is the introduction of resonant defects such as slots, slits and stubs on the ground plane between the antennas. (Kokkinos et al., 2008) has placed two PIFAs on the top and bottom of the mobile chassis to achieve the largest spacing possible (see Fig. 2.4a). Furthermore, two coupled quarter-wavelength slits are inserted into the ground plane between the antennas. The slits introduce resonances and insert transmission zero in the coupling path between the PIFAs. This reduces the coupling without significantly disturbing antenna performance. This technique was also studied by (Karaboikis et al., 2004) for printed PIFAs (see Fig. 2.4b) achieving S_{21} less than -25dB. Fig. 2.4c shows another attempt for reducing port coupling between two PIFAs examined by (Chiu et al., 2007). They achieved coupling better than 15dB across the band. A printed WLAN MIMO antenna with reduced coupling is presented by (Wu et al., 2002). A T-stub section is added to the ground plane as shown in Fig. 2.5a and about 50% improvement comparing to the conventional case is achieved. To support a wider bandwidth for UWB MIMO a multiple branch structure (see Fig. 2.5b) can be replaced with the T-stub (Shuai et al., 2009). In this work, S_{21} less than -10dB is maintained for the UWB band.

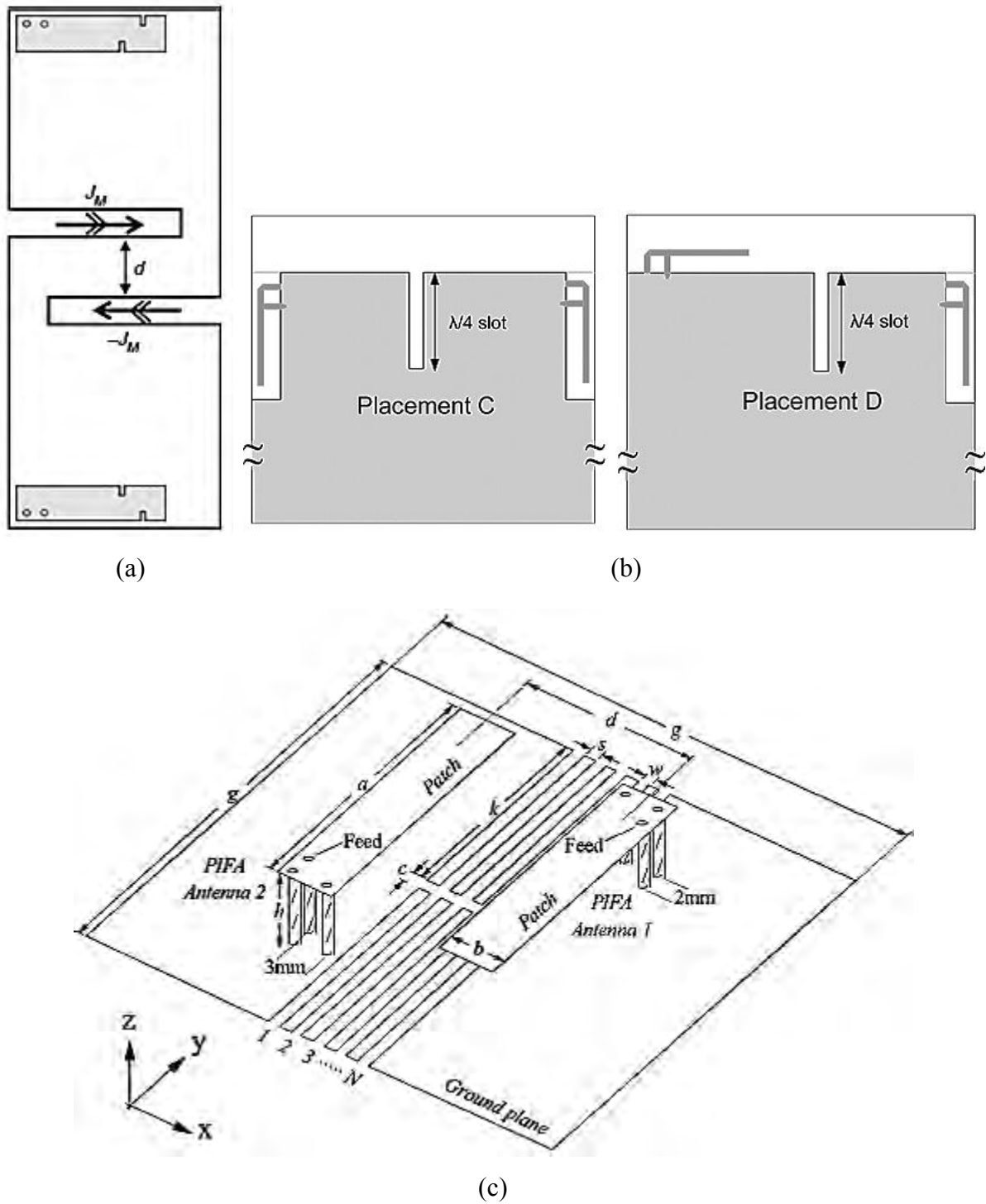
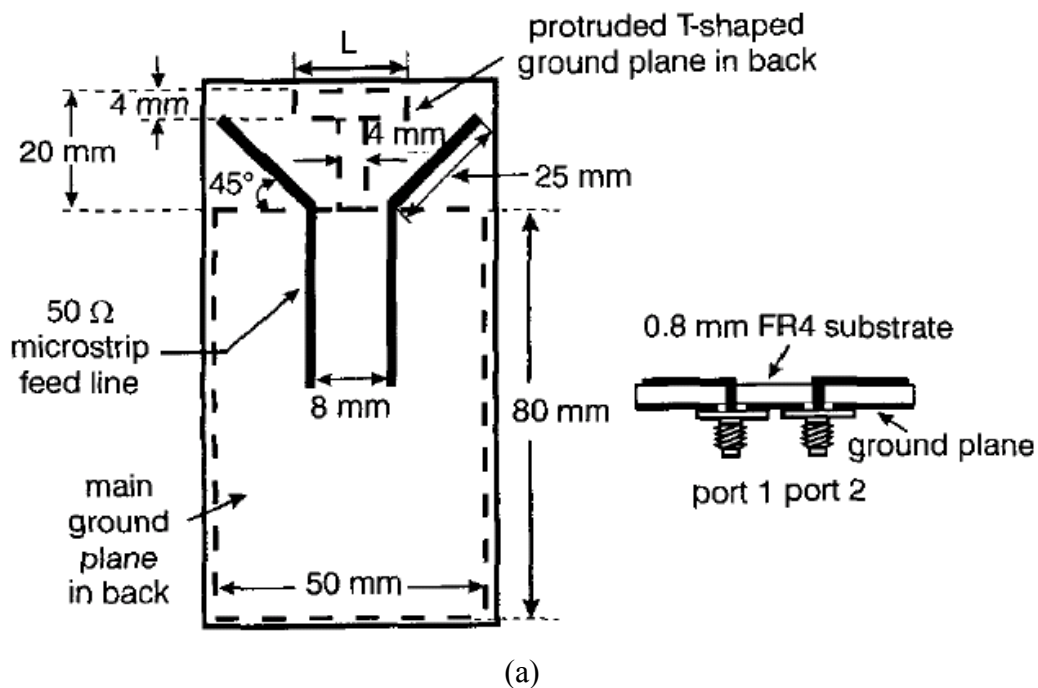


Figure 2.4: Schematic diagram of MIMO antennas with slits in the ground plane, (a) (Kokkinos et al., 2008), (b) (Karaboikis et al., 2004), (c) (Chiu et al., 2007).

Lihao et al. included a split ring resonator on the common ground between the antennas as shown in Fig. 2.6a to limit the port coupling. Furthermore, the cancellation technique is

implemented by inserting a parasitic structure between the dipoles shown in Fig. 2.6b. In principle this method introduces one more coupling path and this coupling path creates another coupled current with pre-determined magnitude and phase in order to cancel out the original coupling. Using this technique, measured S_{21} better than -30dB for the band of interest at 2.45GHz has been achieved. (Lihao et al., 2010). Diallo et al., (2006) introduced a suspended transmission line between the shorting and/or feeding points of two PIFAs, as the cancellation paths (see Fig. 2.6c). When the shorting strips face each other and are linked via the bridging suspended transmission line, the transmission coefficient is stable and better than -20dB across the $0.8\text{-}2.6\text{GHz}$ band. This concept was combined with other techniques such as optimum antenna orientation and position by Park and Jung (2010). As shown in Fig. 2.7 two folded monopoles are printed orthogonally to achieve pattern and polarisation diversity at the same time. High port isolation is obtained by adding a connecting line to the face of the feed-line. The connecting line linking the two antennas is used to cancel the reactive coupling between antennas.



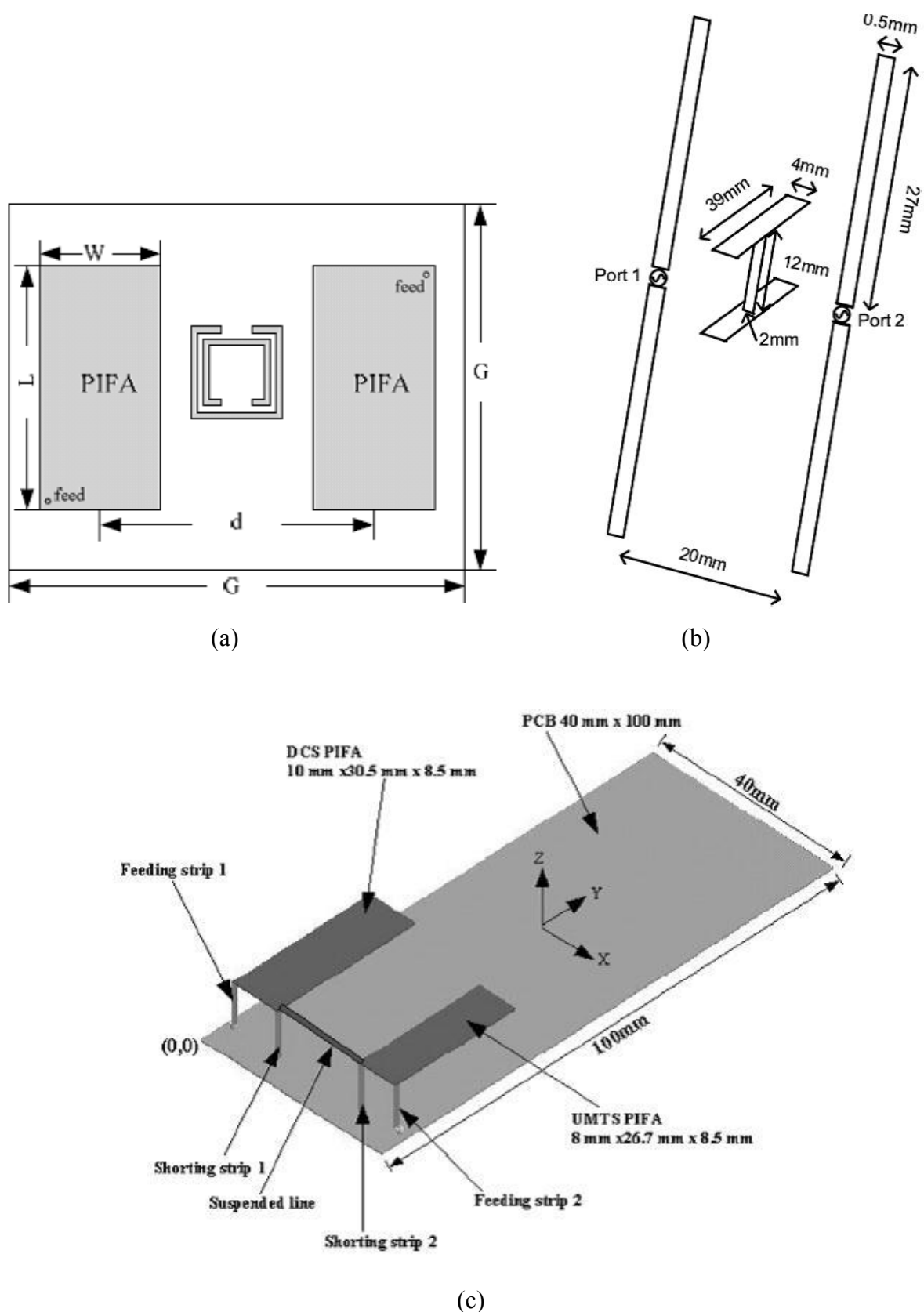


Figure 2.6: Schematic diagram of the PIFAs with (a) split ring resonator (Lihao et al., 2010) (b) parasitic decoupling element (Mak et al., 2008) (c) suspended transmission line (Diallo et al., 2006).

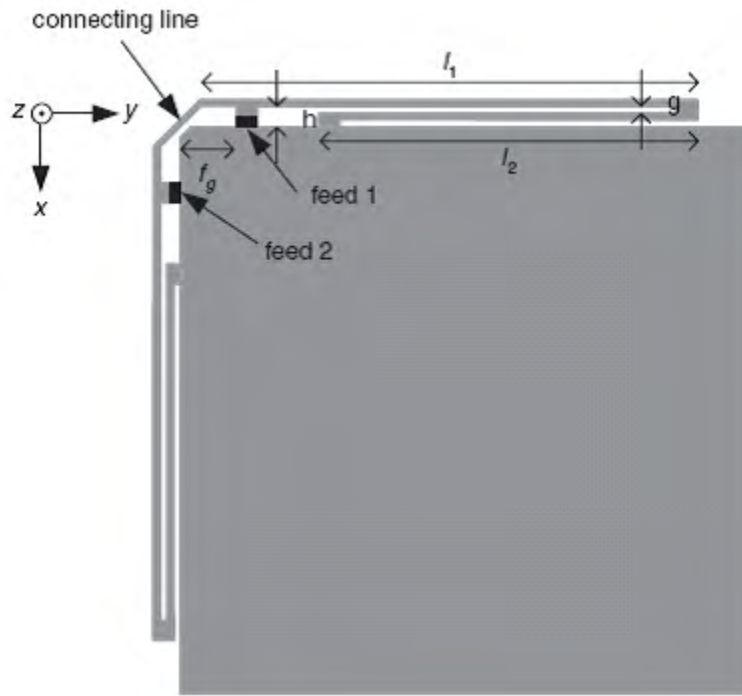


Figure 2.7: Schematic diagram of the antenna with combination of decoupling techniques (Park and Jung., 2010).

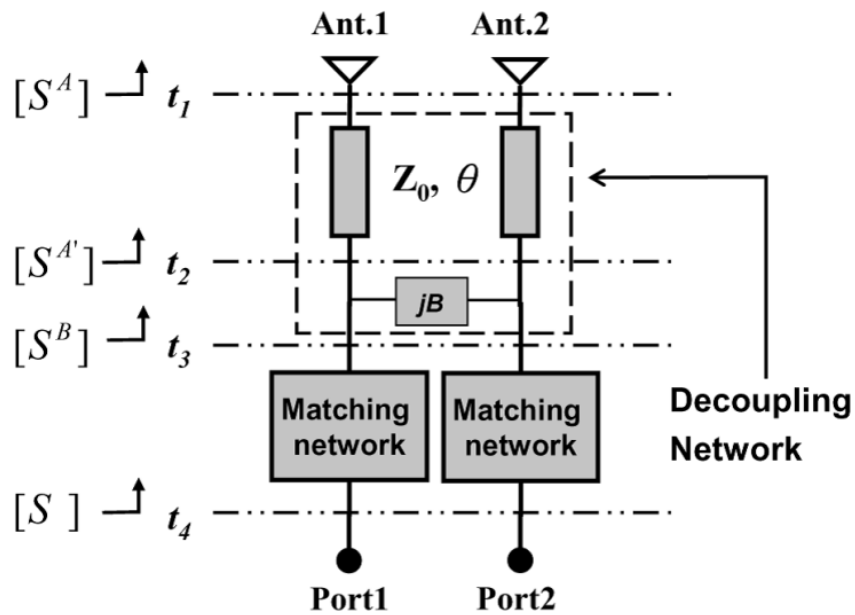


Figure 2.8: The function blocks of the decoupling structure proposed in (Chen et al., 2008).

To compensate the size of the microwave networks, particularly at low frequencies, a lumped element feed network was proposed by Bhatti et al. (2009). An LC-based branch-line hybrid coupler was integrated with the long term evolution (LTE) antenna array as shown in Fig. 2.9. The branch-line hybrid coupler is designed at 710 MHz using the passive inductors and capacitors. Each quarter wavelength transmission line section of the branch line coupler has

been replaced with its equivalent pi-network consisting of a series inductor and two parallel capacitors. Fig. 2.9 shows the configuration of the branch-line coupler. The two monopole antennas have been attached to the hybrid coupler ports 3 and 4, respectively. Ports 1 and 2 of the hybrid coupler are decoupled, which are connected to the input ports. The coupling produced by the hybrid coupler cancels out the mutual coupling between the antenna ports.

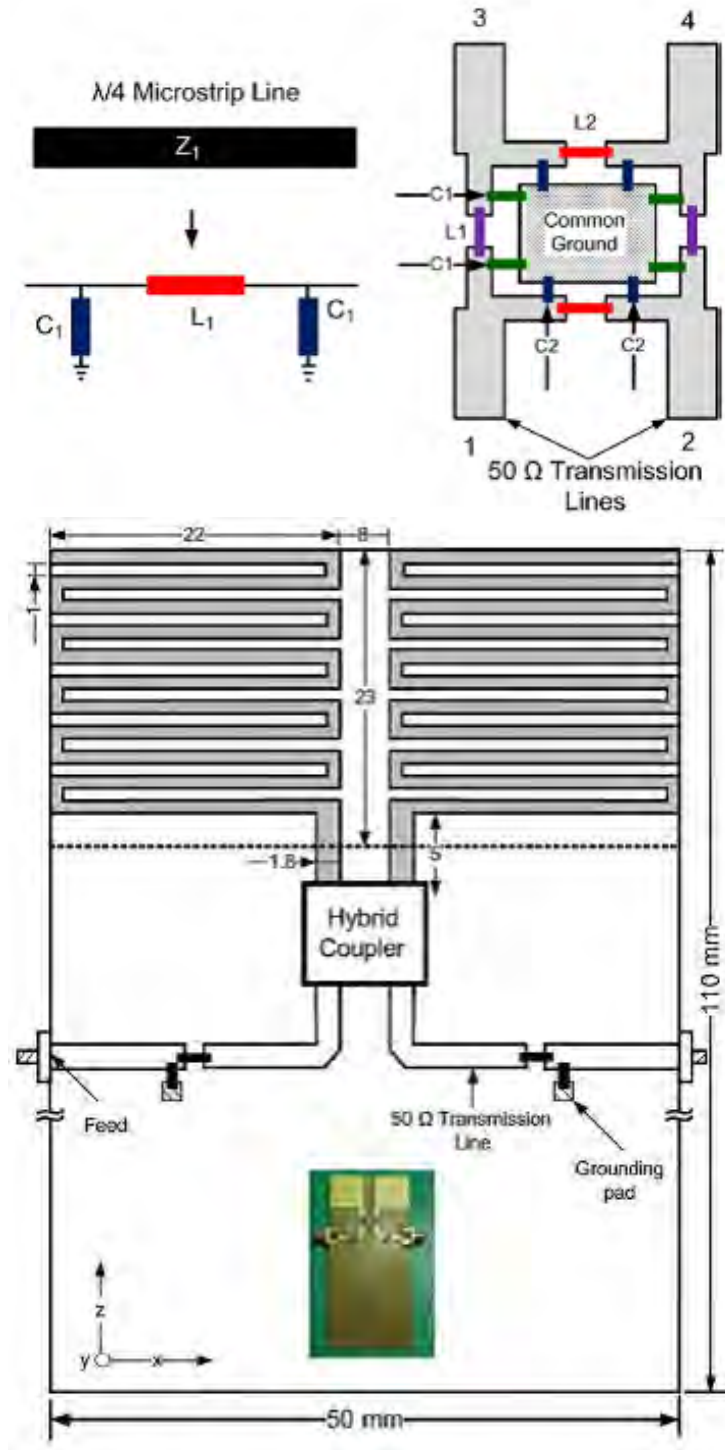


Figure 2.9: Schematic diagram of the LTE antenna with a branchline decoupling feed network (Bhatti et al., 2009).

2.7 Directional Couplers

Directional couplers are passive microwave components used for power division or power combining. The coupler may be a three-port component, with or without loss, or maybe a four port component. Three-port networks take the form of T-junctions and other power dividers, while other networks take the form of directional couplers and hybrids. Power dividers often are of the equal-division (3 dB) type, but unequal power division ratios are also possible. Directional couplers can be designed for arbitrary power division, while hybrid junctions usually have equal power division. (Pozar.1998)

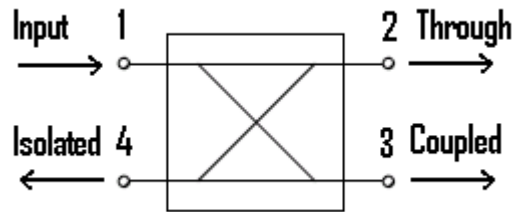


Figure 2.10: Commonly used symbol for directional couplers. (Pozar, 1998)

The $[S]$ matrix of a reciprocal four-port network matched at all ports has the following form:

$$S = \begin{pmatrix} 0 & S_{12} & S_{13} & S_{14} \\ S_{12} & 0 & S_{23} & S_{24} \\ S_{13} & S_{23} & 0 & S_{34} \\ S_{14} & S_{24} & S_{34} & 0 \end{pmatrix} \quad (2.1)$$

If $S_{14} = S_{23} = 0$, the matrix represents a directional coupler,

$$S = \begin{pmatrix} 0 & S_{12} & S_{13} & 0 \\ S_{12} & 0 & 0 & S_{24} \\ S_{13} & 0 & 0 & S_{34} \\ 0 & S_{24} & S_{34} & 0 \end{pmatrix} \quad (2.2)$$

The network is considered to be lossless; Therefore:

$$(2.3a)$$

$$(2.3b)$$

$$(2.3c)$$

$$(2.3d)$$

Which imply that Γ_{12} (using equation 2.3a and 2.3b), and Γ_{13} (using equation 2.3b and 2.3d). Further simplification can be made by choosing the phase references on three of the four ports. Thus, it is chosen to be $\Gamma_{12} = \alpha e^{j\theta}$, $\Gamma_{13} = \beta e^{j\Phi}$, and $\Gamma_{14} = 0$, where α and β are real, and θ and Φ are phase angles to be determined (one of which still free to be chosen).

The dot product of rows 2 and 3 in the matrix (2.2) gives:

Which yields a relation between the remaining phase constants as:

Amplitudes α and β are not independent, as equation (2.3a) requires that:

Thus, apart from phase references, an ideal directional coupler has only one degree of freedom.

The basic operation of a directional coupler can then be illustrated with the aid of Fig. 2.10, which shows a commonly used symbol for a directional coupler and the port definitions. Power supplied to port 1 is coupled to port 3 (the coupled port) with the coupling factor k , while the remainder of input power is delivered to port 2 (the through port) with the coefficient $1 - k^2$. In an ideal directional coupler, no power is delivered to port 4 (isolated port).

The following three quantities are generally used to characterize a directional coupler: (Collin, 1992)

$$S_{11} = \text{Reflection Coefficient (dB)}, \quad (2.4)$$

$$S_{21} = \text{Transmission Coefficient (dB)}$$

$$I = D + C \text{ dB}$$

The coupling factor indicates the fraction of the input power which is coupled to the output port. The directivity is a measure of the coupler's ability to isolate forward and backward waves, as is the isolation. These quantities are then related as:

$$I = D + C \text{ dB} \quad (2.5)$$

The ideal coupler would have infinite directivity and isolation (). Then both α and β could be determined from the coupling factor, C . (Pozar, 1998)

The other parameters which could be defined to characterized the performance of any network such as coupler are: (Collin, 1992)

$$(2.6)$$

$$(2.7)$$

Return Loss is a measure of the input impedance match. The term loss is somewhat anomalous. If the input match is good then the input reflection coefficient is small and only a small amount of incident power is reflected back. Abstractly, the power which passes into the circuit can be thought of as power lost to the feeding circuit. If the reflection coefficient is low then the loss is high. If the reflection coefficient is high (i.e., $G \gg 1$) then the return loss is low.

Insertion Loss is a measure of the amount of power which enters the coupler but fails to make it out of the direct port. A large fraction of the power coupled away would represent a large loss of power to the direct port. When couplers are inserted into a circuit for the purpose of measuring the propagating energy, a low insertion loss is desired to insure that the original circuit is not modified by the measuring system.

Chapter 3

Isolation Using a Hybrid Coupler

This section concerns designing a feed network consisting of a 3 dB rat-race coupler and a phase shifter. The feed network is used to enhance the isolation between the antenna ports. The following is a brief description of the antenna.

3.1 Antenna Description

This section describes a Dual port Ultra Wideband-narrowband antenna suffering from low isolation between the two ports. It has already designed by another member of Antenna and Applied Electromagnetics laboratory.

An integration concept for multi-standard radios was proposed in this section. The method is based on sharing some parts of one antenna between additional antennas. The structure is composed of two printed antennas. The ultra-wideband (UWB) antenna is designed to fulfil the scanning task and the narrowband antenna for narrowband communication. The UWB antenna is a printed wine glass shaped coplanar waveguide (CPW) fed monopole, printed on one side of the substrate. The printed UWB antenna is selected as the main antenna and then a shorted patch antenna is integrated into the main structure.

Fig. 3.1 shows the geometry of the UWB antenna. The structure is printed on a Taconic TLC laminate with a relative permittivity of $\epsilon_r=3\pm 0.05$ and a thickness of 0.79mm.

Since the ground plane is part of the matching network in this class of antennas the dimensions of the ground plane and feed gap are set in a way to provide the optimum matching. The radiating element is a monopole which has been made of a half ellipse and a rectangular segment.

To achieve dual mode operation, an integration of the two antennas has been proposed. The narrowband antenna is printed on the reverse side of the substrate. In other words the UWB antenna is used as the ground plane for the narrowband antenna. Consequently, less space

would be required for this antenna with two states of operation. The antenna can operate at both wide and narrowband state because it has two separate ports-one for each antenna. A shorted microstrip patch antenna is designed and a shorting pin is used to connect the patch to the wideband antenna. As the UWB antenna is a CPW-fed monopole, it can be considered as a defected ground plane for the narrowband antenna. This results in more complicated couplings between the wideband and narrowband antenna. The patch has been fed through a microstrip line. (Ebrahimi and Hall, 2009)

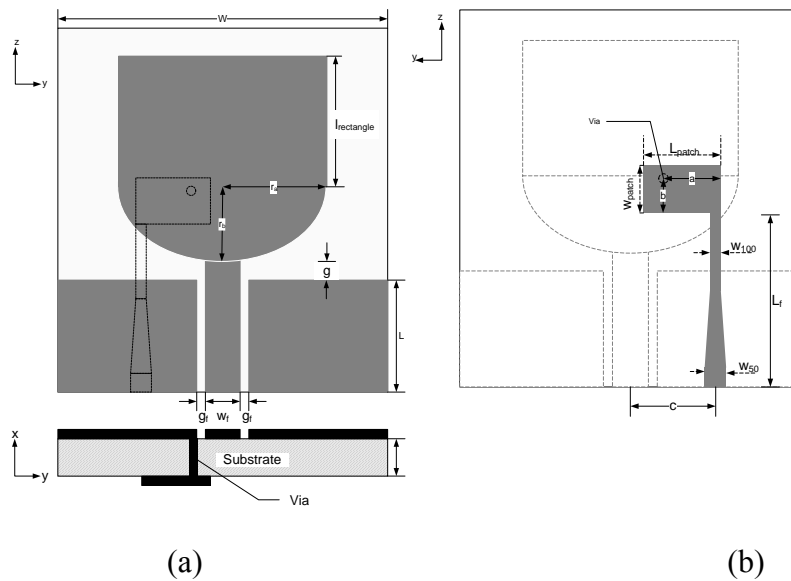


Figure 3.1: Geometry of the proposed antenna. (a) UWB antenna (b) Narrowband antenna (Ebrahimi and Hall, 2009)

Ebrahimi and Hall (2009) carried out a parametric study to achieve the desired performance of the above-mentioned Dual port antenna. Parameters possibly affecting the performance include the narrowband antenna feed line length and the ground plane dimensions. The following section explains some aspects of the parametric study to demonstrate the challenge involved in the design of an external decoupling network.

3.1.1 Ground Plane Width (W_g)

Variation in ground plane size changes the current path and therefore antenna matching. Fig. 3.2 shows that the ground plane width (W_g) varies from 46mm to 62mm while other parameters are fixed. Evidently, both ends of the band are considerably affected by a change in ground width, while the band ranging from 4GHz to 7GHz stay less than -10dB for all

values of W_g . While the first resonance is not significantly affected by the width of the ground plane the second resonance is shifted along the band. As the optimal width of the ground plane is 54 mm, it is important to note that the -10dB bandwidth has reduced for both narrower and wider ground planes. As can be seen in Fig 3.3, increasing the length of the ground plane improves the return loss at lower frequencies and reduces the lower cut-off frequency.

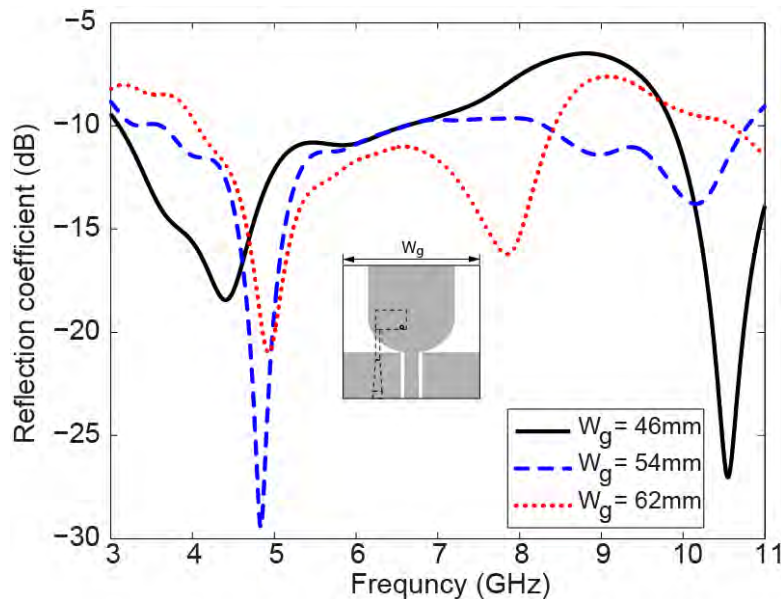


Figure 3.2: Simulated reflection coefficient curves for different W_g , wideband antenna (Ebrahimi, 2011)

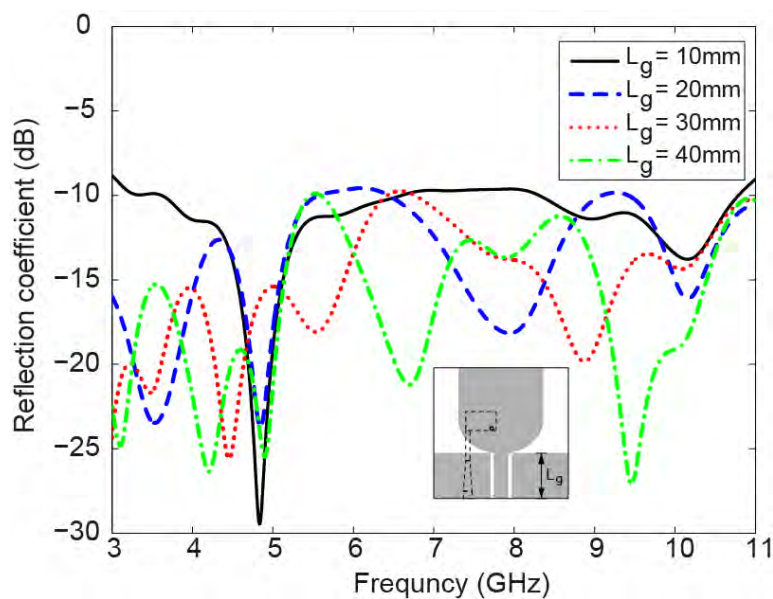
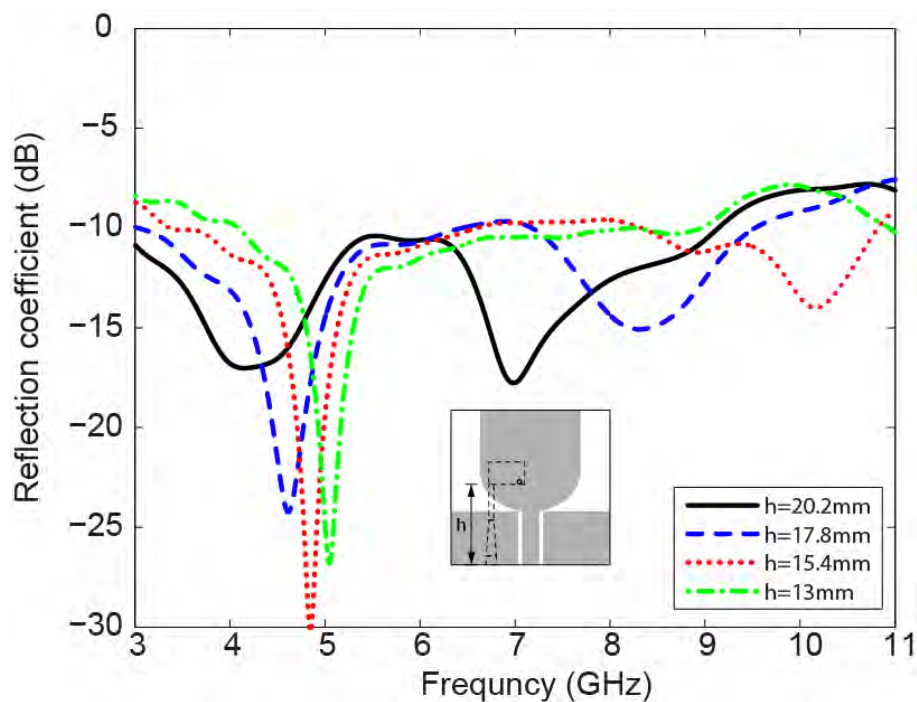


Figure 3.3: Simulated reflection coefficient curves for different L_g , wideband antenna (Ebrahimi, 2011)

It follows that the ground plane can be considered as part of the antenna and contributes to radiation. Variation in ground plane size thus changes antenna matching. The narrowband antenna reflection coefficient is independent of ground plane width. This is understandable because the wideband antenna ground plane is used as the ground plane for narrowband antenna microstrip feeding; therefore variation of ground plane width does not change narrowband feeding impedance or the current distribution.

3.1.2 Narrowband antenna feed line

Fig. 3.4a shows that increasing the length of the narrowband antenna feeding (h) improves matching at lower frequencies. However, it has a reverse effect on the higher end of the frequency band ranging from 9GHz to 11GHz. Increasing the narrowband antenna height relative to the edge of the board creates considerable variation in the return loss of the patch antenna at 6GHz to 11GHz frequency range, as depicted in Fig. 3.4b. Increasing the length of the feeding from 13mm to 20.2 mm decreases expected resonance frequency from 5.5GHz to 4.8GHz. In the frequency range of 6-11GHz the change is dramatic and has no clear pattern. Increasing the feeding length changes its impedance; however this does not follow a clear pattern, perhaps owing to the effect of the feed crossing the gap between the monopole and its ground plane.



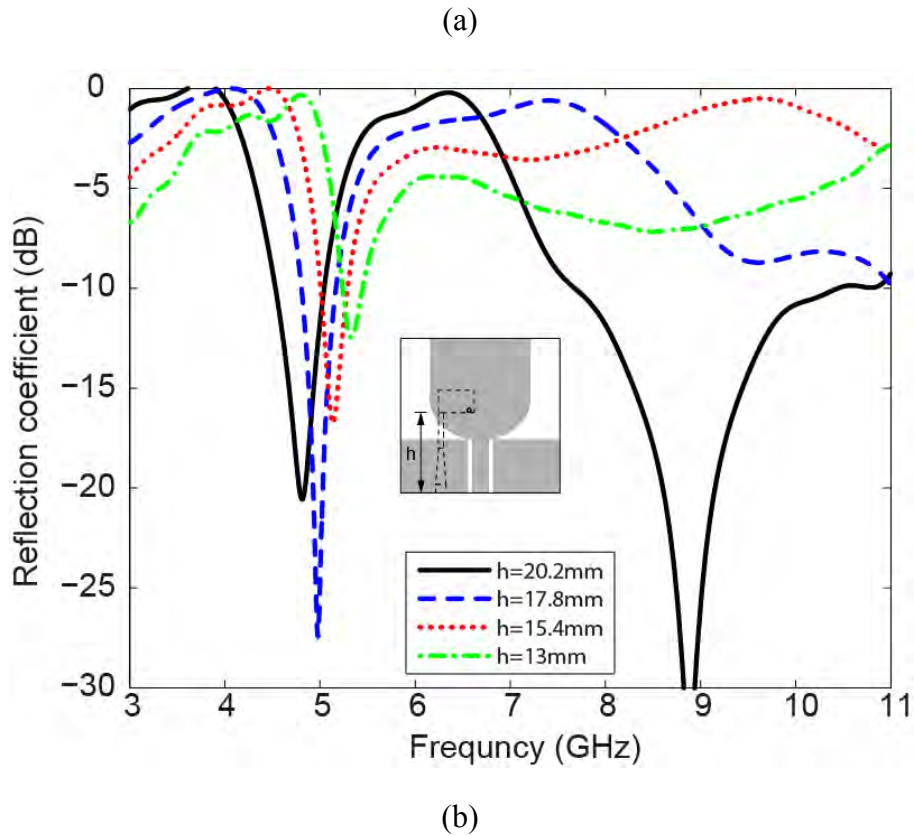


Figure 3.4: Simulated reflection coefficient curves for different h (a) wideband antenna, (b) narrowband antenna (Ebrahimi, 2011)

It can be concluded that changing the narrowband antenna feed length as well as ground plane dimensions affects the narrowband and/or wideband reflection coefficient. As a result, adding a feed network to the antenna might change the ground plane size and narrowband antenna feed line which should be taken to account.

Another conclusion is that adding any feed network to the antenna will change the size of the ground plane. This might influence the narrowband antenna's feed length and will certainly affect the antenna's reflection coefficient.

3.1.3 Electric current distributions on the antenna

In order to explore the EM behaviour of the antenna, the current distributions on the antenna are shown in Figs. 3.5 and 3.6. Fig. 3.5 shows the current distribution on both sides of the structure when the UWB antenna is excited and the narrowband antenna is terminated to a 50Ω load. Currents are more concentrated on the edge of radiator and ground plane. Hence, a significant amount of power couples to the narrowband antenna. The asymmetrical current distribution on the UWB antenna is due to the presence of narrowband antenna. Moreover it can be seen that when UWB port is excited, some current couples to the narrowband port.

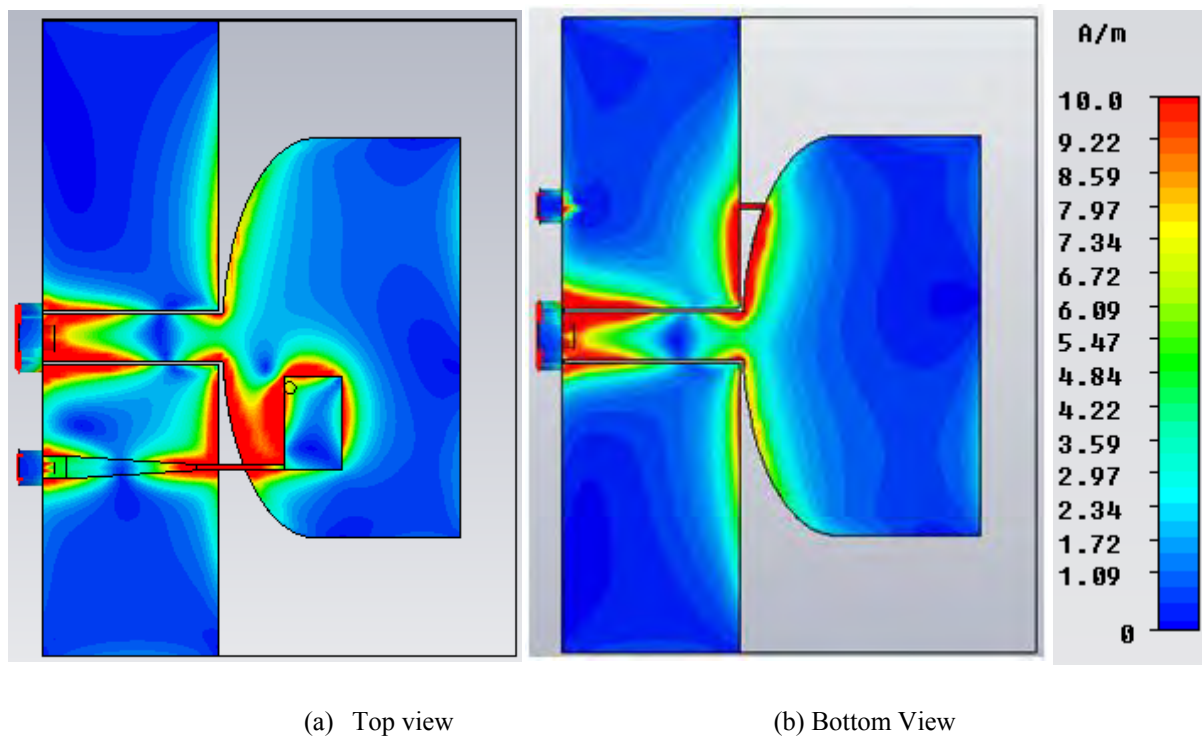


Figure 3.5: Current distributions when the wideband antenna is excited and the narrowband antenna is terminated to a 50Ω load at 5 GHz.

Fig. 3.6 shows the current distributions on the structure when the narrowband antenna is excited and the UWB antenna is terminated to a 50Ω load. Since the narrowband antenna is fed in this case, the currents are highly concentrated around it. At the narrowband antenna resonant frequency, 5.15 GHz, high concentration of currents can also be observed on the edge of the UWB radiator and ground plane. This is due to the current coupled through the UWB antenna from the narrowband antenna. The coupling is because of the close spacing of the antennas in the designed structure. This coupling could be cancelled out by redesigning the spacing of the two antennas. However, it is not the concern of this thesis. The purpose of this project is to reduce the mutual coupling at the antenna ports.

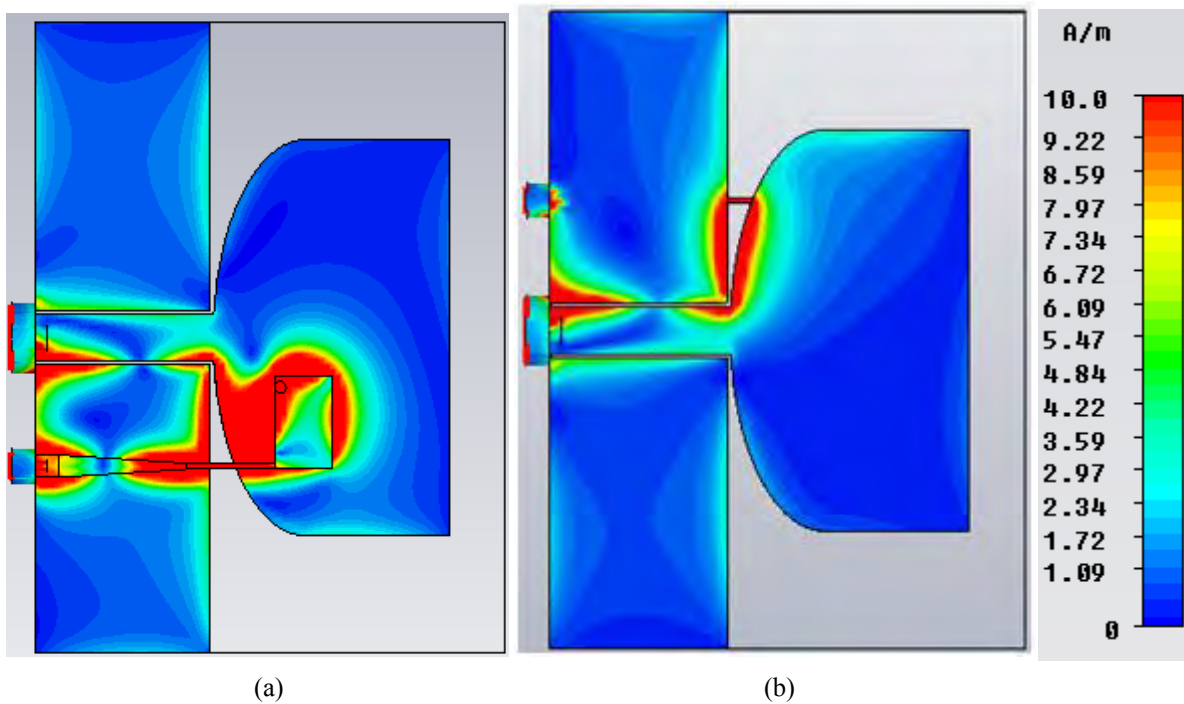


Figure 3.6: Current distributions when the narrowband antenna is excited and the wideband antenna is terminated to a 50Ω load at 5 GHz. (a) Top view, (b) Bottom view.

3.2 Coupler Design

The following was the initial approach to reduce the mutual coupling between the antenna ports. The idea was to cancel the coupling existing between the antenna ports by creating another coupling path. This coupling could be produced by a coupler.

A 3dB rat-race coupler was chosen to create the coupling path. It should be mentioned that a phase shifter was also required because the coupler itself would not necessarily create the right phase shift to cancel the mutual coupling between the antennas. Another degree of freedom was therefore necessary. According to (Pozar, 1998) the scattering matrix for a rat-race coupler is

$$S = -j/\sqrt{2} \begin{pmatrix} 0 & 1 & 1 & 0 \\ 1 & 0 & 0 & -1 \\ 1 & 0 & 0 & 1 \\ 0 & -1 & 1 & 0 \end{pmatrix} \quad (3.1)$$

The 180° hybrid junction is a four port network with a 180° phase shift between the two output ports. It can also be operated so that the outputs are in phase. With reference to the 180° hybrid symbol shown in Fig 3.7, when port1 is excited, the signal is evenly split into two in-phase components at ports 2 and 3, and port 4 is isolated. If the signal is applied to port 4, it is equally split into two components with a 180° phase difference at ports 2 and 3, and port 1 is isolated. If the input signals are applied at ports 2 and 3, the sum of the inputs appears at port 1, while the difference appears at port 4; in this case the 180° hybrid is operating as a combiner. Thus, ports 1 and 4 are referred to as the sum and difference ports, respectively.

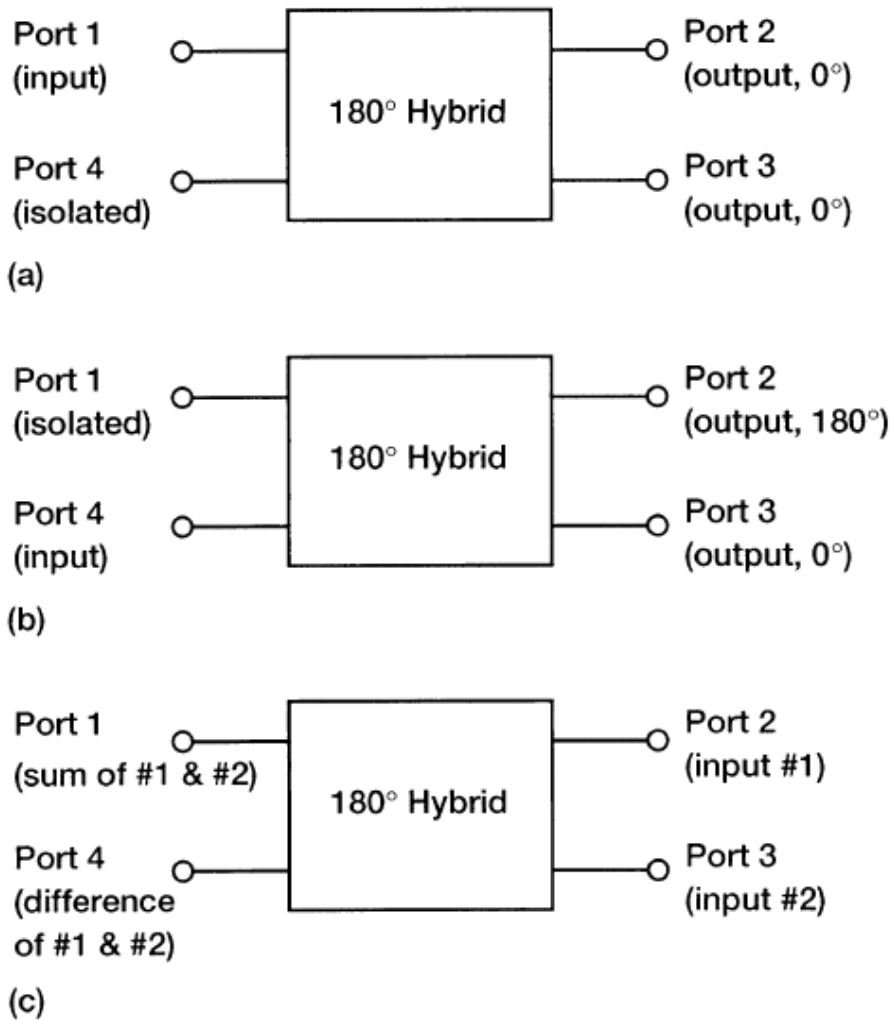


Figure 3.7: Representation of a 180° hybrid: (a) As a power divider with port 1 as input; (b) as a power divider with port 4 as input; (c) as a power combiner with ports 2 and 3 as input. (Simons, 2001)

The 180 hybrid can be fabricated in different forms. The ring hybrid or rat-race, shown in Fig 3.8 can be constructed in planar (microstrip or stripline) form, although a waveguide version is also possible.

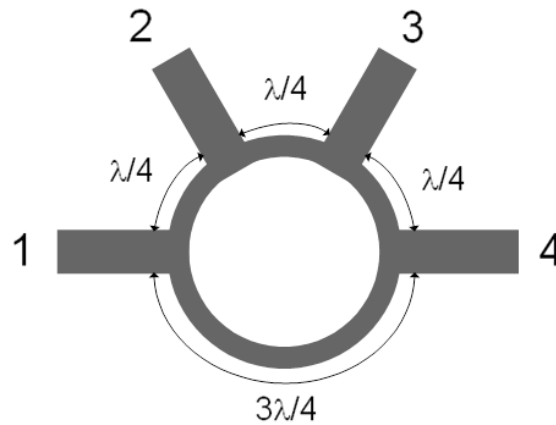


Figure 3.8: The ring hybrid or rat-race coupler (Gardner, 2010)

The bandwidth of the ring hybrid is limited by the frequency dependence of the ring lengths, but is generally of the order of 20-30%. Increased bandwidth can be obtained by using additional sections, discussion of which is outside the scope of this project.

The ring lengths and feed lines are calculated as follows:

For equal split 3 dB coupler (equal power split and 180° phase shift between ports 3 and 4):

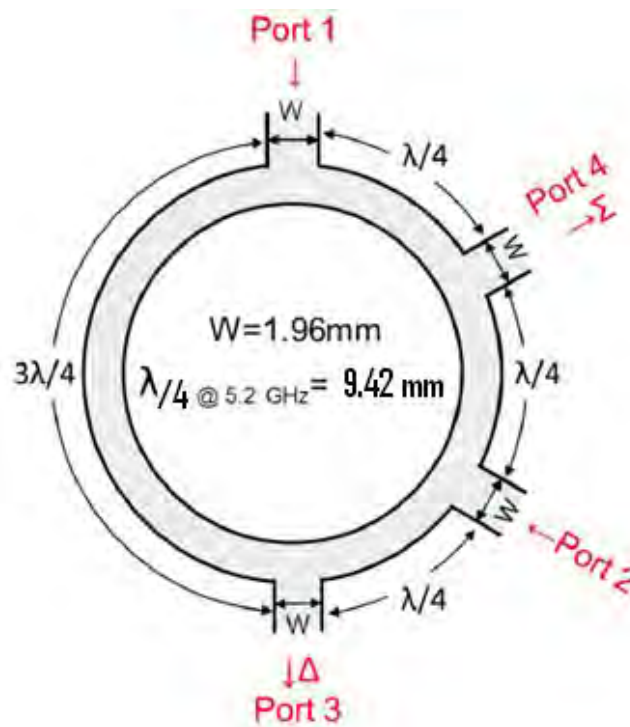


Figure 3.9: The ring hybrid or rat-race coupler

In Fig. 3.9:

The port impedances are 50Ω . The ring has a characteristic impedance of factor $\sqrt{2}$ compared to port impedance.

The effective guided wavelength is given by (Pozar, 1998):

$$\text{---} \quad (3.2)$$

Where, to a first approximation (ignoring the metal thickness and losses):

$$\text{---} \quad (3.3)$$

λ_{eff} is calculated for the high performance RF Laminate (TLC-30) substrate with a relative permittivity of $\epsilon_r=3\pm 0.05$ and a thickness of $h=0.79$ mm. By substituting, $\epsilon_r=3$ (relative permittivity), $H=0.79$ mm and $W=1.96$ mm in equation (3.3)

$$\epsilon_{\text{eff}} = 2.4$$

Then by substituting $\epsilon_{\text{eff}} = 2.4$ into equation (3.2) at $f=5.2$ GHz, where

$$\lambda_{\text{eff}} = 37.713 \text{ mm}$$

To calculate the width of the ring and feed lines the TXLine is used a useful tool of the *Microwave Office* (AWR) software. The ring's width is equal to 0.2 mm at 5.2 GHz. The rat-race coupler is been simulated in *CST Microwave Studio*; it was implemented and measured.

In order to draw the coupler, the radius of the ring is required. Fig. 3.9 shows that the ring's circumference is equal to $C = 56.56$ mm. By applying circle's circumference formula, $C = 2\pi r$, the radius of the ring works out at 9.54 mm.

Fig. 3.10 shows the simulated S-parameter magnitude for the 180° hybrid coupler designed at 5.2 GHz. All four ports are matched. The 3dB power coupling is achieved between the input and output ports. The input ports are isolated from each other. (S_{11} less than -10 dB at 5.2 GHz)

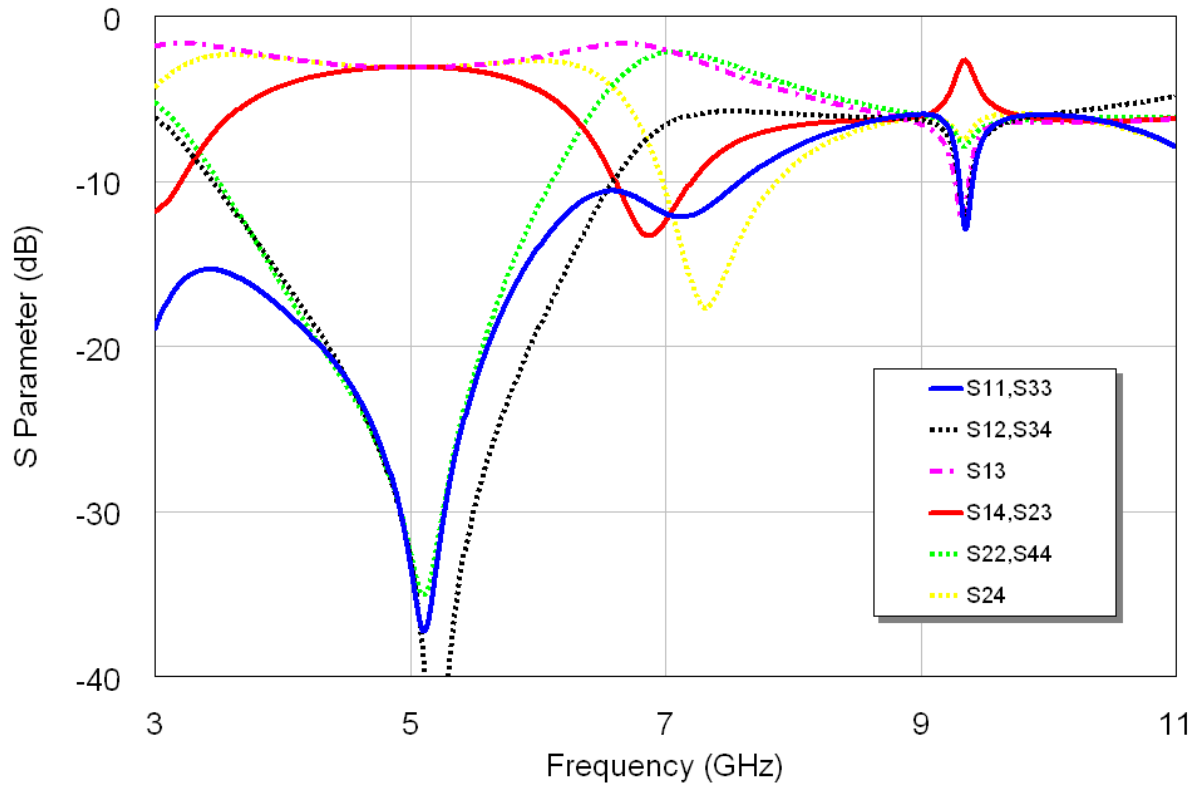


Figure 3.10: Simulated Rat-race coupler S-parameters

As it was mentioned earlier, a phase shifter is required to achieve the appropriate phase. The value of the phase shift will be achieved by manual optimization. The optimum value of phase shift is equal to 84° ; therefore the phase-shifter length is equal to 8.7 mm (Using TXline). In order to find the optimum value for the phase shift, different values have been tried. Figs. 3.11 and 3.13 show the results of S_{11} and S_{22} for the phase shift value of 55° and 110° respectively. Fig. 3.12 shows that a better isolation achieved by a phase shift of 84° .

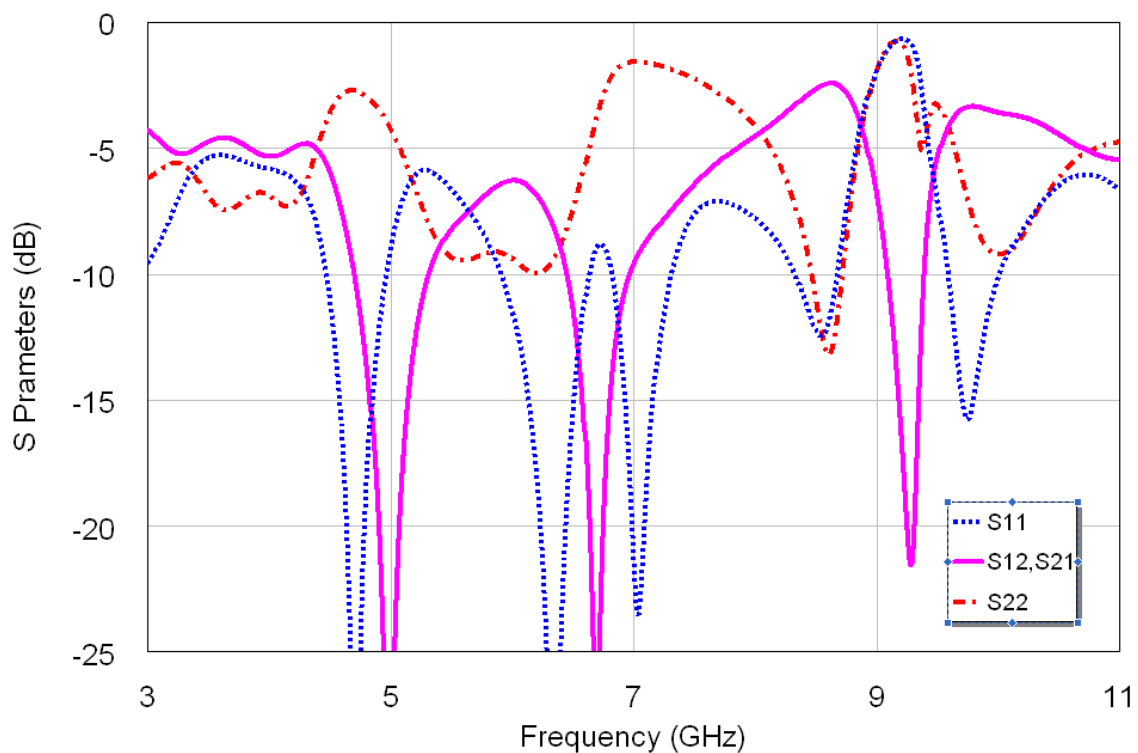


Figure 3.11: S-parameters of the antenna and feed network, phase shifter value is equal to 55 °.

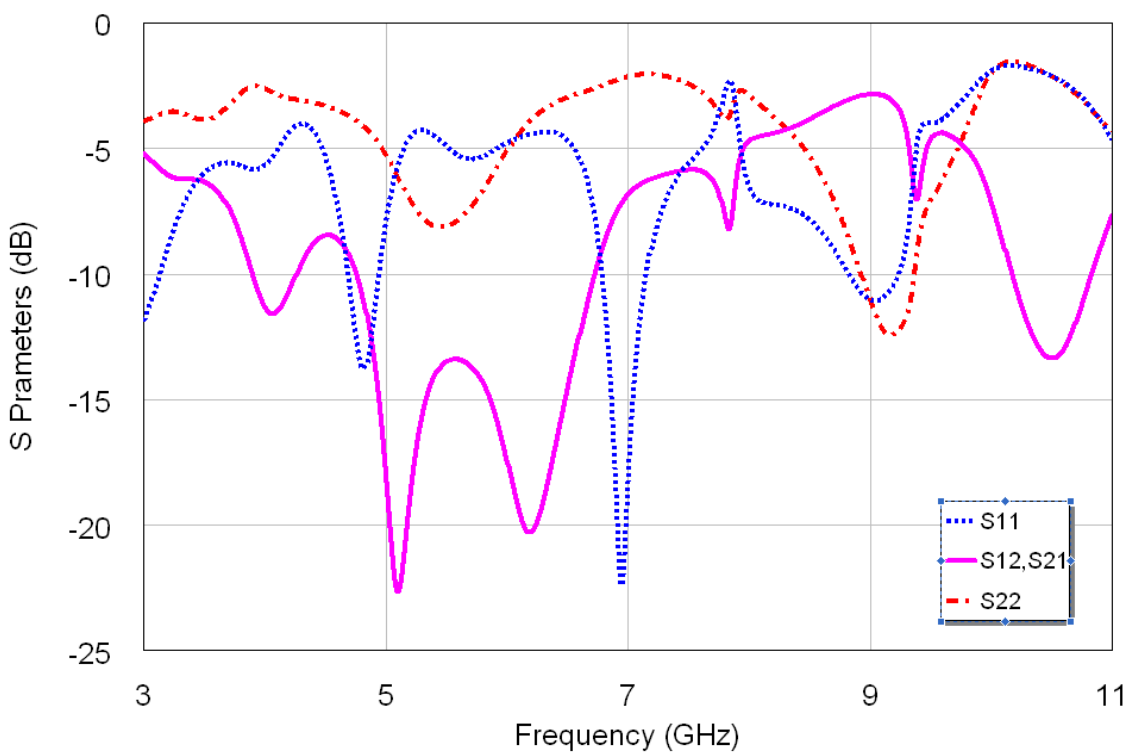


Figure 3.12: S-parameters of the antenna and feed network, phase shifter value is equal to 84 °.

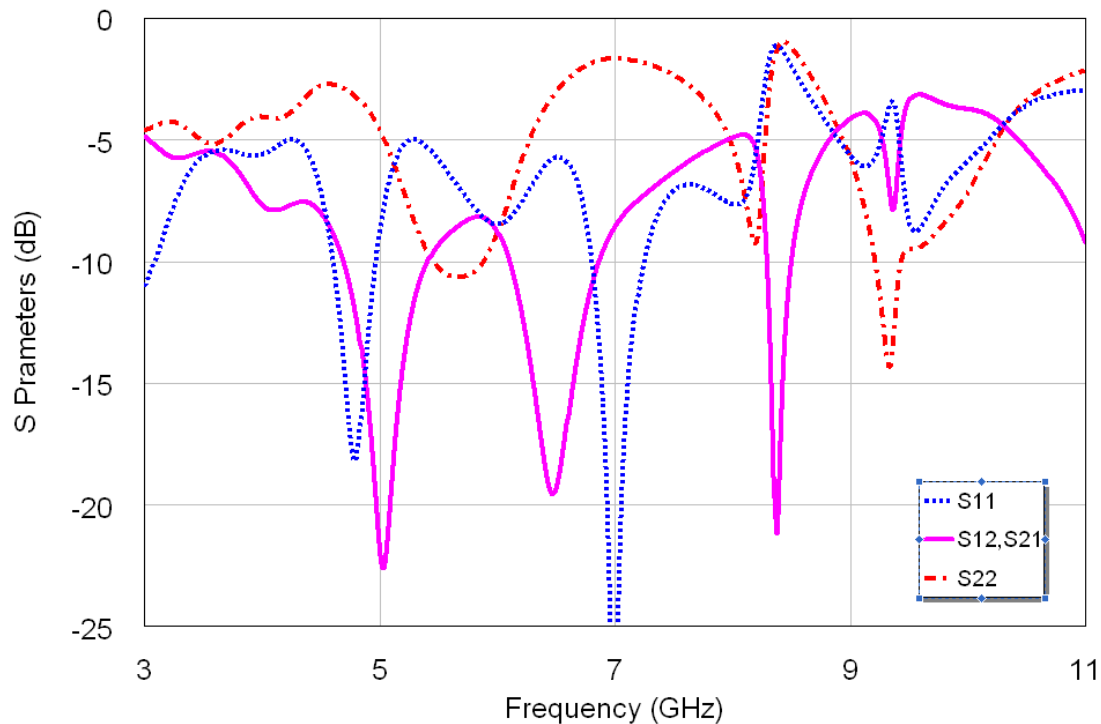


Figure 3.13: S-parameters of the antenna and feed network, phase shifter value is equal to 110° .

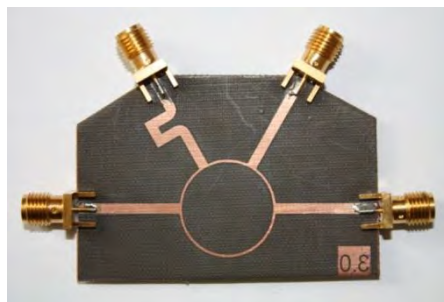


Figure 3.14: Prototype of the retraced coupler + phase shifter

The designed network, a 180° hybrid rat-race coupler and a phase shifter, are fed to the antenna ports; the antenna and feed network are implemented on the same substrate board. The structure is printed on a Taconic TLC laminate with a relative permittivity of $\epsilon_r=3\pm 0.05$, and a thickness of 0.79 mm (same as the antenna).

As can be seen in Fig. 3.15, the two ports of the coupler, which are connected to the antenna ports via microstrip lines, have a length difference of 8.7 mm. This length was chosen to produce the required phase shift between the antenna ports.

The feed network (coupler) which is a microstrip structure, is connected to the CPW-mictristrip antenna, so there is a microstrip structure of coupler and narrow band PIFA which is connected together via microstrip feed lines [see Fig 3.15(a)]. On the reverse side of the substrate, is the microstrip coupler's ground plane connected to the CPW antenna's ground plane [see Fig. 3.15(b)].

The UWB port of the antenna is connected to the coupler's port (on the reverse side of the substrate) via a shorting pin [see Fig. 3.15]. The shorting pin position through the CPW feedline and the gap dimensions are simulated by parametric studies to achieve a 50Ω matching between the microstrip line of the coupler and the CPW antenna's feed line.

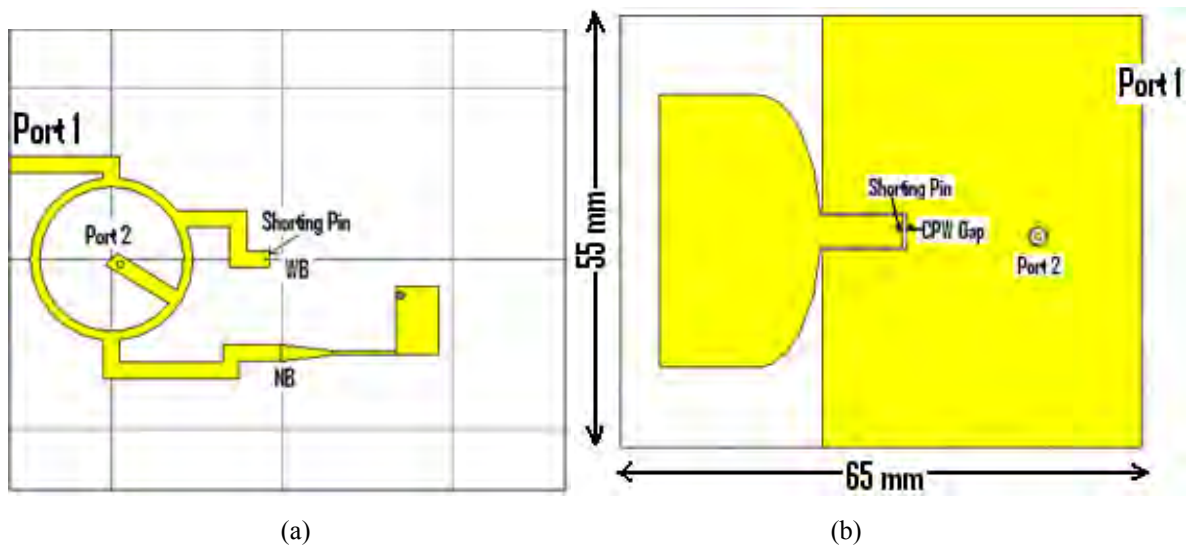


Figure 3.15: Geometry of the final structure in CST design environment. (a) microstrip (b) CPW and ground plane

The designed structure was simulated in *CST Microwave Studio* and it was fabricated on Taconic TLC laminate substrate board (Fig. 3.16).

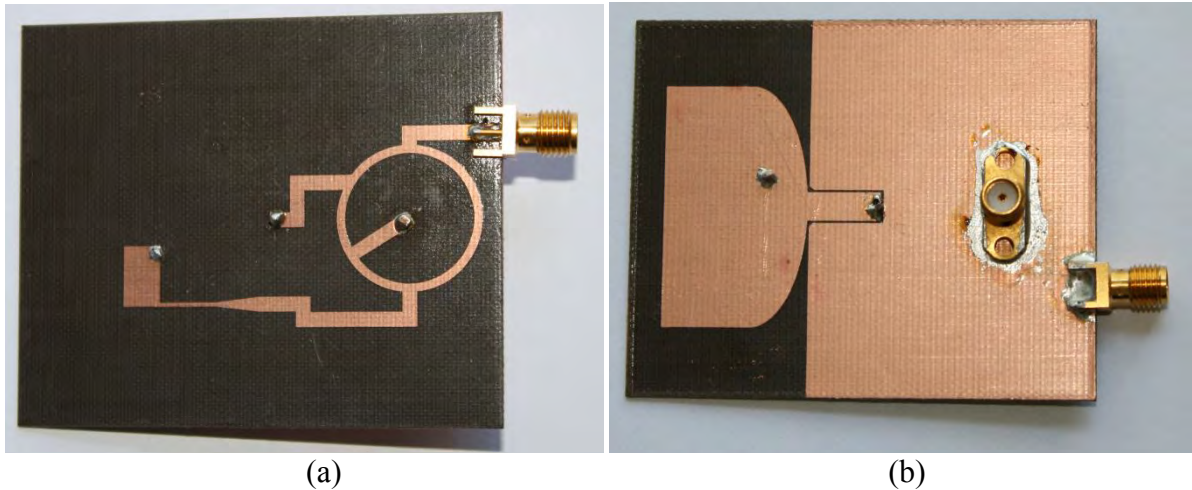


Figure 3.16: Prototype of the designed structure (a) Top view (b) Bottom view

3.3 Results

In this section all the simulated and measured S-parameters are considered for comparison. Fig 3.17 is a comparison between the isolation before and after adding the feed network to the antenna (See Fig 1.1). As can be seen, the value of coupling is reduced considerably at 5.2 GHz. The level of coupling (reflection coefficient) is below the commonly applied -10dB benchmark for the 4.8-6.3 GHz frequency range. This -10dB benchmark is an agreed standard as far as power loss and safety point are concerned.

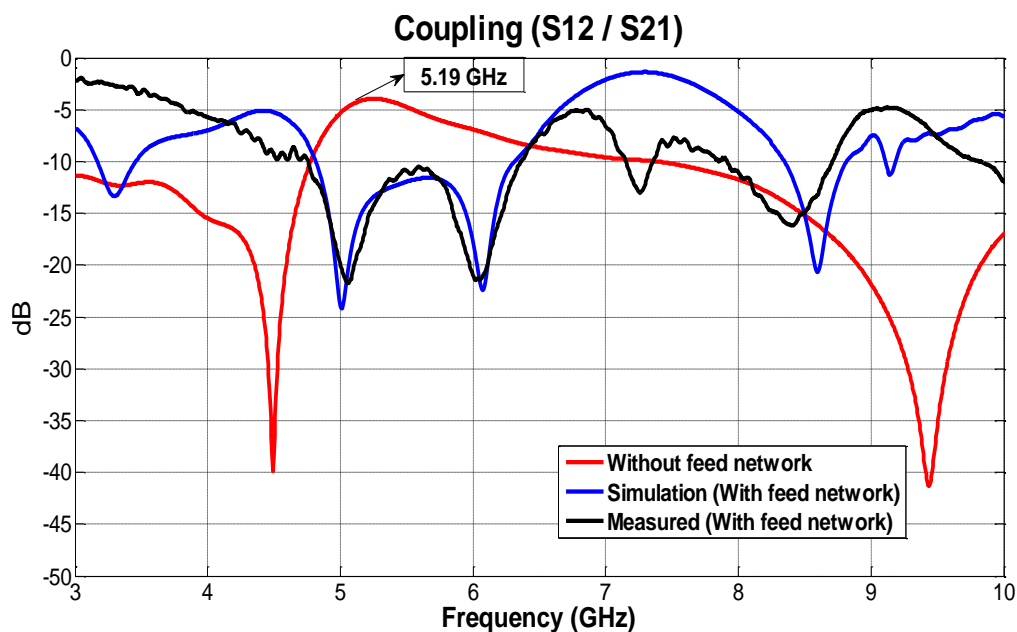


Figure 3.17: Coupling between the composite network ports (before and after adding the feed network).

Fig. 3.18 represents the measured reflection coefficient of the port 1 of the composite structure. It is compared to wideband antenna's reflection coefficient before and after adding the feed network. According to the commonly applied benchmark noted above the new simulation/measurement results indicates unsatisfactory wideband performance with $S_{11} > -10$ dB.

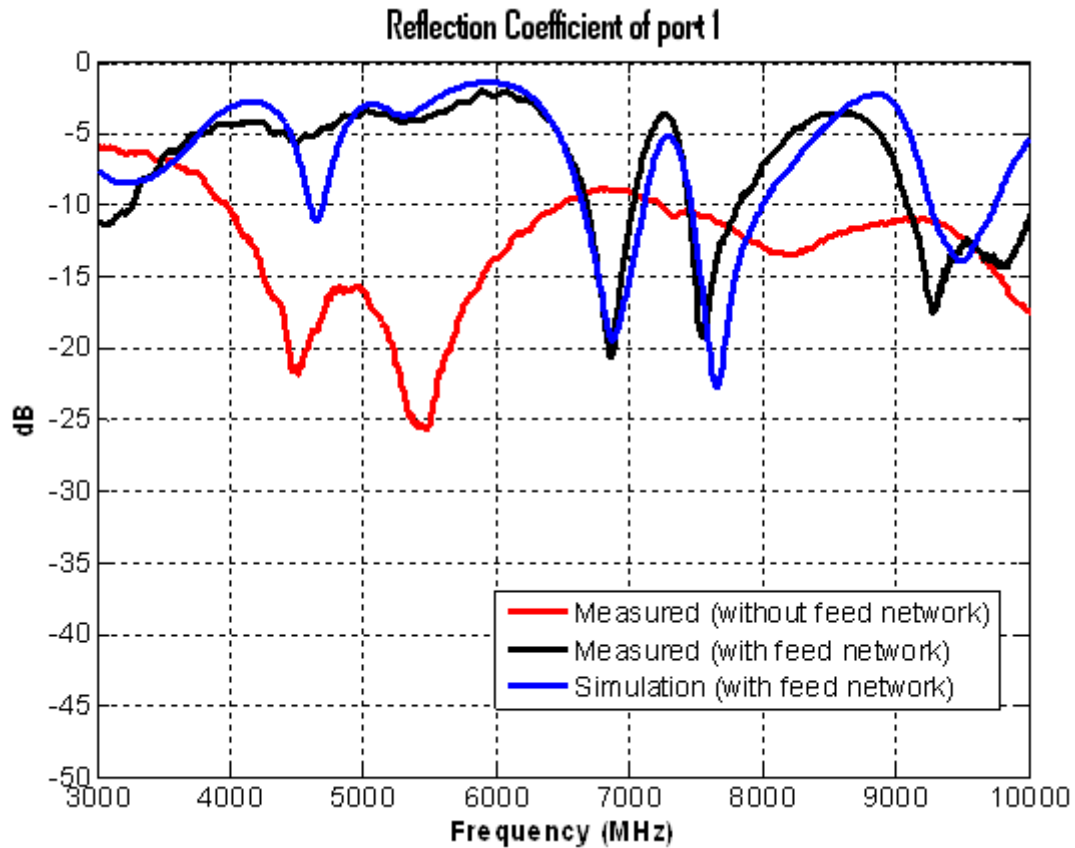


Figure 3.18: Measured and simulated return loss for port 1 (with and without feed network).

Fig. 3.19 represents port 2 of the composite structure. It is compared to the narrowband antenna reflection coefficient before and after adding the feed network. The resonating frequency of the narrowband antenna is changed by 0.8 GHz.

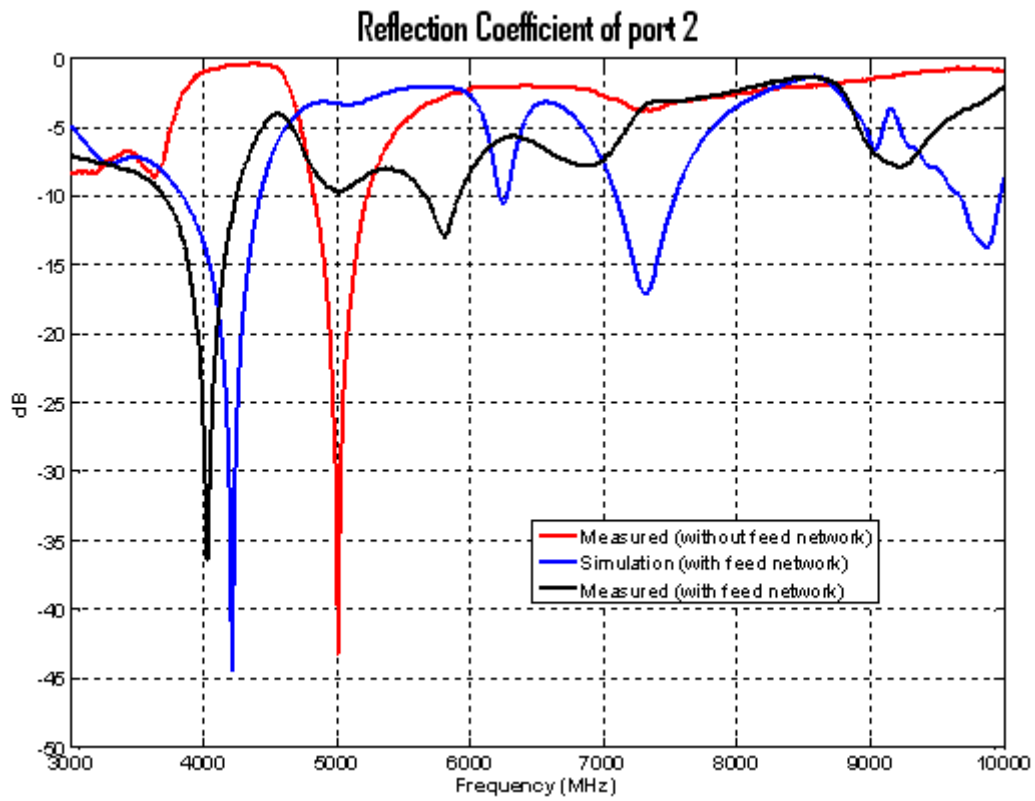


Figure 3.19: Measured and simulated return losses for port 2 (S22)

Fig. 3.20 shows the current distribution on both sides of the structure when port 1 is excited and port 2 is terminated to a 50Ω load. Port 1 and Port 2 of the rat-race coupler are isolated. Comparing Fig. 3.20 with Fig. 3.5, it could be concluded that after adding the feed network to the antenna, the UWB antenna is excited, but the coupled current to the narrowband antenna port is reduced.

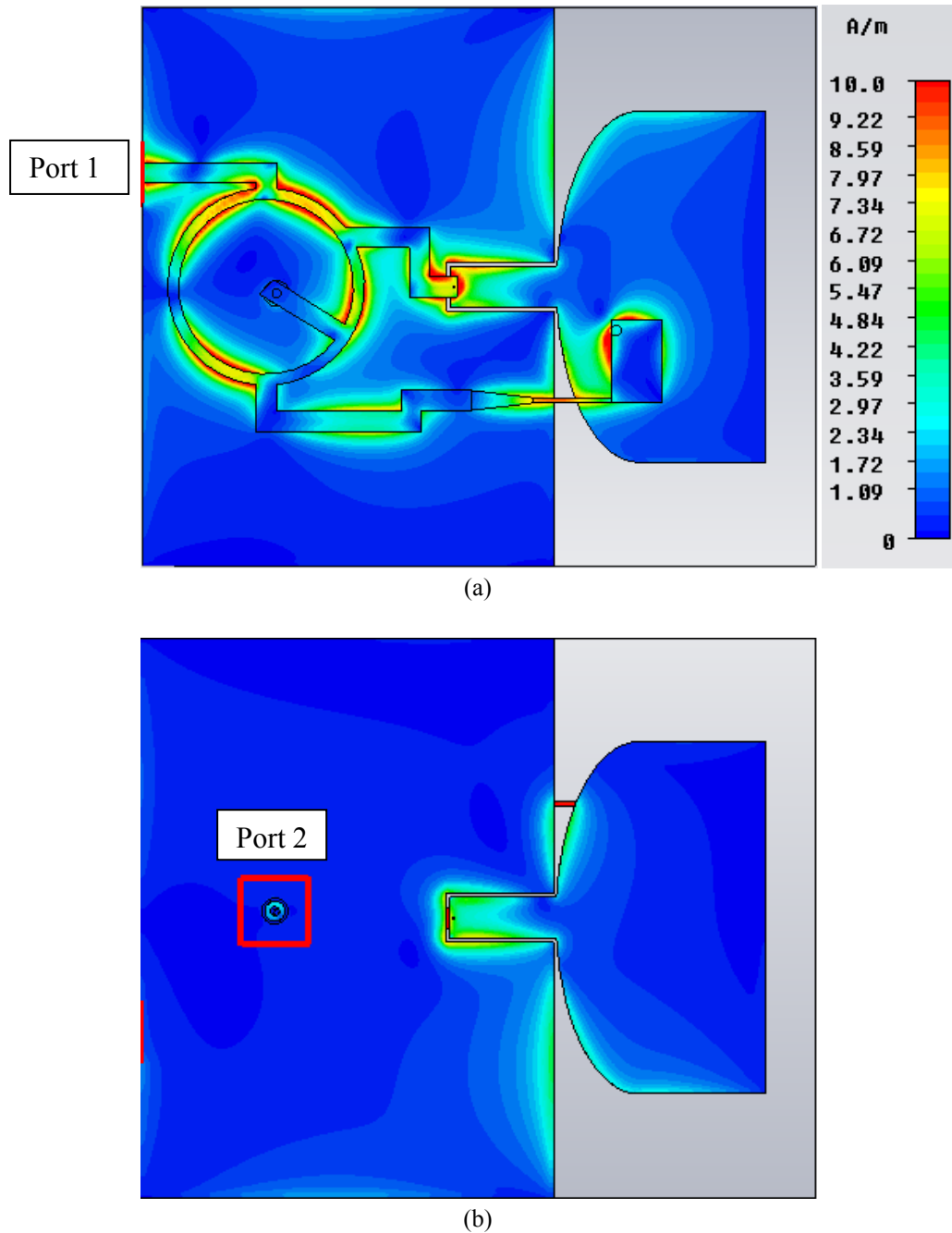
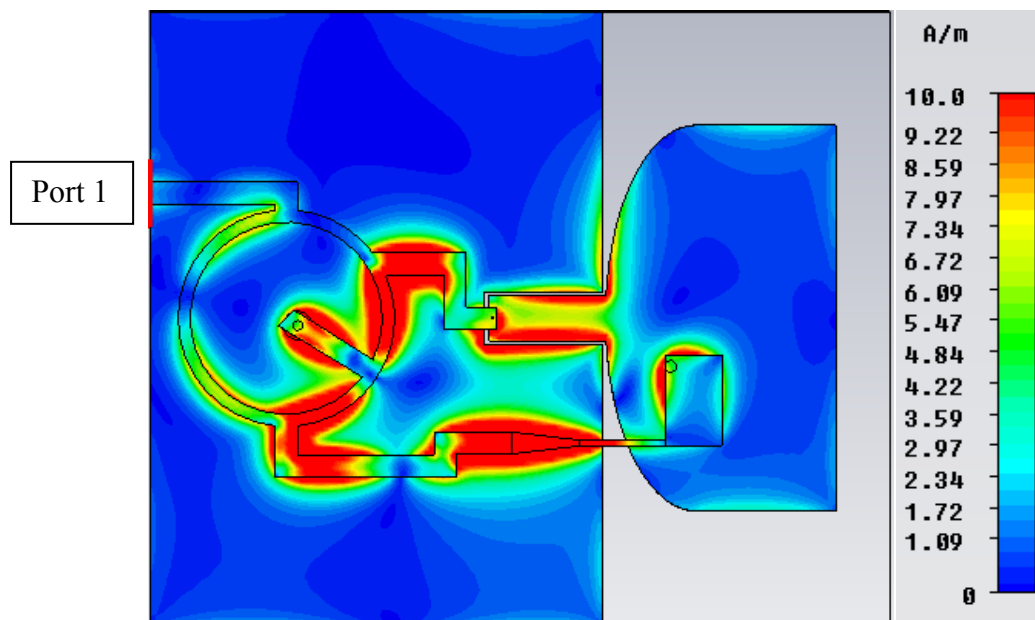
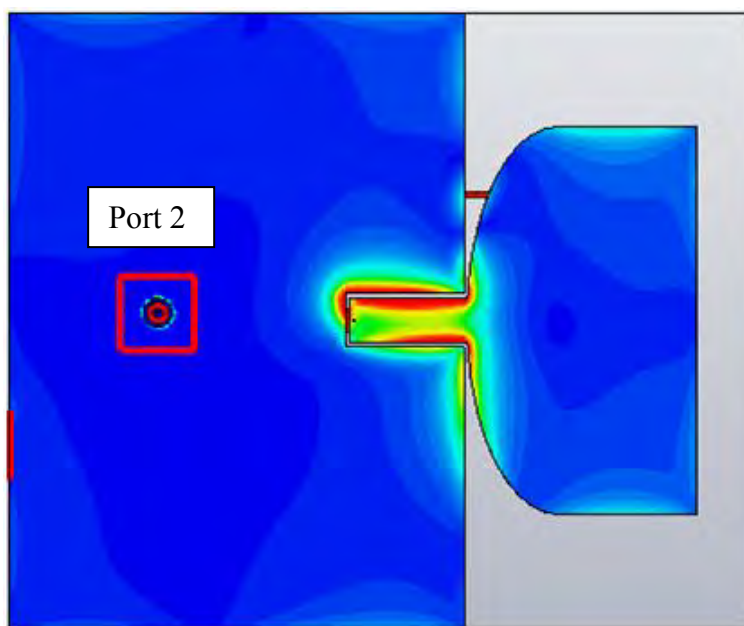


Figure 3.20: Current distributions when the port1 is excited and the port 2 is terminated to a 50Ω load at 5 GHz. (a) Top View (b) Bottom View.

Fig. 3.21 shows the current distribution on both sides of the structure when port 2 is excited and port 1 is terminated to a $50\ \Omega$ load. Port 1 and Port 2 of the rat-race coupler are isolated.



(a)



(b)

Figure 3.21: Current distributions when port 2 is excited and the port1 is terminated to a $50\ \Omega$ load at 5 GHz. (a) Top View (b) Bottom View.

The simulated 3D radiation patterns of wideband and narrowband antennas after adding the feed network are shown in Fig. 3.22 and Fig. 3.23, respectively.

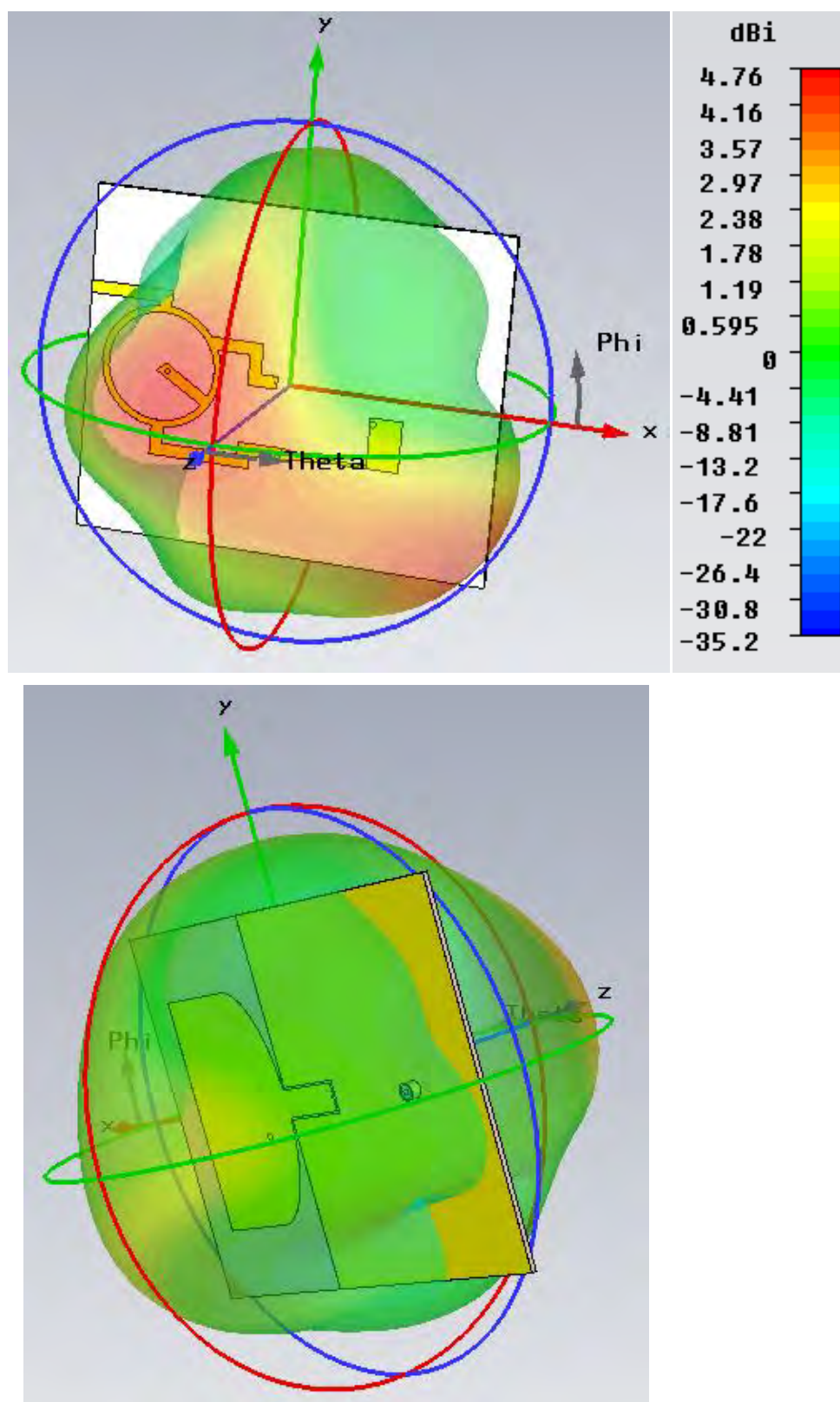


Figure 3.22 : Simulated 3D radiation pattern of the structure when port 1 is excited.

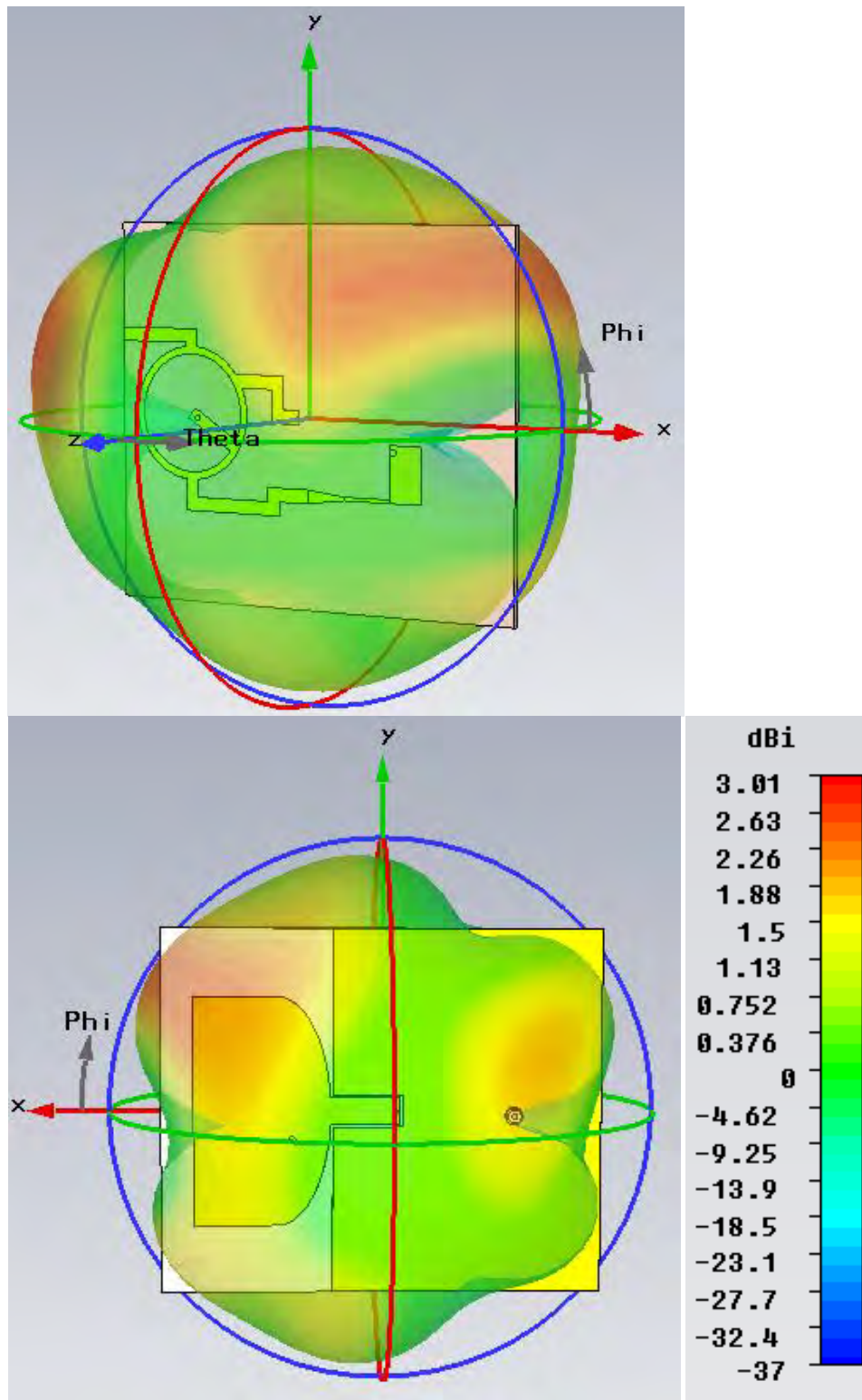


Figure 3.23: Simulated 3D radiation pattern of the structure when port 2 is excited.

3.4 Discussion

A 3dB rat-race coupler and a phase-shifter have been used to enhance the isolation between antenna ports. As is evident from the measured results, this approach improves the isolation of the antenna up to -25 dB at 5.2 GHz, which is the operating frequency of the narrowband antenna. This approach promises to achieve good isolation, but fails to maintain the antennas' wideband and narrowband characteristics.

In section 3.3, the reflection coefficient of port 1 of the composite structure (antenna and feed network) was called $\Gamma_{1'}$ and was compared to wideband antenna's reflection coefficient in isolation. In Fig. 3.24, 2 ports of the composite structure are called 1' and 2'. Equation (3.4b) approximates reflection coefficient of port 1'. As can be seen, the narrowband antenna contributes to $\Gamma_{1'}$ as well as the wideband antenna. Therefore $\Gamma_{1'}$ should not be approximated as wideband antenna's reflection coefficient. This can be described using Equation (3.4b). The same argument is true for ($\Gamma_{2'}$).

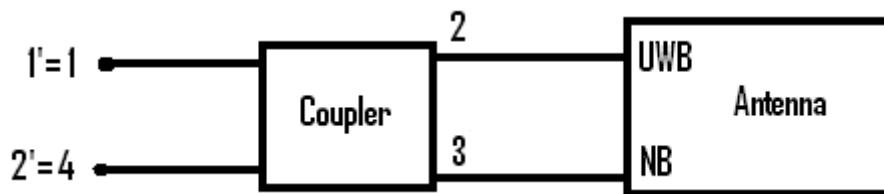


Figure 3.24: Composite Structure consists of coupler and antenna

$$(3.4a)$$

$$(3.4b)$$

In equation (3.4), $\Gamma_{1'}$ stands for the reflection coefficient of port 1 of the coupler. The same argument is true for port 2 and 3. According to matrix (3.1), for a rat-race coupler:

and $\Gamma_{2'}$. Therefore equation

(3.4b) could be simplified as:

$$(3.5)$$

The same equation could be written for the other port of the composite network (2'). It could be concluded that when a 3 dB coupler is being used, reflection coefficient of port 1 of the composite network () is not a good approximation for wideband antenna's reflection coefficient. The same argument is true for . Therefore, 3 dB coupling ratio is not a suitable value to achieve all the goals of this project.

The alternative solution proposed in the next chapter is a compromise between reducing the coupling (isolation) and not disturbing the antenna's return loss: to enable control of the coupling ratio. Thus the next chapter is about designing a coupler with a different coupling ratio.

Chapter 4

Isolation Using a Branch-line Coupler

The aim of this section is to design and build a branch-line coupler (as a feed-network) for enhancing port isolation in a dual port wideband-narrowband antenna. As shown in the previous chapter a conventional 3 dB (hybrid) branch-line coupler is not suitable. The challenge is to find the appropriate coupling value (C), in order to maintain wideband and narrowband antennas S-parameters, as well as improving the isolation between them. The approach is applied to the sample dual port antenna which has been introduced earlier.

4.1 Branch-line Coupler Design

Fig. 4.1 shows the geometry of the branch-line coupler, which is a type of directional coupler with 90° phase difference in the outputs of the through and coupled arms. A branch-line coupler is made by two main transmission lines shunt-connected by two secondary (branch lines). As it can be seen from the figure, it has a symmetrical four port. The First port is the Input port; second and third ports are output ports, and the fourth port is the isolated port. The second port is also named as the Direct or Through port and the third port is a coupled port. Evidently, owing to the symmetry of the coupler, any of these ports can be used as the Input port; but should this be the case, the Output and isolated ports change accordingly. The result of this symmetry is also evident in the scattering matrix of the coupler. Branch-line couplers are often made in microstrip or stripline. (Pozar, 1998)

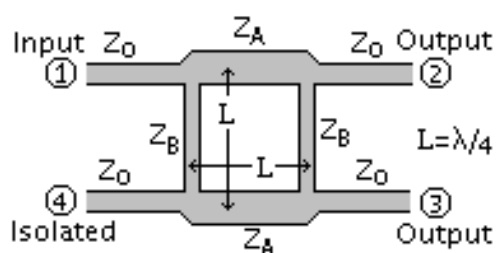


Figure 4.1: Geometry of a branch-line Coupler. (Pozar, 1998)

The aim is to design a branch-line coupler with unequal power division. For this reason the coupling value (C) should be found. In view of the dimensions of the coupler, the length of the branch line and series line is generally chosen as the fourth of the design wavelength. According to Fig. 4.1, if the length of series and stub-transmission lines are named as L, then L can be find as follows:

$$(4.1)$$

By using equation (3.2), the effective guided wavelength is given by: (Poazar, 1998)

$$\lambda_{eff} = \frac{c}{f \sqrt{\epsilon_{eff}}}$$

Where, to a first approximation (ignoring the metal thickness and losses); using equation (3.3)

$$\epsilon_{eff} = \epsilon_r \left(\frac{W}{W + H} \right) + \epsilon_r \left(\frac{H}{W + H} \right)$$

λ_{eff} is calculated for the high performance RF Laminate (TLC-30) substrate with a relative permittivity of $\epsilon_r=3\pm 0.05$ and a thickness of $h=0.79$ mm. By substituting, $\epsilon_r=3$ (relative permittivity), $H=0.79$ mm and $W=1.96$ mm in equation (3.3)

$$\epsilon_{eff} = 2.4$$

Then by substituting $\epsilon_{eff} = 2.4$ into equation (3.2) at $f=5.2$ GHz, where

$$\lambda_{eff} = 37.713 \text{ mm}$$

—

The next step is to find the impedance of the series lines and branch lines, and . As branch-line couplers are a type of directional couplers, therefore:

$$S = \begin{pmatrix} 0 & S_{12} & S_{13} & 0 \\ S_{12} & 0 & 0 & S_{24} \\ S_{13} & 0 & 0 & S_{34} \\ 0 & S_{24} & S_{34} & 0 \end{pmatrix} \quad (4.2)$$

For any branch-line coupler: (Gardner, 2010)

$$\text{---} \quad \text{and} \quad (4.3)$$

$$\begin{array}{c} \text{-----} \\ \text{---} \end{array} \quad (4.4)$$

;

$$\text{=====} \quad (4.5)$$

Therefore, for calculating S_{11} and S_{22} , and S_{12} (S-parameters matrix) of the coupler is required. The network is considered to be lossless; thus (By using equation 2.3 from chapter 2):

Which imply that $S_{11} = -S_{22}$ (using equation 4.8a and 4.8b), and $S_{12} = S_{21}$ (using equation 4.8b and 4.8d).

If $S_{11} = 0$, then $S_{22} = 0$ and $S_{12} = S_{21}$.

Branch-line coupler's matrix could be written as:

$$\begin{pmatrix} 0 & 0 & A & -90 & \sqrt{1-A^2} & -180 & 0 & 0 \\ A & -90 & 0 & 0 & 0 & 0 & \sqrt{1-A^2} & -180 \\ \sqrt{1-A^2} & -180 & 0 & 0 & 0 & 0 & A & -90 \\ 0 & 0 & \sqrt{1-A^2} & -180 & A & -90 & 0 & 0 \end{pmatrix} \quad (4.6)$$

The even columns represent the phase of the S-parameters. In order to find the value of A, the branch-line couplers matrix was imported to the *Microwave Office* (AWR) as a Touchstone file. The antenna's already measured S-parameters were also imported. The Antenna's S-parameters matrix is represented by a 2-port element called Sub-circuit. The coupler's S-parameters appeared as a 4-port sub-circuit. The two sub-circuits were connected together in

the simulator (*Microwave Office*). The composite structure is a 2 port network. Γ_{1c} and Γ_{2c} are the reflection coefficient of port 1 and port 2 of the composite structure respectively. They are approximated as the reflection coefficient of the wideband and narrowband antennas respectively.

It should be mentioned that a phase-shifter is also required because the coupler itself will not necessarily create the right phase shift to cancel the mutual coupling between the antennas. This is achieved by optimizing an arbitrary phase shift between the coupler and antenna ports. The phase shift is created with a piece of microstrip line.

The value of A should be optimized to enhance the isolation between the new composite structure ports. The narrowband antenna's resonating frequency should be maintained as well as wideband antenna's reflection coefficient agreement to the wideband antennas benchmark. An arbitrary value of A = 0.1 is chosen to start with. Different values of A such as: 0.1, 0.2, 0.25, 0.3, 0.4, 0.6, 0.707, 0.8, 0.9 were tried in the simulator. An acceptable value for A is one which produces the optimum results considering, isolation and UWB and narrowband antenna performances. Finally the optimum value for A was found to be 0.3.

As it was mentioned earlier Γ_{1c} and Γ_{2c} are calculated using equations (4.3) and (4.4). Thus Γ_{1c} and Γ_{2c} are calculated. By using equation (4.5):

$$\underline{\underline{\Gamma_{1c} = 0.3 \angle -90^\circ}}$$

..

, therefore the coupler's matrix is as follows:

$$\begin{pmatrix} 0 & 0 & 0.3 & -90 & 0.95 & -180 & 0 & 0 \\ 0.3 & -90 & 0 & 0 & 0 & 0 & 0.95 & -180 \\ 0.95 & -180 & 0 & 0 & 0 & 0 & 0.3 & -90 \\ 0 & 0 & 0.95 & -180 & 0.3 & -90 & 0 & 0 \end{pmatrix} \quad (4.7)$$

Even columns represent the phase.

According to equation (2.4) (Pozar, 1998):

$$- \quad \text{dB}$$

dB

dB= 12 dB

By having the values and , the next step is to simulate the branch-line coupler with the Coupling value of 12 dB:

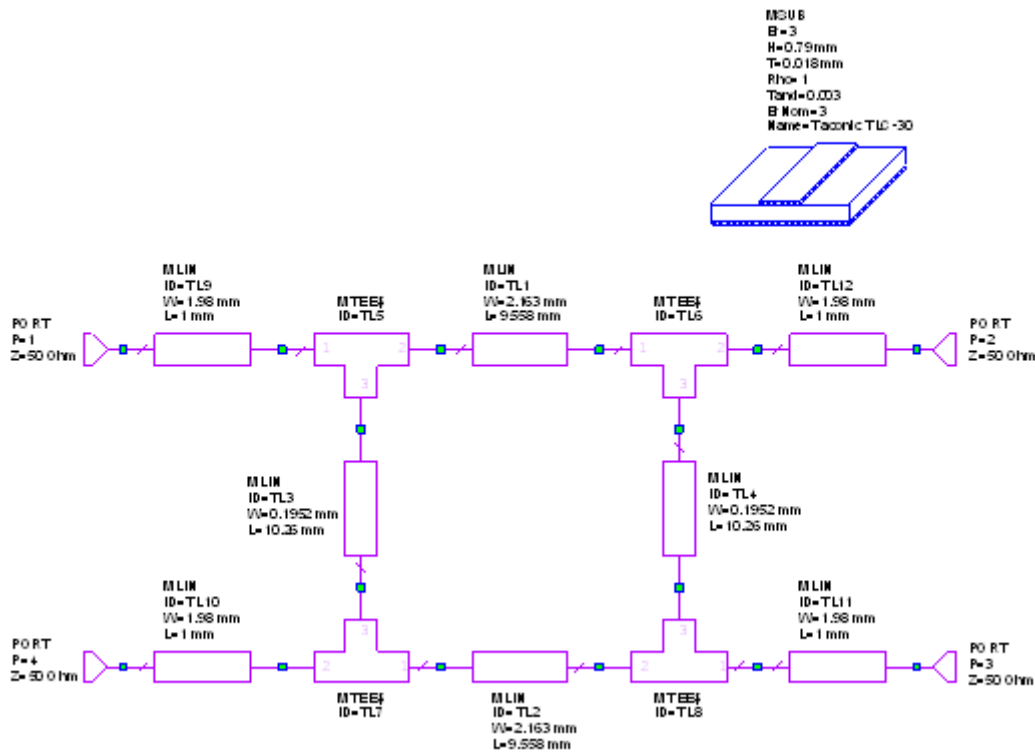


Figure 4.2: Schematic of a 12 dB Branch-line coupler Schematic in Microwave Office.

Fig. 4.3 is the branch-line coupler S-parameters, which is evidently operating at the desired frequency of 5.2 GHz. is the coupling value of the coupler, expected to be -12 dB at 5.2 GHz. However, it is shown in Fig. 4.3 to be -9.5 dB at 5.2 GHz. This could be due to the discontinuities in the design.

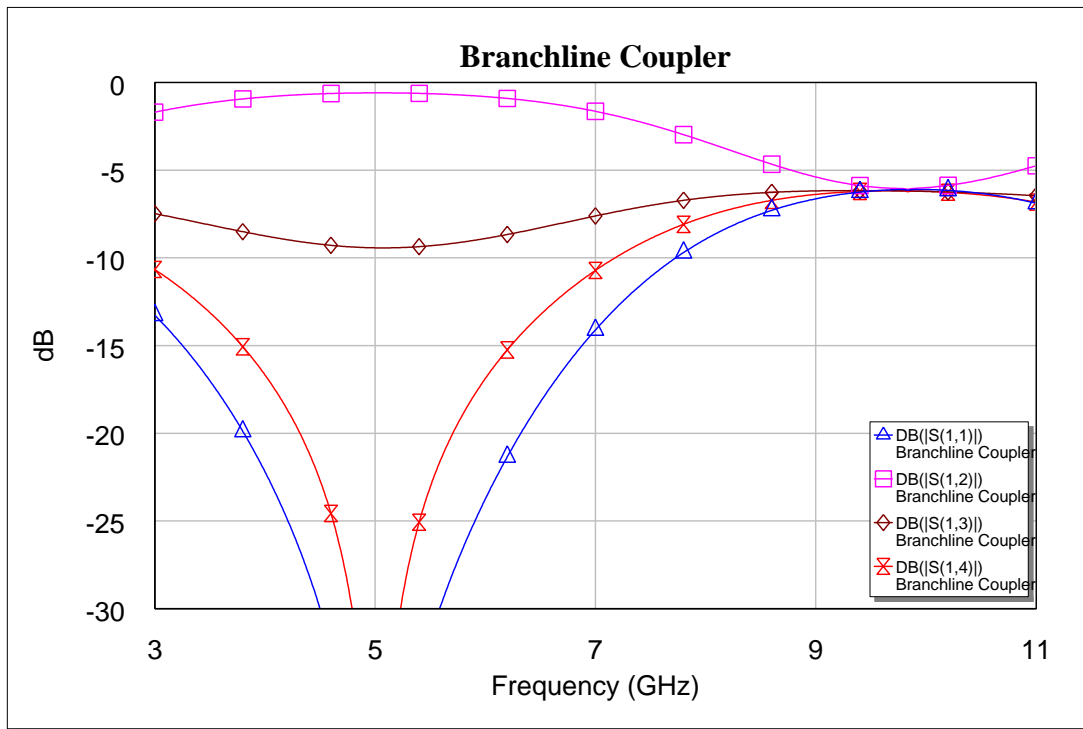


Figure 4.3: S-parameters of the 12 dB Branch-cline coupler designed at 5.2 GHz.

As can be seen in Fig 4.4, the coupler and the antenna are simulated together. The sub-circuit, called Antenna, is the Antenna's simulated results, which are imported into the simulator so as to be combined by the branch-line coupler for isolation enhancement between the ports. Some degree of phase-shift was also required between antenna and coupler ports. The optimized value for the phase-shifter was determined by tuning the value to 89°.

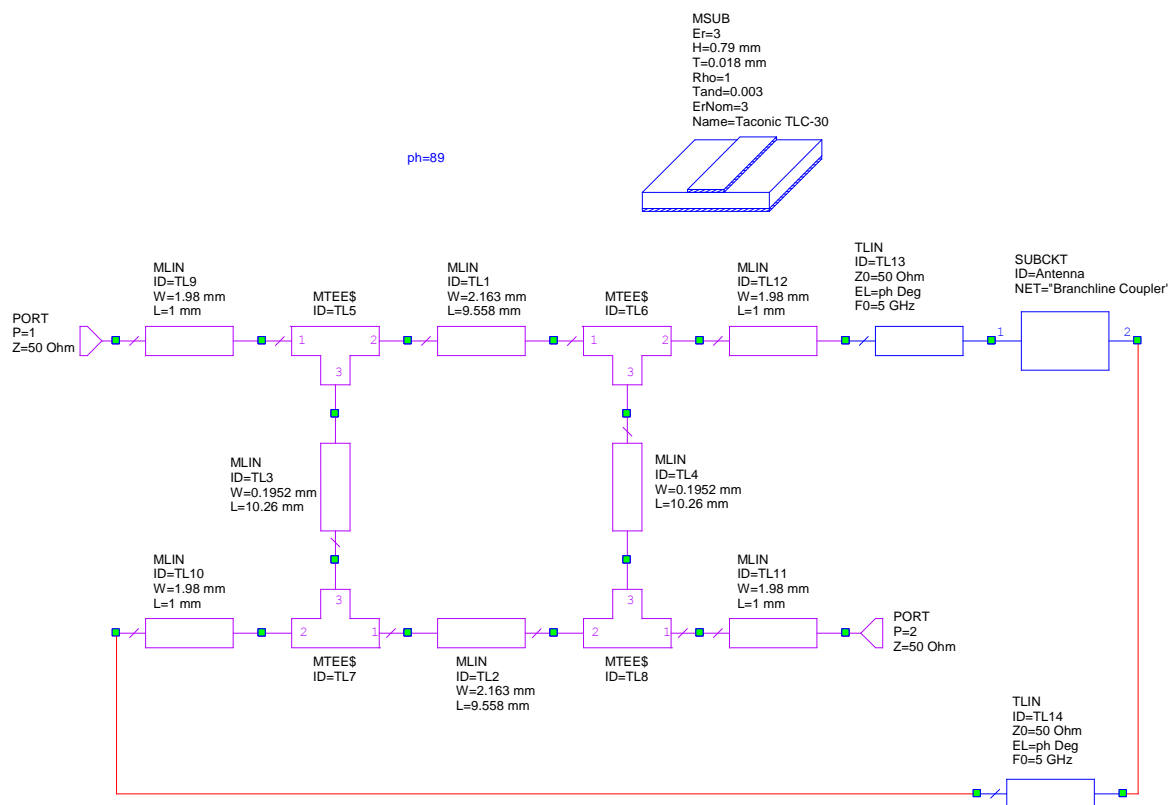


Figure 4.4: Schematic of the branch-line coupler + phase shifter + antenna in Microwave Office

Fig 4.5, represents the S-parameters of the composite network (antenna+ coupler+ phase-shifter), with the optimized coupling value ($C=12$ dB). As can be seen, is the transmission coefficient between antenna ports and shows that it's about -14 dB at 5.2 GHz, which is a reasonable isolation. The narrowband antenna reflection coefficient (resonating frequency is maintained at 5.2 GHz. The wideband antenna's reflection coefficient is acceptable (less than -10 dB) from 3-8 GHz. It then peaks at approximately 8.5 GHz, which is not very good for an UWB performance.

Figs. 4.6 and 4.7 show simulated S-parameters of the composite network after adding the feed network consisting of 5 dB and 16 dB coupler to the antenna, respectively. Comparing Fig. 4.6 and 4.7 to Fig. 4.5 leads to a better understanding of how important it is to find the optimum value of the coupling.

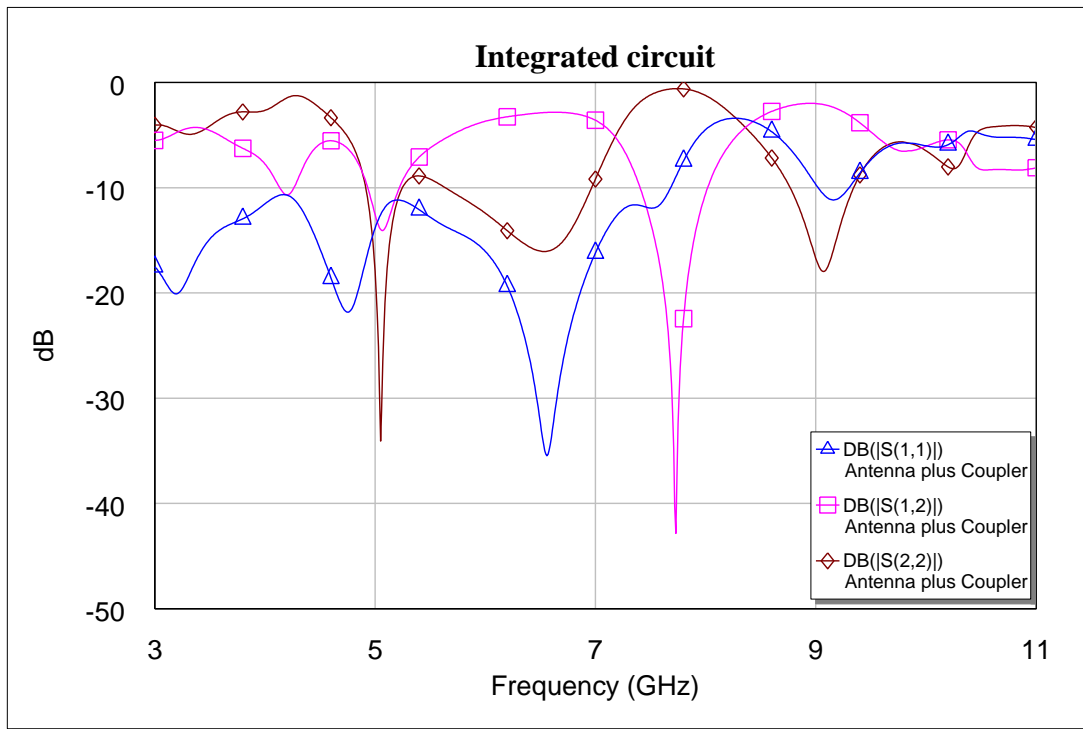


Figure 4.5: Simulated S-parameters of the composite network after adding the feed network to the antenna (Feed network consists of a 12 dB coupler).

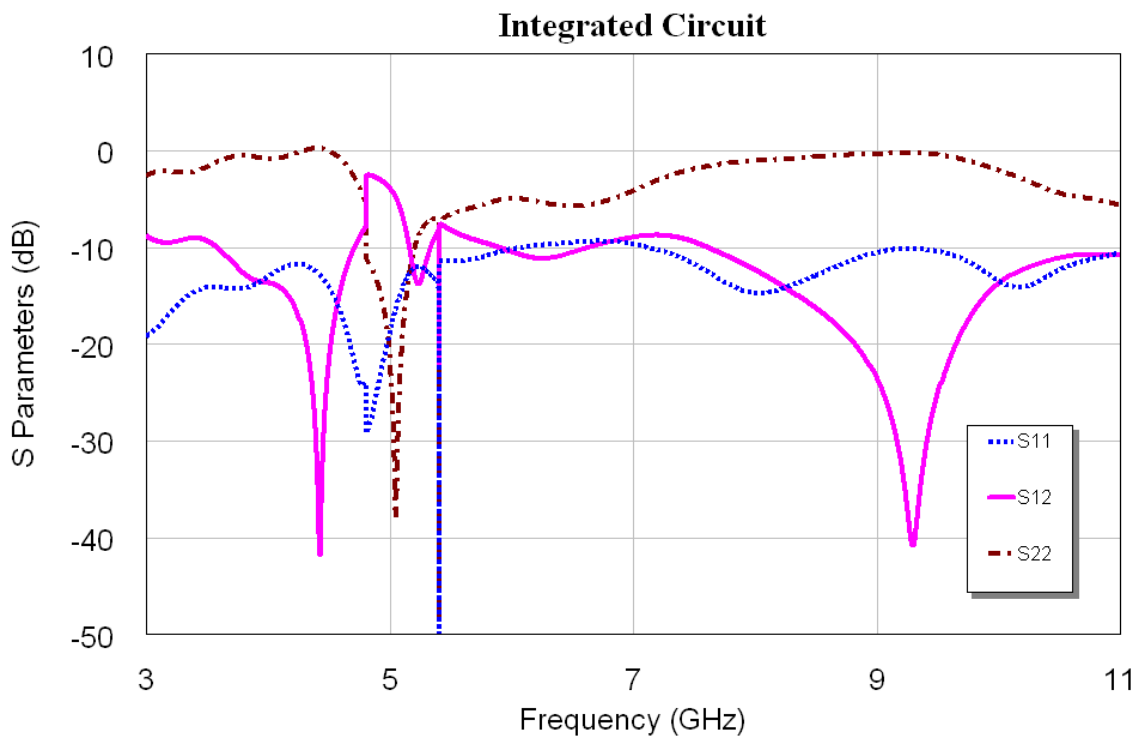


Figure 4.6 : Simulated S-parameters of the composite network after adding the feed network to the antenna (Feed network consists of a 5 dB coupler).

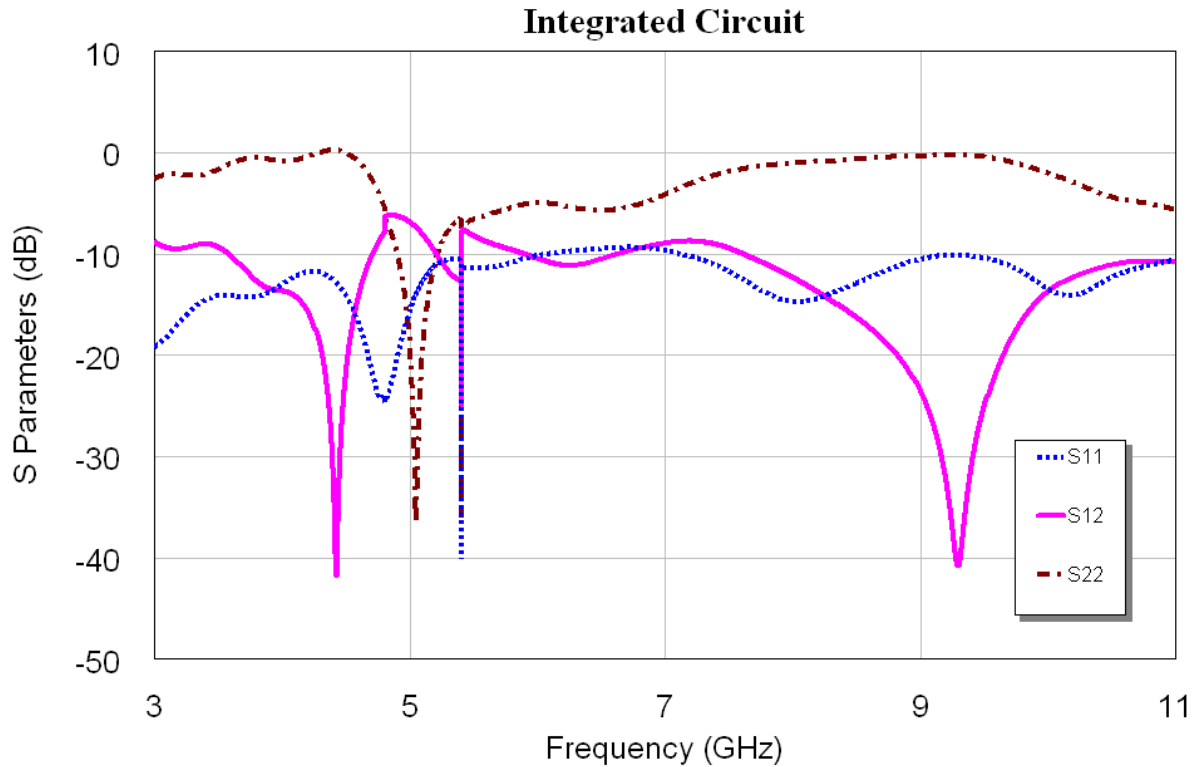


Figure 4.7 : Simulated S-parameters of the composite network after adding the feed network to the antenna (Feed network consists of a 16 dB coupler).

The next step, having received the simulation results, is fabrication of an actual PCB. According to the Fig. 4.8, the two ports of the coupler connected to the antenna ports via microstrip lines are different in length by 9.1 mm. This length produces the required phase shift (89°) between the antenna ports. The length of the transmission lines between the antenna and the coupler is very critical because they cause a phase shift which consistently affects the results.

The feed network (coupler) which is a microstrip structure, is getting connected to the CPW-microstrip antenna. Thus, there is a microstrip structure of coupler and narrow band PIFA ; it is connected via microstrip feed lines [See Fig. 4.8(a)]. On the reverse side of the substrate, there is the ground plane of the microstrip coupler connected to the CPW antenna's ground plane [See Fig. 4.8 (b)].

The UWB antenna port is connected to the coupler's port (on the reverse side of the substrate) via a shorting pin [see Fig. 4.8]. The shorting pin position through the CPW feedline and the gap dimensions are simulated by parametric studies to achieve a 50Ω matching between the microstrip line of the coupler and the CPW antenna's feed line.

As the design was based on a pre-designed dual port antenna with a small separation between the two ports, all the dimensions were limited, due to the antenna's two sided structure. The branch-line coupler is rotated by 90° so as to fit into the antenna's geometry.

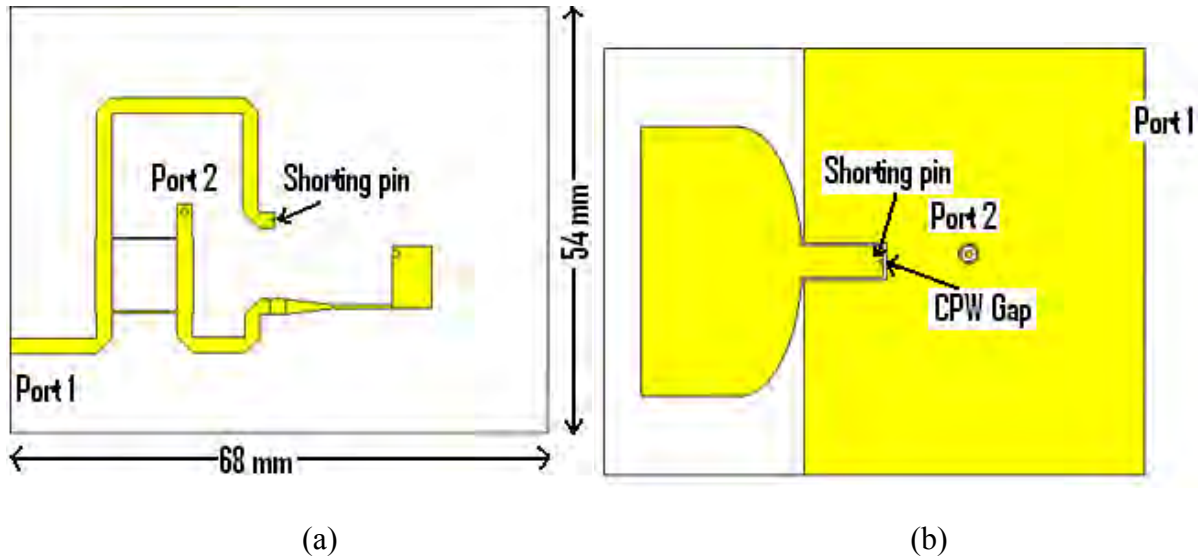


Figure 4.8: Geometry of the final structure in CST Microwave Studio. (a) microstrip (b) CPW and ground plane

Fig. 4.9 represents the simulated results in CST *Microwave Studio*. S_{11} , the transmission coefficient of the composite network, decreased to -14 dB at the desired frequency of 5.2 GHz. If Fig 4.9 compared to Fig 1.1, the isolation between two ports can be seen to have been enhanced by approximately 11 dB. It is also clear that the narrowband antenna resonating frequency is maintained at 5.2 GHz. The wideband antenna's reflection coefficient S_{11} , is almost less than -10 dB in most of the frequency range except at frequencies from 6.3 to 7.1 GHz and at the high end of the band about 11 GHz. These results are the optimized value of the coupling in order to maintain the narrowband-wideband characteristics of the antenna. More solutions for further improving the results will be examined in the Discussion section at the end of this chapter, and in the next chapter.

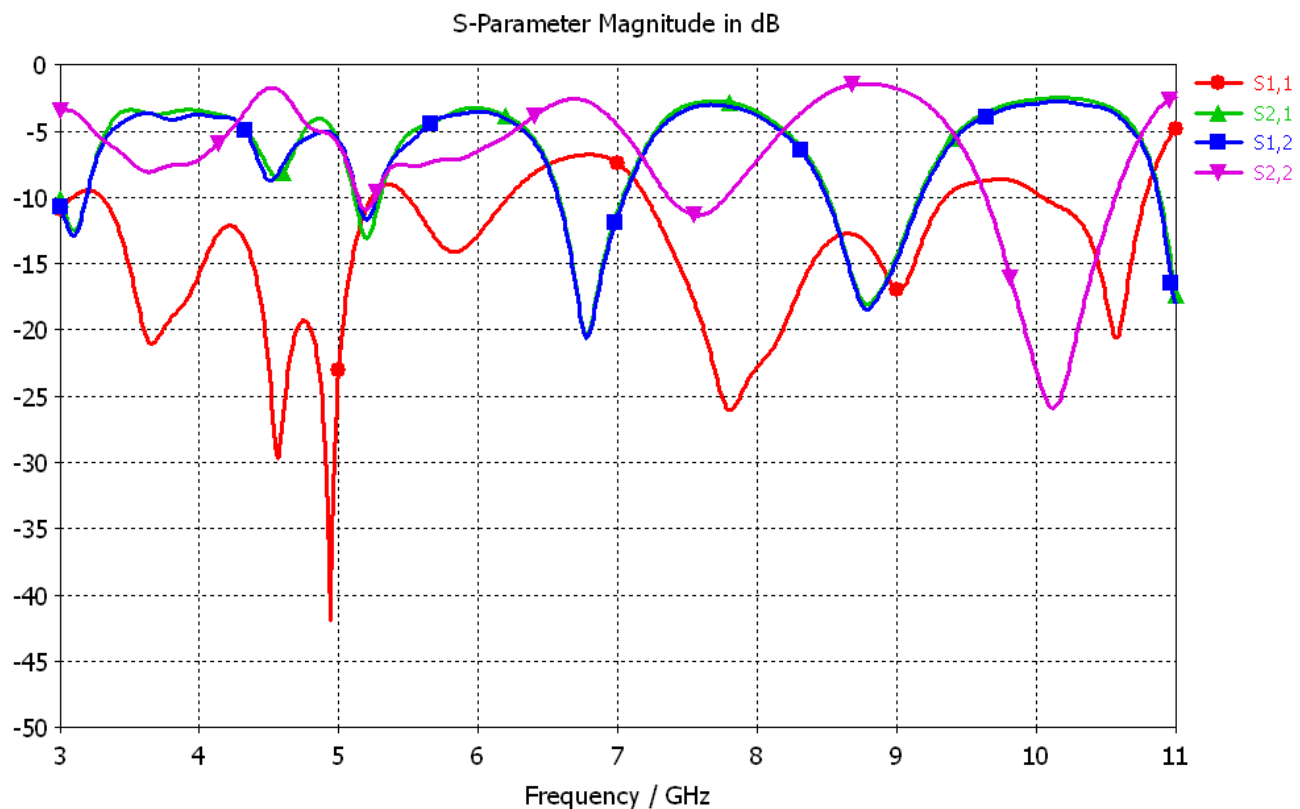


Figure 4.9: Simulation S-parameters results of the composite structure by CST

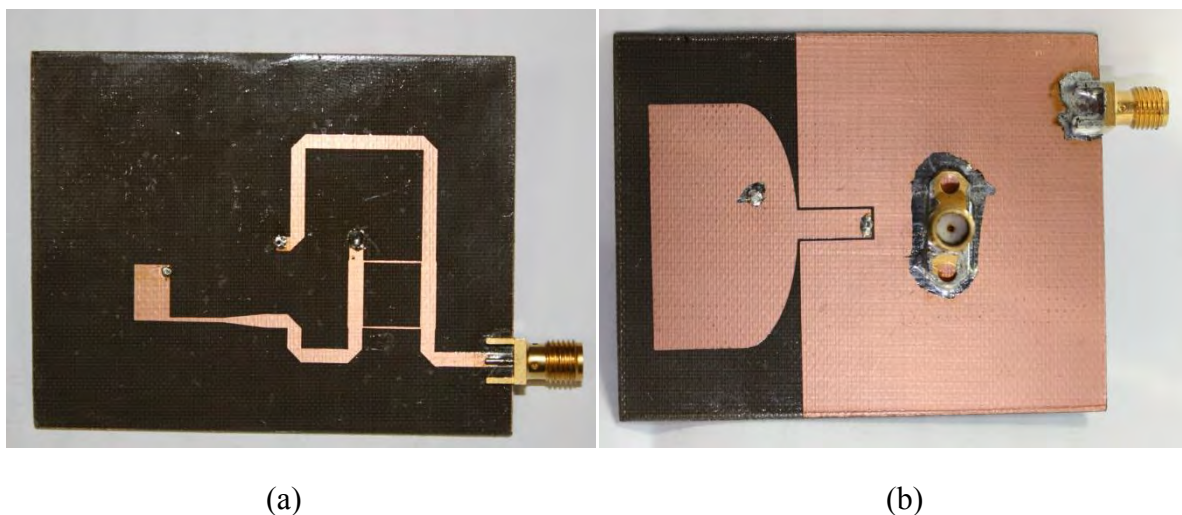


Figure 4.10: PCB of the designed structure (a) Microstrip (NB Antenna+ phase-shifter + branch-line coupler) (b) CPW + ground plane (UWB antenna+ ground)

4.2 Results

Fig. 4.11 shows the measured S_{12} of the composite structure and should be compared with Fig. 1.1, where the coupling value is about -3 dB. The coupling at 5.2 GHz is reduced to approximately -14 dB. The solid line represents the measured result which agrees quite well with the simulated result.

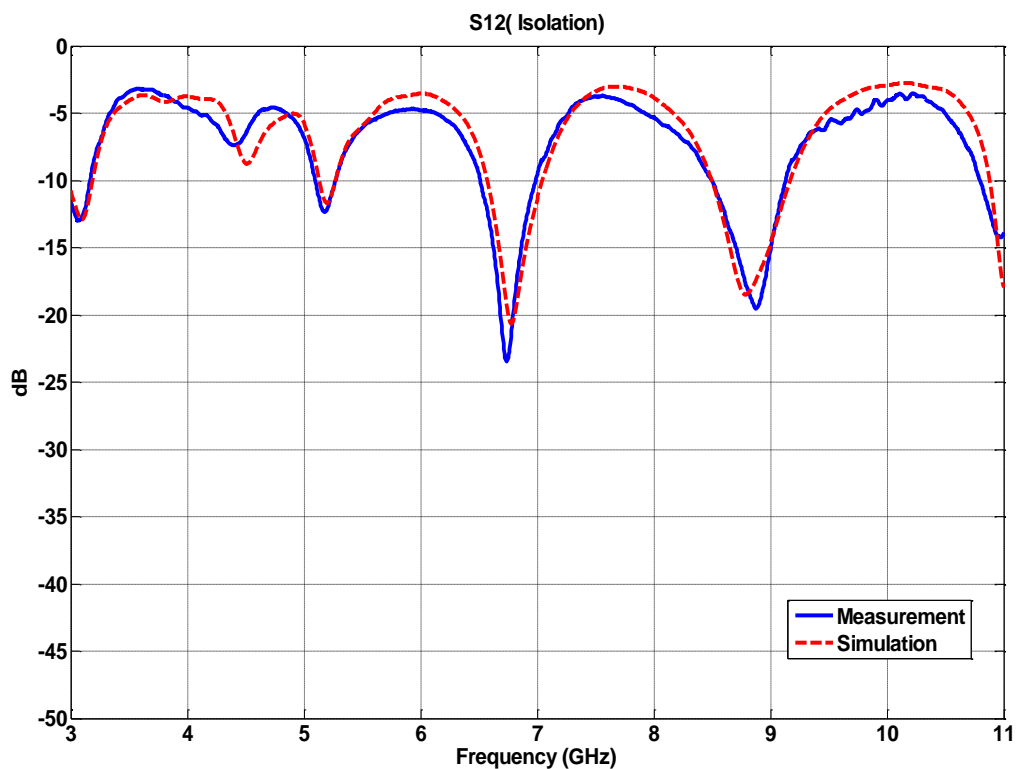


Figure 4.11: Measured transmission coefficient of the composite structure

Fig. 4.12 shows the S_{11} , the reflection coefficient of port one, which is connected to the UWB antenna via the through port of the branch-line coupler. It could be considered as the UWB antenna's reflection coefficient (minus the Return loss). S_{11} is less than -10 dB in most of the UWB antenna's operating frequency range. The value of S_{11} peaks at frequencies of about 6.58 GHz and 9.5 GHz. This happens because the whole structure of the antenna is changed as a result of adding a narrowband feed network to it.

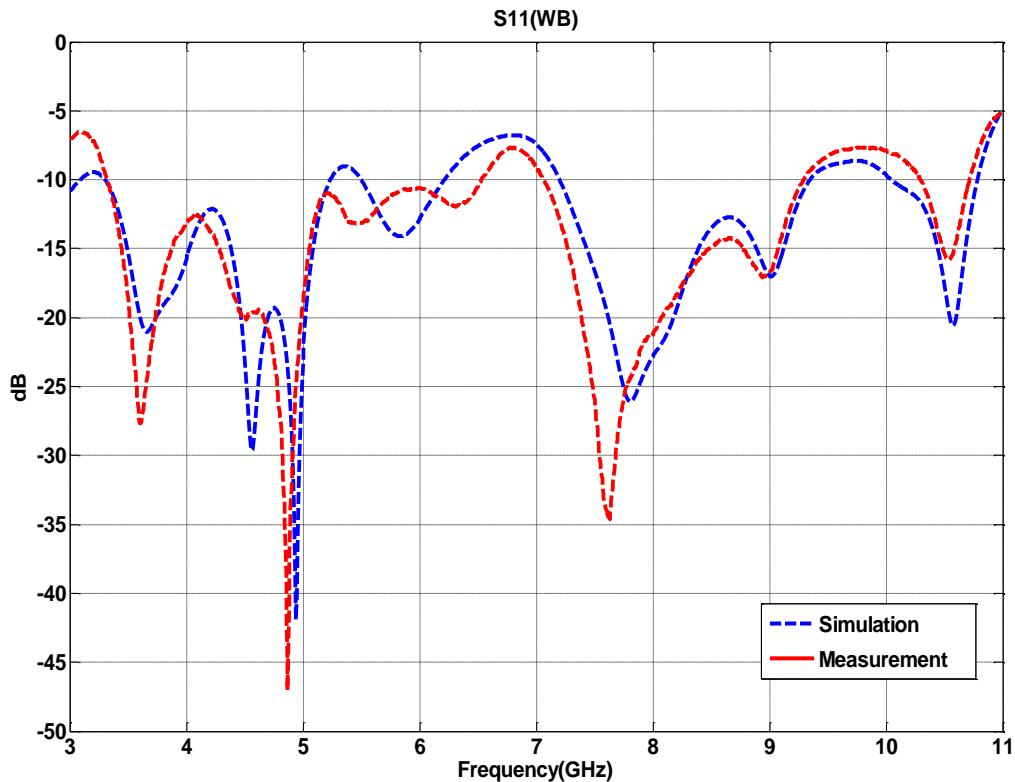


Figure 4.12: Reflection Coefficient of port 1 of the composite structure: represents UWB antenna

Fig. 4.13 represents the S_{22} , the reflection coefficient of port two, which is connected to the narrowband antenna via the through port of the branch-line coupler. It could be considered as the narrowband antenna's reflection coefficient (minus Return loss). As can be seen, the measured and simulated results have a good agreement. The value of S_{22} is about -14 dB at 5.2 GHz. Thus the narrowband antenna's resonating frequency is unchanged and the narrowband antenna resonates at the original value of 5.2 GHz.

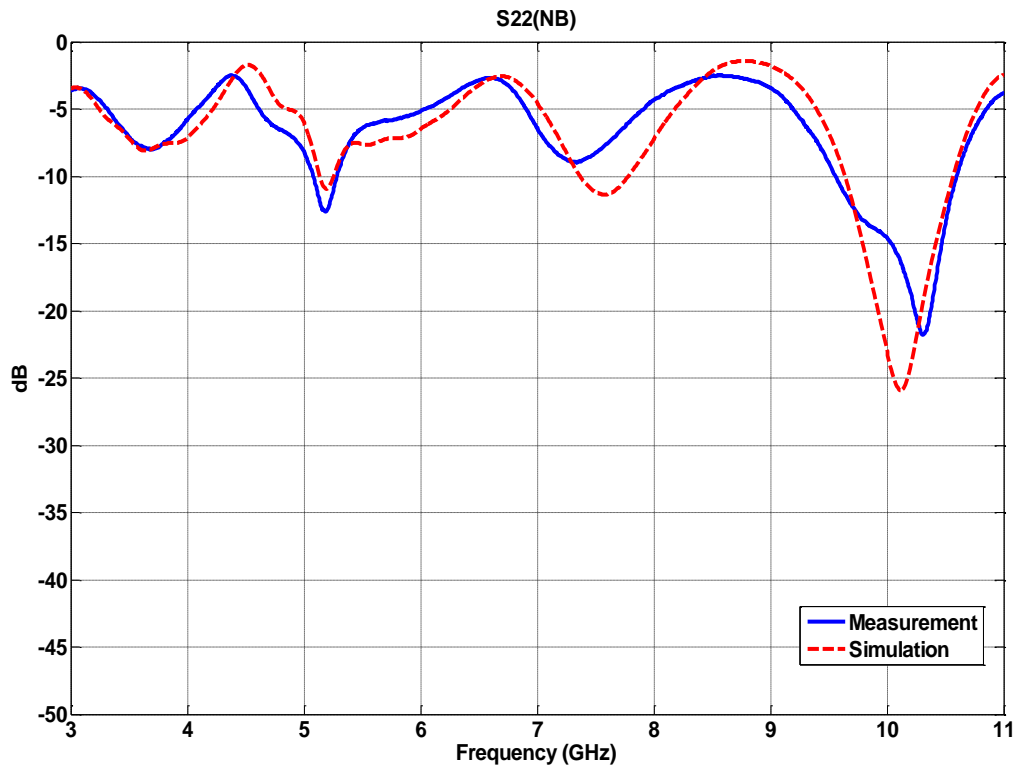
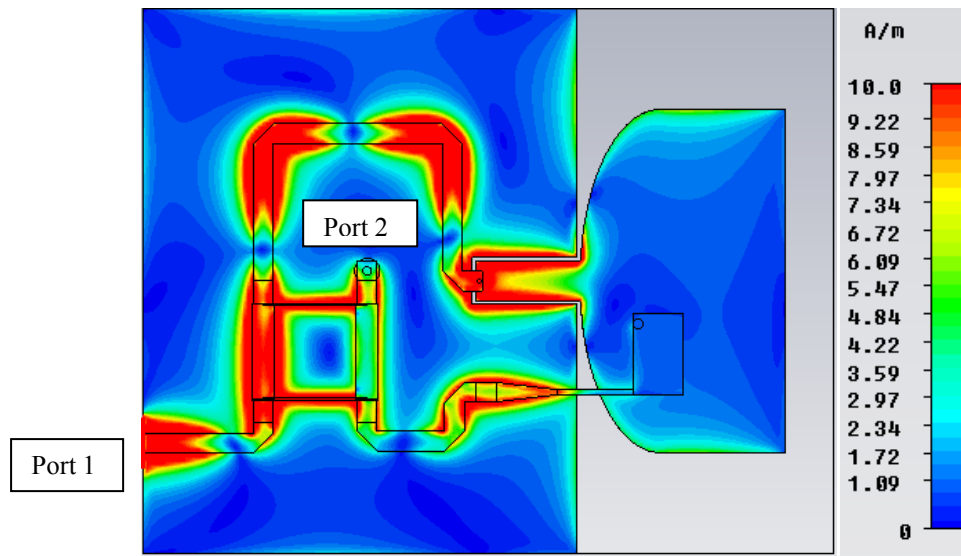
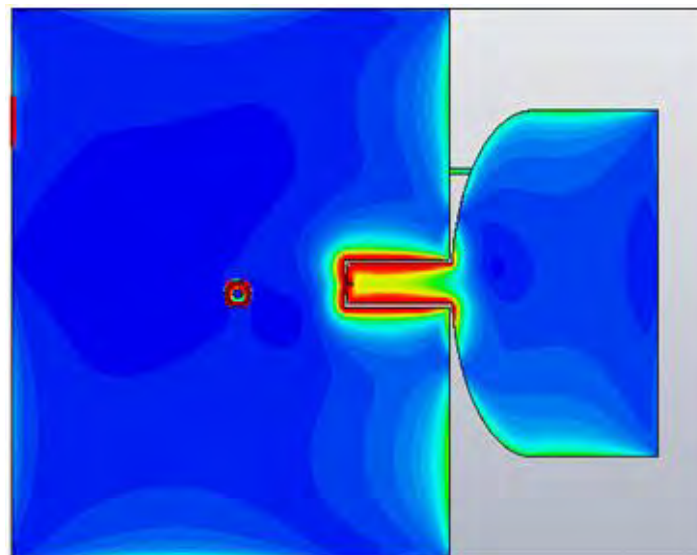


Figure 4.13: Reflection coefficient of port 2 of the composite structure: represents narrowband antenna

Fig. 4.14 shows the current distribution on both sides of the structure when port 1 is excited and port 2 is terminated to a 50Ω load. Port 1 is the ‘Input’ port of the coupler. Wideband antenna is connected to the ‘Through’ port of the coupler. Port 2 is connected to the ‘Coupled’ port of the coupler and the narrowband antenna is connected to the ‘Isolated’ port of the coupler. It is evident that when port 1 is excited, the wideband antenna is excited but the narrowband antenna is isolated. This agrees well with the S-parameters of the structure, showing that the coupling between the antenna ports is reduced.



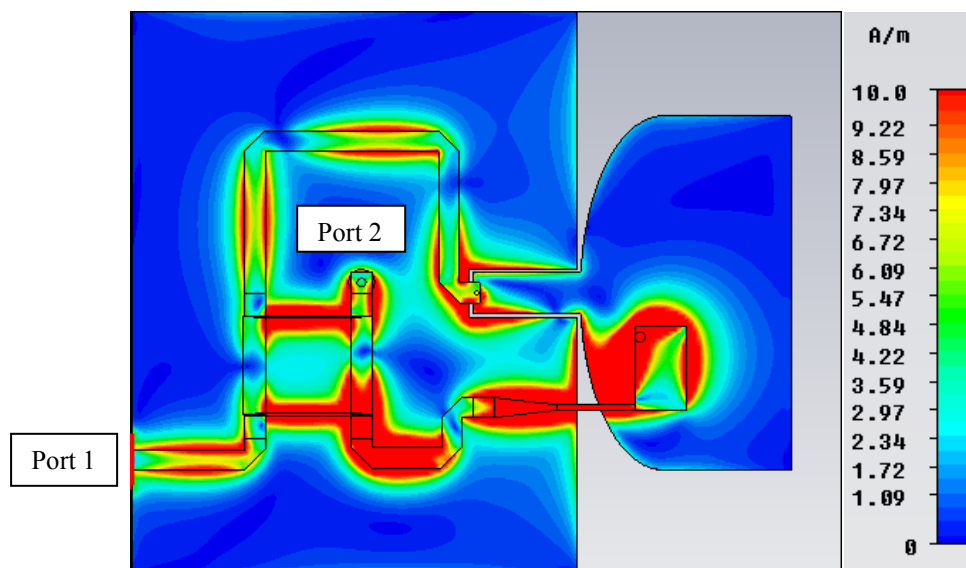
(a)



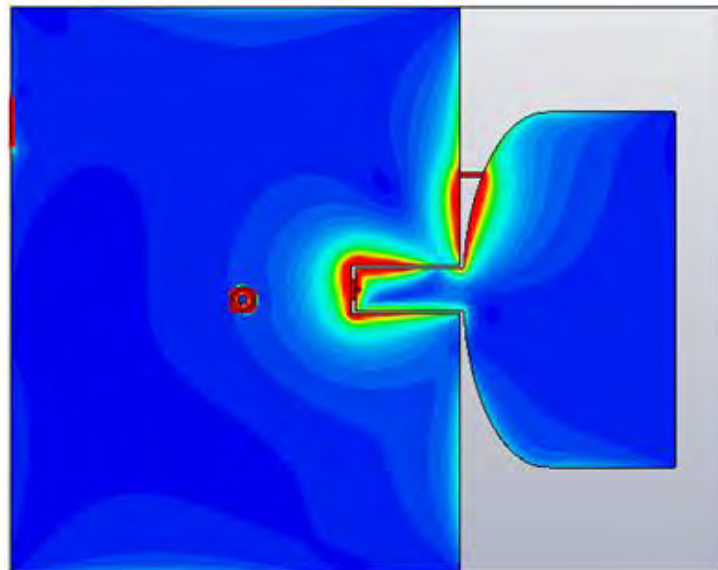
(b)

Figure 4.14 : Current distributions when the port1 is excited and the port 2 is terminated to a 50Ω load at 5 GHz. (a) Top View (b) Bottom View.

Fig. 4.15 shows the current distribution on both sides of the structure when port 2 is excited and port 1 is terminated to a $50\ \Omega$ load. In this case, Port 2 is the 'Input' port of the coupler. The narrowband antenna is connected to the 'Through' port of the coupler. Port 1 is connected to the 'Coupled' port of the coupler and the wideband antenna is connected to the 'Isolated' port of the coupler. As can be seen in Fig. 4.15, when port 2 is excited, the narrowband antenna is excited too. The wideband antenna is expected to be isolated, but it is not. The reason is that the current couples from narrowband antenna to the wideband antenna near the gap edges (see Fig. 4.15(b)). The induced current in the wideband antenna goes back to the 'Isolated' port of the coupler.



(a)



(b)

Figure 4.15 : Current distributions when the port1 is excited and the port 2 is terminated to a 50Ω load at 5 GHz. (a) Top View (b) Bottom View.

By comparing Fig. 4.14 and 4.15 with Fig. 3.5 and 3.6 respectively, it could be concluded that by adding the feed network to the antenna, the mutual coupling at the antenna ports is reduced considerably. In the other words when one port is being excited, there is just a very small value of current couples to the other port. The coupling caused by the structure of the antenna could be reduced by changing the position of the narrowband antenna relative to the UWB antenna, in a way that there is less coupling at the gap edges.

4.3 Discussion

In this section, a 12 dB branch-line coupler was designed, fabricated and measured to enhance the port isolation of the dual port antenna. The simulation and measurement results have a good agreement. The narrowband and UWB reflection coefficients were found to be reasonable; the narrowband characteristic of the antenna was maintained quite well. However the UWB antenna's reflection coefficient () was marginally above the desired value at some higher frequencies such as 6.8 GHz.

The reason for this improvement is that the coupling value (C) was optimized to achieve the desired results, whereas in the previous section it was fixed at 3dB (see 3.4 Discussion). In equation (3.4), stands for the reflection coefficient of port 1 of the coupler. The same argument is true for port 2 and 3. According to matrix (4.7), for a 12 dB branch-line coupler and , Therefore equation (3.4b) could be approximated as (without considering the phases):

$$\text{---} \quad (4.9)$$

It could be concluded that when a 12 dB coupler is being used, UWB antenna's reflection coefficient dominates the reflection coefficient of port 1 of the composite network (), and narrowband antenna has less influence. The similar equation could be written for the other port of the composite network (2'). Thus, () and () could be approximated by UWB and narrowband antenna reflection coefficients respectively.

The results suggest that frequency selectivity is required within the coupler in order to control the modified antenna S-parameters over the whole 3 to 11 GHz bandwidth. This further approach is discussed in the next chapter.

Chapter 5

Investigation into use of filters in a branch-line Coupler

As mentioned in the previous chapter, the 12 dB branch-line coupler with effective bandwidth of 4.8-5.2 GHz disturbed the UWB antenna's reflection coefficient () at 6.8 GHz and 11 GHz. This happens because, the feed-network does not necessarily perform as a coupler out of its bandwidth but, it's still connected to the antenna and affects its reflection coefficient.

Couplers are generally narrowband components. Their behaviour is not well controlled out of their operating band. In order to achieve control over the feed network's behaviour also out of the coupler's bandwidth, its scattering matrix need to be carefully controlled at those frequencies too. This will give control on the feed network response all over the UWB (3-11 GHz) bandwidth.

The solution is to define such a feed network to behave as a coupler in the desired frequency band; and it should not couple in the rest of 3-11 GHz band. This could be implemented by embedding a filter inside the branch-line coupler.

5.1 Investigation of the Filtering Action

The feed network must produce the C coupling in the desired (4.8-5.4 GHz) frequency band. Everywhere else in the 3-11 GHz band of the antenna's operating frequency, the network should not couple. In order to examine this concept, a simplified approach in the simulator was taken.

As seen in the previous chapter (matrix 4.7), the S-parameters matrix of the 12 dB branch-line coupler is as follows:

$$\begin{pmatrix} 0 & 0 & 0.3 & -90 & 0.95 & -180 & 0 & 0 \\ 0.3 & -90 & 0 & 0 & 0 & 0 & 0.95 & -180 \\ 0.95 & -180 & 0 & 0 & 0 & 0 & 0.3 & -90 \\ 0 & 0 & 0.95 & -180 & 0.3 & -90 & 0 & 0 \end{pmatrix}$$

The desired feed-network's behaviour should also be defined outside of the coupler's frequency band (4.8-5.2 GHz). If the feed network does not couple in the rest of the band, it's not going to affect the UWB return loss in higher frequencies. The scattering matrix representation of the feed network in this approach is as follows,

From 3 to 4.8 GHz

$$\begin{pmatrix} 0 & 0 & 0 & 0 & 1 & 0 & 0 & 0 \\ 0 & 0 & 0 & 0 & 0 & 0 & 1 & 0 \\ 1 & 0 & 0 & 0 & 0 & 0 & 0 & 0 \\ 0 & 0 & 1 & 0 & 0 & 0 & 0 & 0 \end{pmatrix}$$

From 4.805 to 5.4 GHz

$$\begin{pmatrix} 0 & 0 & 0.3 & -90 & 0.95 & -180 & 0 & 0 \\ 0.3 & -90 & 0 & 0 & 0 & 0 & 0.95 & -180 \\ 0.95 & -180 & 0 & 0 & 0 & 0 & 0.3 & -90 \\ 0 & 0 & 0.95 & -180 & 0.3 & -90 & 0 & 0 \end{pmatrix}$$

From 5.405 to 11 GHz

$$\begin{pmatrix} 0 & 0 & 0 & 0 & 1 & 0 & 0 & 0 \\ 0 & 0 & 0 & 0 & 0 & 0 & 1 & 0 \\ 1 & 0 & 0 & 0 & 0 & 0 & 0 & 0 \\ 0 & 0 & 1 & 0 & 0 & 0 & 0 & 0 \end{pmatrix}$$

These matrices were imported to *Microwave Office* (AWR) as a Touchstone file; Fig 5.1 shows the simulated S-parameters of the 4-port feed-network. S_{11} is the coupling value equal to -12 dB in the 4.8-5.4 GHz frequency band. In the rest of the bandwidth, S_{11} is equal to zero. S_{21} and S_{31} are equal to zero (-inf dB) in all 3-11 GHz frequency range. S_{41} is matched, and ports 1 and 4 are isolated.

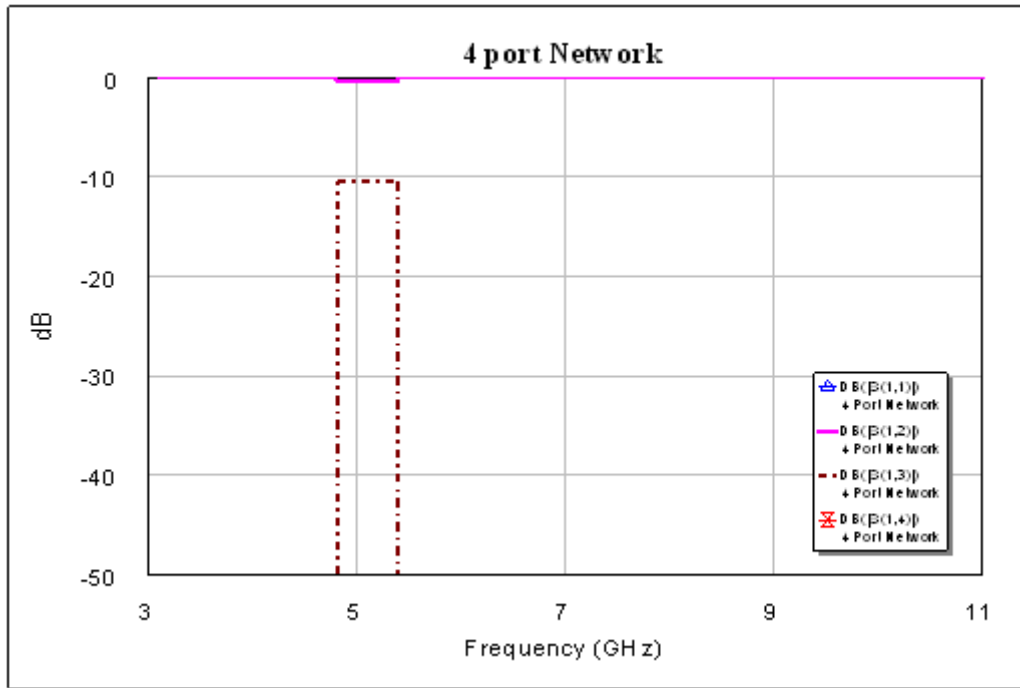


Figure 5.1: Simulated S-parameters of the 4 port feed-network

The antenna's already measured S-parameters are also imported to *Microwave office*. Antenna's S-parameters matrix is represented by a 2-port element called Sub-circuit. The two sub-circuits are connected together in the simulator (*Microwave Office*). The composite structure is a 2 port network. The two ports of the composite structure are approximated as antenna's new ports. $\Gamma_{wideband}$ and $\Gamma_{narrowband}$ are the reflection coefficient of wideband and narrowband antennas respectively. As has been mentioned above, a phase shifter is required to achieve the appropriate phase. The value of the phase shift can be achieved by manual optimization. The required phase shift is equal to 144° .

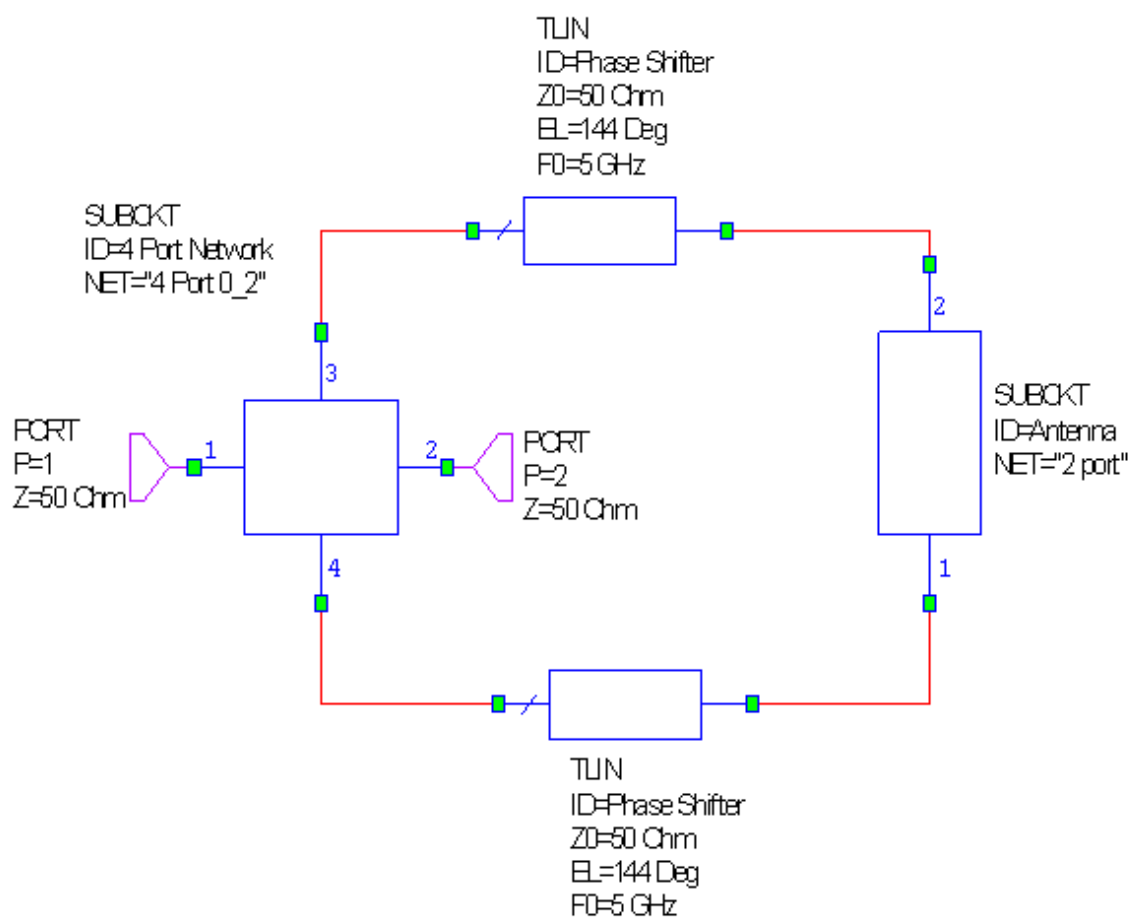


Figure 5.2: 4-port feed network connected to the antenna with a 144° phase-shift at both antennas ports

Fig 5.3 represents the simulated S-parameters of the composite structure (antenna+phase-shifter + feed-network). As can be seen, the reflection coefficients of the UWB and narrowband antennas are not changed outside the 4.8-5.4 GHz frequency band. Narrowband antenna resonating frequency is maintained at 5.2 GHz. S_{11} is about -24 dB at 5.2 GHz; thus two ports of the antenna are well isolated at the desired frequency after the addition of the feed-network. The UWB antenna's reflection coefficient is approximately -10dB or less throughout the 3-11 GHz.

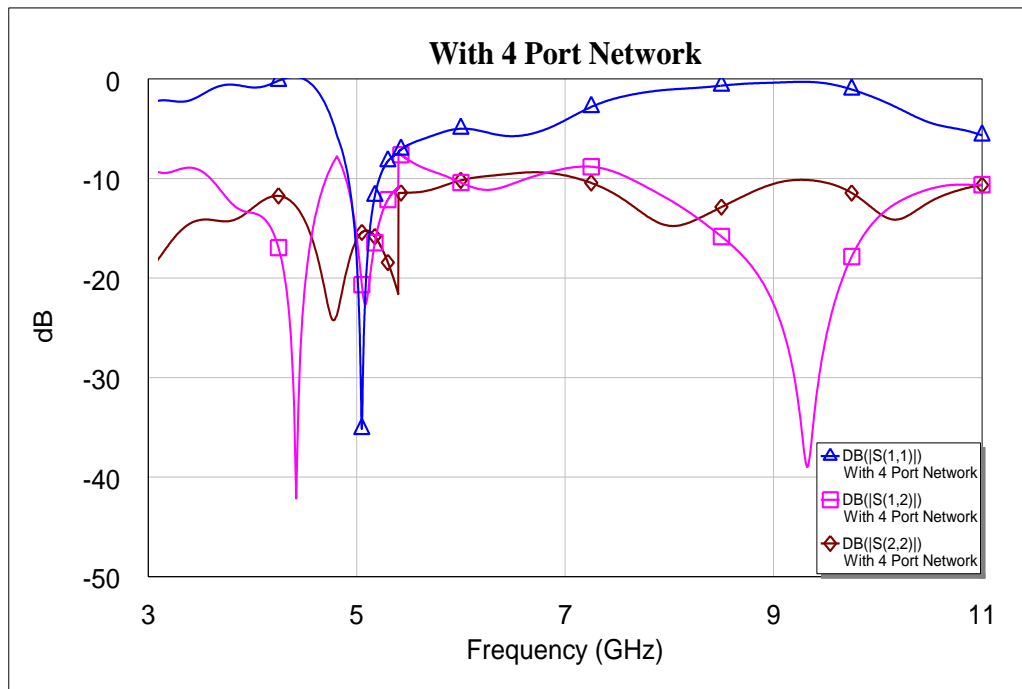


Figure 5.3: Simulated s-parameters of the composite structure

As the 4-port feed network's response was acceptable, the 4-port network could be written as two 2-port networks. These 2-port networks are embedded in branch-line coupler. As seen in the previous chapter, in a 12 dB branch-line coupler with a centre frequency of 5.2 GHz, and . Now that the characteristic impedances of the branch-line coupler lines are found, then the scattering matrix for a quarter wavelength line (when $\beta L=90^\circ$) is as follows (Gardner, 2010):

S- Parameters matrix of the shunt line in Fig 4.1: (5.1)

$$\begin{matrix} \text{---} \\ \text{---} \end{matrix}$$

Thus the S-Parameter of the shunt line with the Impedance of is the matrix S, which is a 2- port network matrix:

(5.2)

in the out of band matrices represent and open circuit in the shunt line. Hence;

In the 3-4.8 GHz frequency band the matrix associated with the shunt line is . In the

4.8-5.4 GHz frequency band matrix associated with the shunt line is . In

the 5.4-11 GHz frequency band matrix associated with the shunt line is . Therefore

the Touchstone file of the 2-port network is as follows (the even columns represents the phase);

From 3 to 4.8 GHz
$$\begin{pmatrix} 1 & 0 & 0 & 0 \\ 0 & 0 & 1 & 0 \end{pmatrix}$$

From 4.805 to 5.4 GHz
$$\begin{pmatrix} 0.76 & 0 & 0.64 & -90 \\ 0.64 & -90 & 0.76 & 0 \end{pmatrix}$$

From 5.405 to 11 GHz
$$\begin{pmatrix} 1 & 0 & 0 & 0 \\ 0 & 0 & 1 & 0 \end{pmatrix}$$

The Touchstone file was imported to *Microwave Office* and appeared as a 2-port sub-circuit in the schematic editor. Fig 5.4 represents a 12 dB branch-line coupler with a 2 port sub-circuit (network) substituted in it's shunt line. This 2 port networks represents () the 137 Ω shunt line with a 90° phase shift.

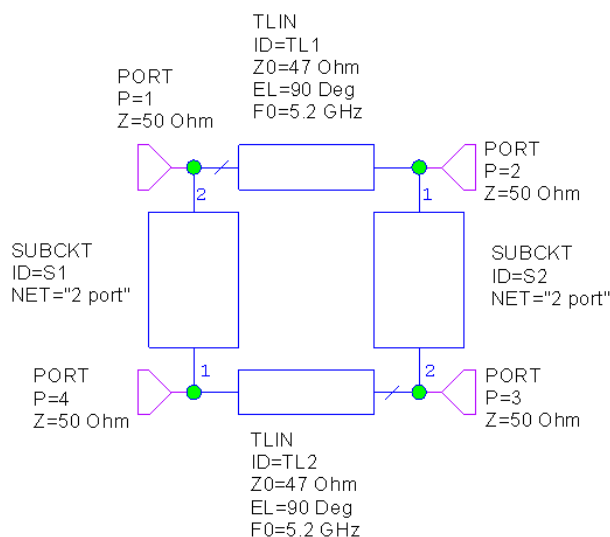


Figure 5.4: Schematic of a 12 dB branch-line coupler ; the shunt line is replaced by a 2 port network

Fig 5.5 shows the simulated S-parameters of the 12 dB branch-line coupler shown in Fig 5.4. As it is evident from the figure, which represents the coupling value (c) is almost -9 dB instead of -12 dB (which is the nominal coupling value). This is due to design's discontinuities. and are well matched at 5.2 GHz. is equal zero in the entire band, responding as a kind of ideal branch-line coupler.

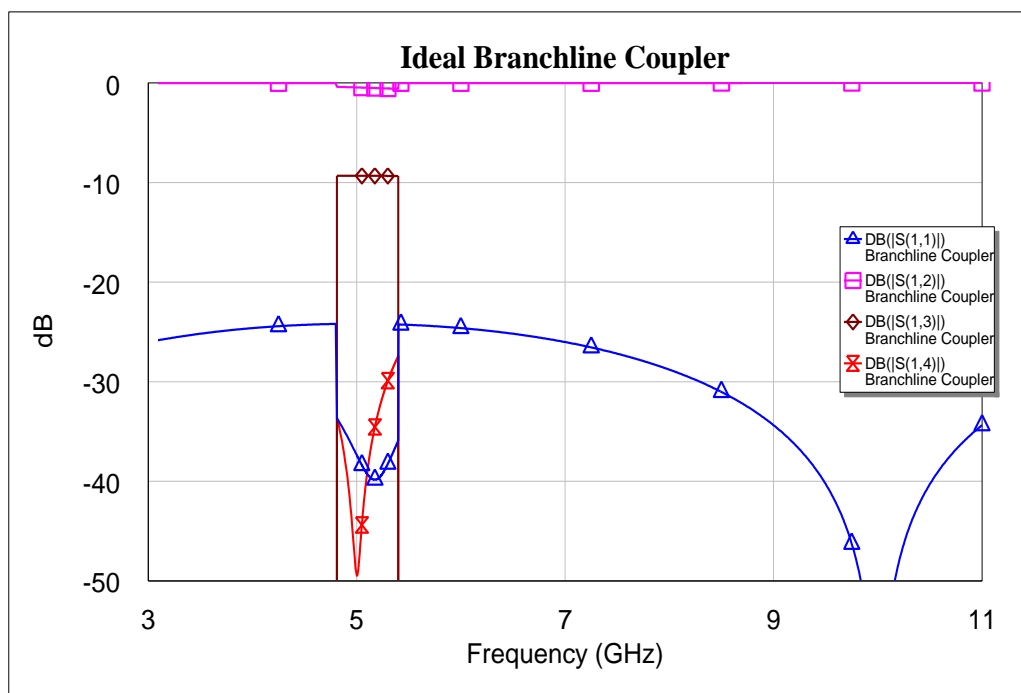


Figure 5.5: simulated s-parameters of the Branch-line coupler with embedded 2-port networks instead of shunt lines

Once the branch-line coupler is seen to be working as expected, it is connected to the antenna. A phase shifter is required to adjust the phase. The value of the phase shifter is optimized manually.

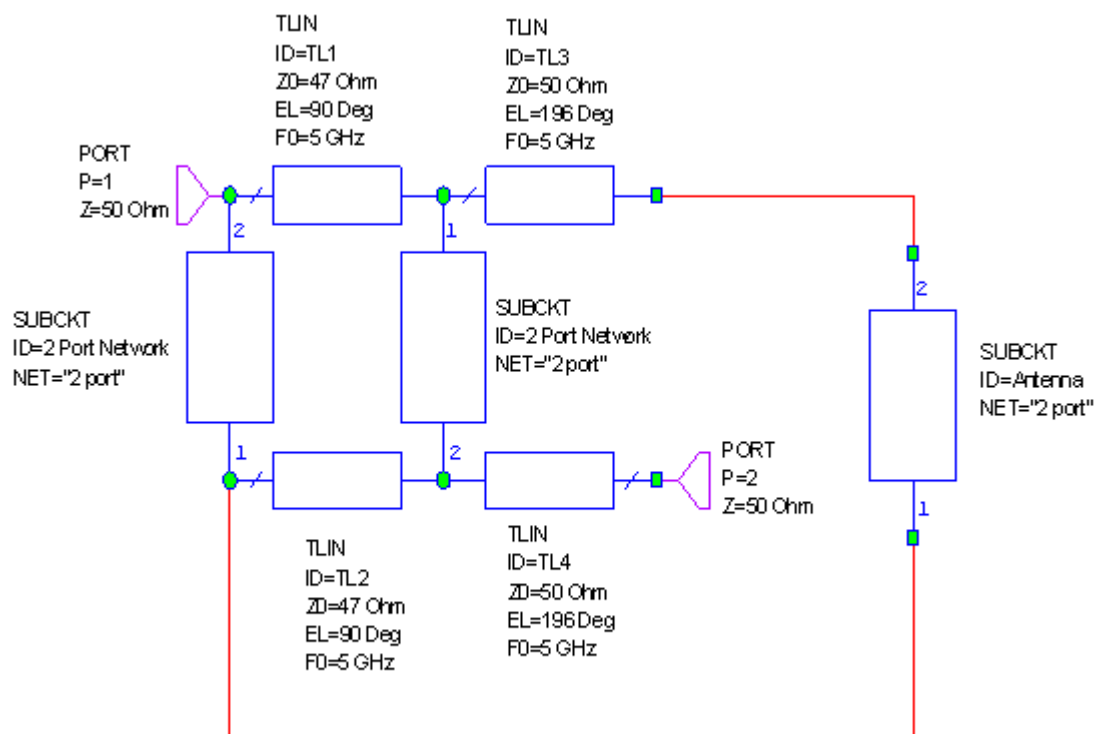


Figure 5.6: Schematic of the ideal branch-line coupler connected to the antenna via phase shifter

Fig 5.7 represents the simulated S-Parameters of the feed-network (ideal coupler and the phase-shifter) connected to the antenna (cf Fig 1.1). The UWB antenna reflection coefficient () is less than -10 dB throughout the 3-11 GHz bandwidth. The narrowband antenna's resonating frequency remains the same (at 5.2 GHz). The isolation is acceptable throughout the 3-11 GHz band and is noticeably reduced to -14 dB at 5.2 GHz. It could be concluded that all the antenna's S-parameters are reasonable after the addition of the feed-network.

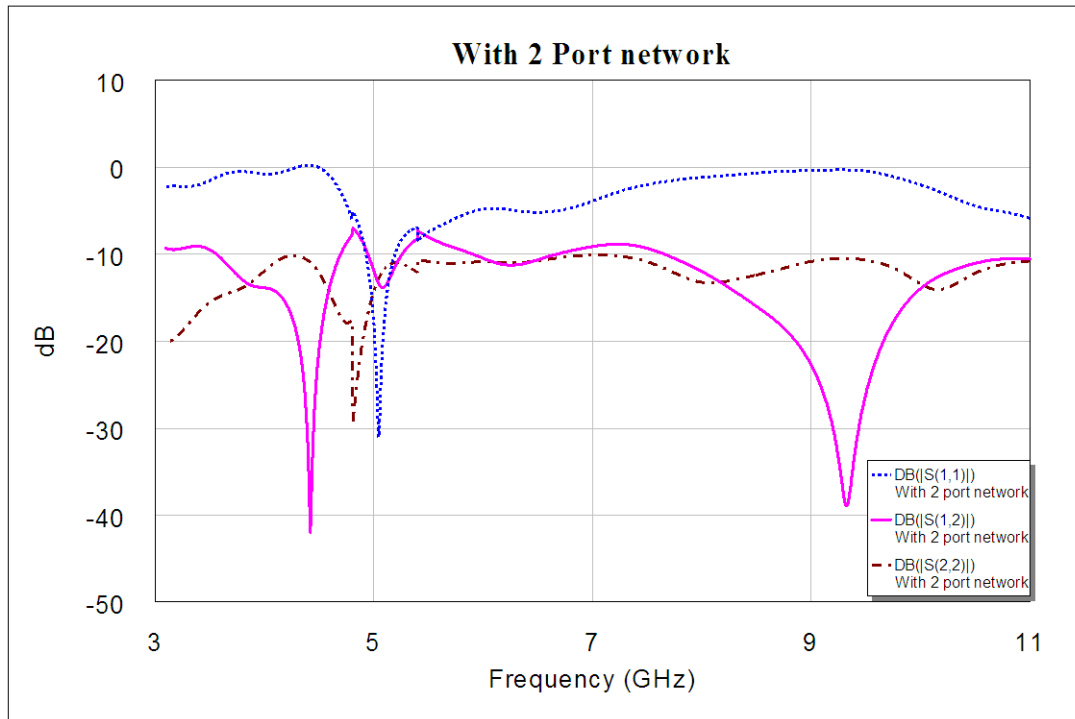


Figure 5.7: Simulated S-parameters of the composite network.

5.2 Filter Design

The realization of the 2 port network is now considered. The S matrix of the shunt line represents a quarter wavelength (90° phase shift) transmission line with 137Ω impedance. This line should be thus characterised exclusively in the branch-line coupler's frequency band (4.8-5.4 GHz). This characteristic could be satisfied by a band-pass filter.

The first solution considered is to design a lumped element band-pass filter satisfying 137Ω impedance and having a 90° phase shift. As designing lumped element filter with such requirements is a challenging task; different combinations of 2nd-, 3rd- and 4th-order filters have been tried in a bid to achieve the right phase and impedance. Lumped element filters of an order of more than 3 can be quite bulky and not suited to compact systems. One of the difficulties encountered in designing this filter was the change in the wideband antenna characteristics due to cut off frequencies on band edges.

The band pass filter’s schematic, shown in Fig. 5.8, is the lumped element filter with 137 Ω of impedance. It provides a 90°-phase shift. The band pass filter has a pass band of 4.8 GHz to 5.4 GHz. As can be seen in the figure, the filter consists of one 3rd-order (Butterworth) band pass filter, two 2nd-order band stop filters (with centre frequency of 4.7 GHz and 5.1 GHz) and two 56°-phase shifters at each end of the band pass filter. The filter coefficients were calculated using *Microwave Office* “Filter Synthesis Wizard”. The whole structure has been kept symmetrical to get the appropriate results. Fig 5.9 shows the sub-circuit overview of the lumped element band-pass filter in Fig. 5.8. *Microwave Office* optimizer has been used for further optimization of the filter parameters.

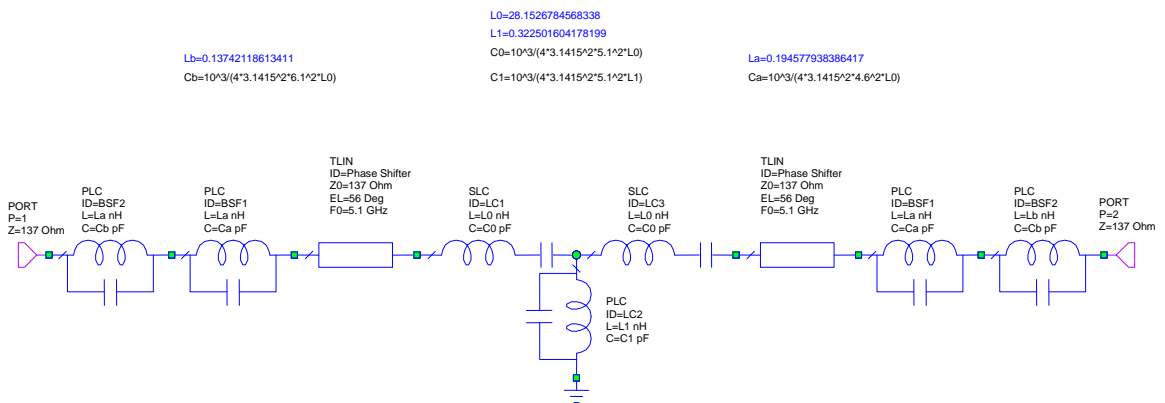


Figure 5.8: Schematic of the lumped element band-pass filter

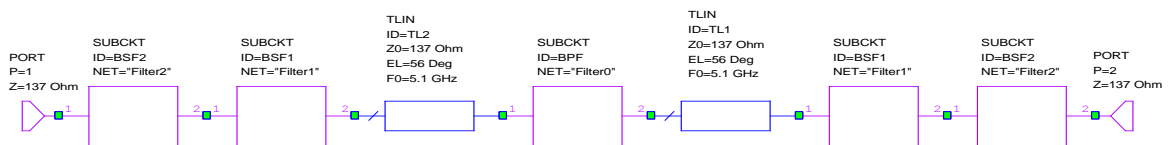


Figure 5.9: Sub-circuit overview of the lumped element band-pass filter in Fig 5.8

Microwave Office “Filter Synthesis Wizard” calculates the filter parameters using the design theories. More details of filter design theories are found in Pozar (1998).

Fig. 5.10 represents the band-pass filter's response, shows a good match inside the pass-band of the filter (4.8-5.4 GHz); everywhere else it is almost zero. The filter thus passes the waves with a frequency of between 4.8-5.4 GHz and blocks all other frequency waves. As expected, it can be seen that the filter has a finite roll off rate on either side of the pass-band.

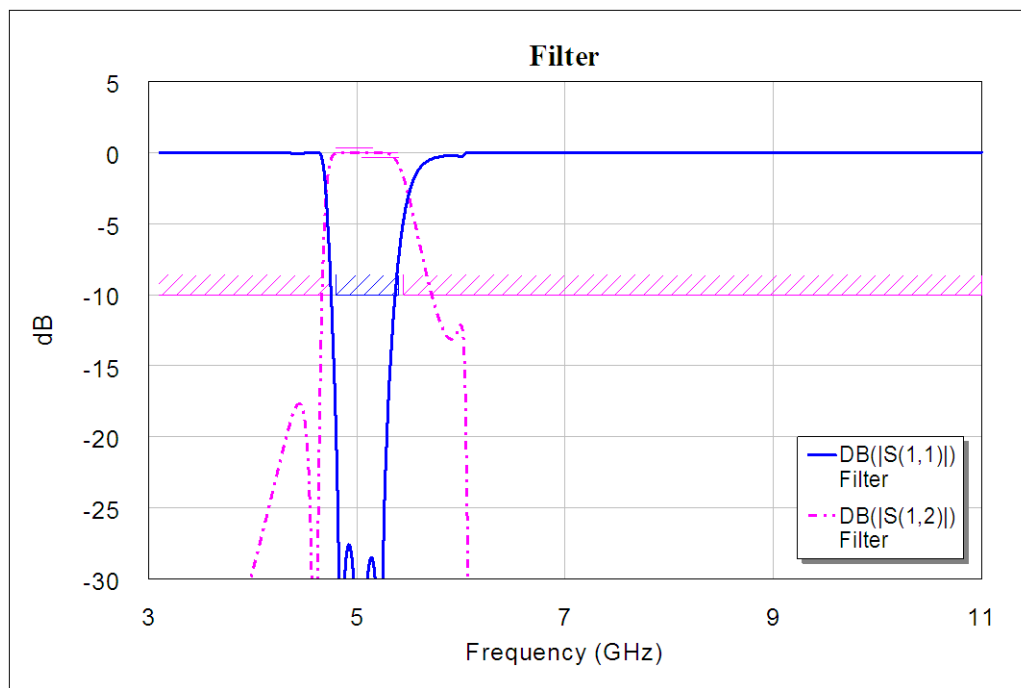


Figure 5.10: Simulated S-parameters of the lumped element band -pass filter

Fig. 5.11 shows the branch-line coupler, containing the band-pass filter.

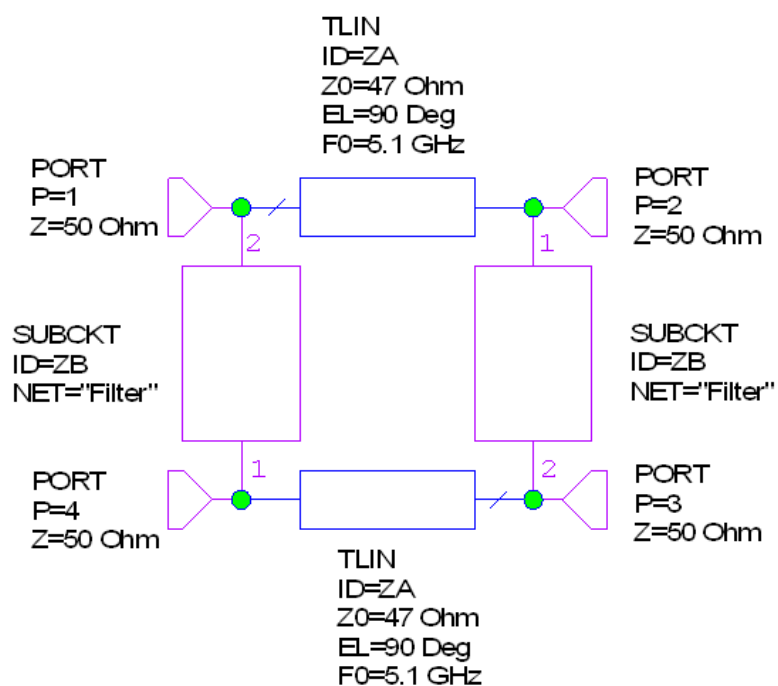
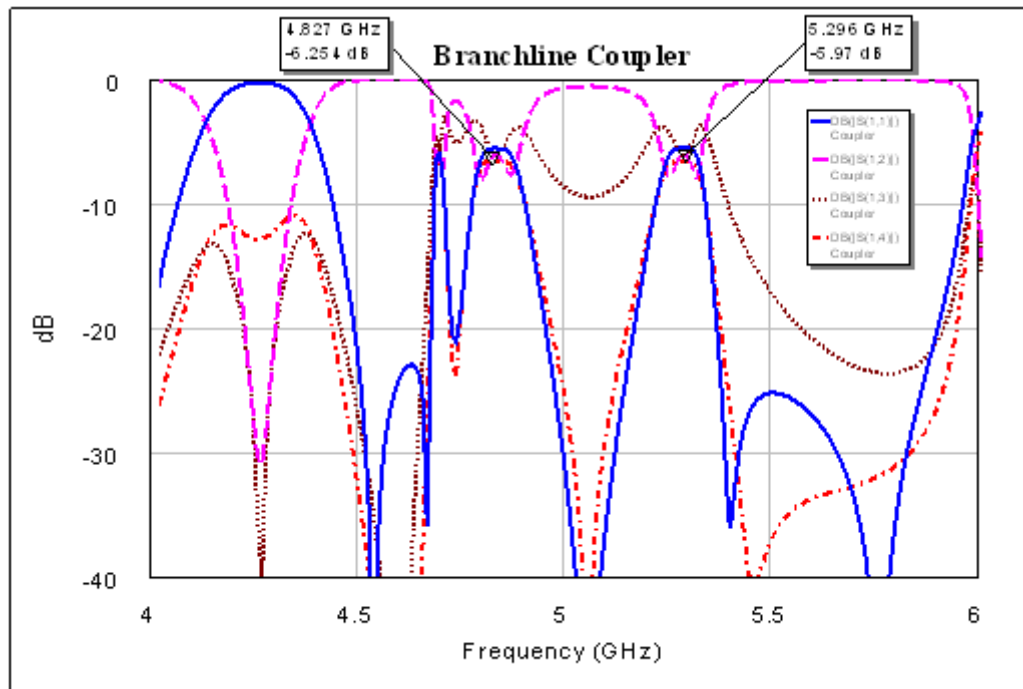


Figure 5.11: Schematic of the 12 dB branch-line Coupler with emended filters

Fig. 5.12 represents the simulated S-parameters of the branch-line coupler shown in Fig. 5.11 from 4-6 GHz. The coupler works well from 4.82-5.29 GHz but outside of the band, it's response is not well controlled. This is due to the imperfections in the design of the lumped element filters. The value of S_{11} is equal to -9 dB instead of the expected -12 dB, due to discontinuities of the design.



- DB(|S(1,1)|)
Coupler
- - - DB(|S(1,2)|)
Coupler
- ... DB(|S(1,3)|)
Coupler
- . - DB(|S(1,4)|)
Coupler

Figure 5.12: Simulated S-parameters of the branch-line coupler with embedded filters.

In Fig. 5.13, the branch-line coupler in Fig. 5.11 is connected to the antenna via phase shifter. The phase shifter has the optimized value of 103° . The value of the phase shift is achieved by manual optimization.

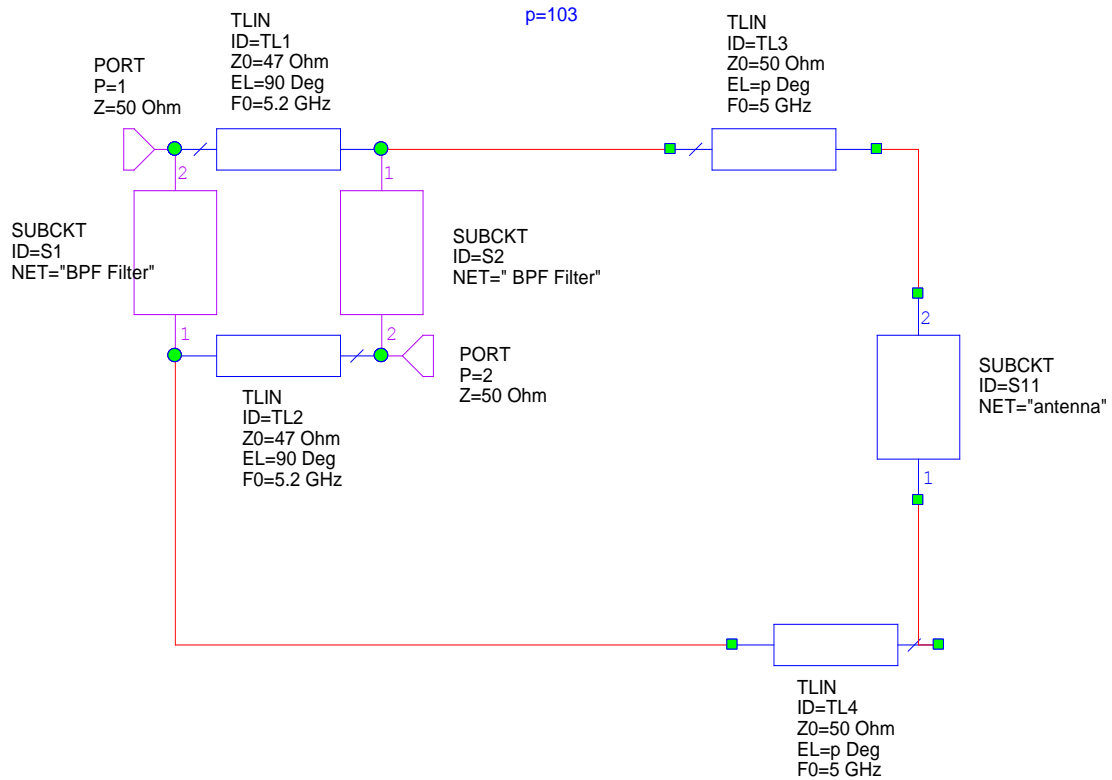


Figure 5.13: Schematic of the branch-line coupler with embedded BPF connected to the antenna

Fig. 5.14 shows the simulated S-parameters of the composite structure. The S_{11} (isolation) is reduced to -14 dB at 5.2 GHz, and the S_{21} and S_{31} parameters within the pass-band of the filter also indicate good impedance matches. Outside the pass-band, the roll-off of the filter characteristic is not fast enough to prevent problems at the band edges. The result is the high values of S_{11} , S_{21} and S_{31} just outside of the pass band.

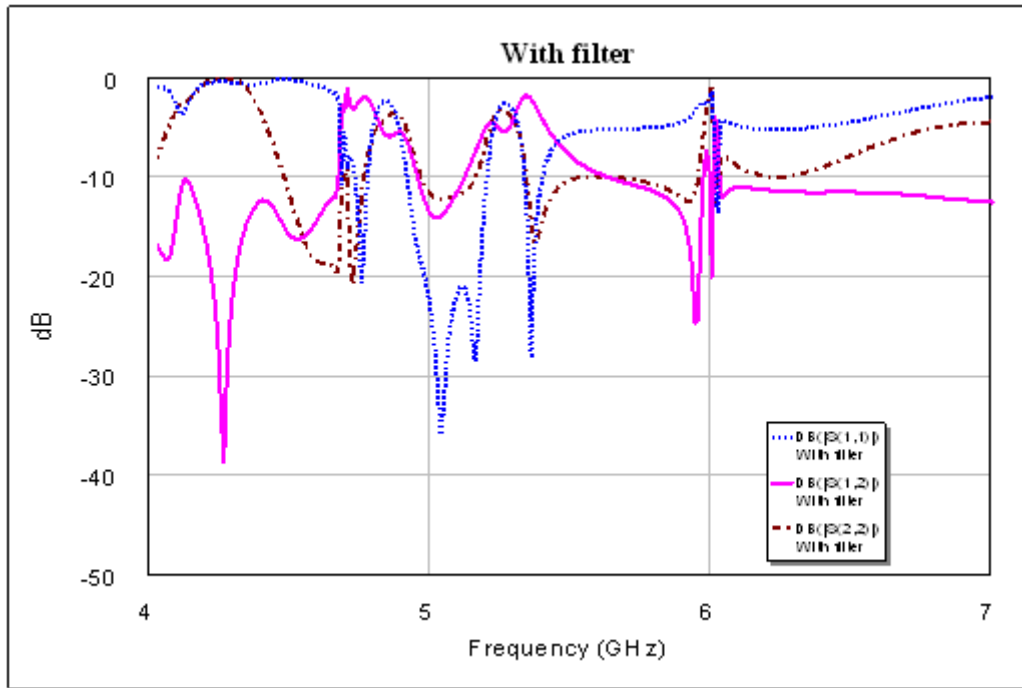


Figure 5.14: Simulated S-parameters of the antenna connected to the branch-line coupler

5.3 Discussion

The difference between an ideal and a real filter is evident from the simulation results. In the ideal case, the results confirm the theory. When a Lumped Element filter was simulated, the results in the optimized case were ideal in just a very narrow band and the filter was not as sharp as in the ideal case. Therefore, the UWB performance of the circuit is slightly distorted out of the 4.8-5.2 GHz band.

Time constraints prevented this filter being realised. Some comments on realisation are now made. There are different methods of manufacturing a filter in the 5 GHz frequency range. Lumped element filters have reasonable size at intermediate frequencies (500 MHz to 1 GHz); fabricating elements at higher frequencies becomes impractical. Lumped element filters have been made up to approximately 3 GHz; manufacturing them at higher frequencies such as 5 GHz is not viable.

There are other types of filters that can be manufactured in this frequency range. Distributed filters, using transmission lines to produce appropriate impedance where they are needed, could be used; however it is likely that they will not fit in the branch line structure. Another option might be to make such filters using YIG resonators or dielectric resonators. However these are outside the scope of this project. They are discussed briefly in the “Future work” section of this dissertation.

Chapter 6

Conclusions and Future Work

Several decoupling techniques have been reported in papers, most of which suggest making changes to the antenna structure such as an increase of the spacing between them. However, Ultra Wideband-Narrowband antenna decoupling has not been done before. This project is about adding a feed-network to the antenna to enhance the isolation between the two ports.

6.1 Conclusions

Approaches to the problem of improving the isolation between the ports of a two-port antenna have been investigated. An initial experiment showed that a rat-race coupler with appropriate phase-shift could produce some useful effect, but the coupling ratio and the out of band responses need very careful attention.

A series of simulations based on ideal filters introduced into branch-line couplers (non -3dB) showed that such couplers could provide the required narrowband isolation improvement without degrading the response out-of-band. Simulations based on lumped element filters suggested that the ideal response needed could not be approximated closely enough with a practical number of sections.

A practical demonstration using a branch-line coupler with the designed coupling ratio (non -3dB) but without the frequency selectivity features demonstrated the general principle.

The approaches didn't make modify the antenna structure itself. Thus the advantage of these methods is that the decoupling feed network could get connected to any other similar dual-port antenna with slight design modifications. These changes are, for instance: re-designing

the coupler and/or filter for a new frequency and/or optimizing the required phase shifter value.

6.1.1 Challenges

The isolation enhancement approach was examined by connecting the feed-network to a pre-designed dual port antenna, of which the two ports are very close to each other. Thus all the dimensions were limited due to the antenna's two sided structure.

For practical purpose, the wide-narrowband characteristics of the antenna should be unchanged after the addition of the feed network. Thus the effect of adding this feed network should be reduced as much as possible (out of 4.8-5.4 GHz band) and, ideally, the antenna characteristics and S-parameters should be unchanged. However, this is not practical, so these values have to be reduced to their minimum.

Section 3.1 of this thesis shows that the ground plane is considered as part of the antenna and contributes to the radiation. Therefore variation in ground plane size changes antenna matching. Changing the narrowband antenna feed length also affects the narrowband and/or wideband reflection coefficient. Thus adding a feed network to the antenna changed the ground plane size and narrowband antenna feed line, and this should be taken into account.

The effect of the change in narrowband antenna feed-length (see Fig 4.8(a) and Fig. 3.15) is cancelled by optimizing the value of phase-shift between the antenna and coupler's ports (length of the 50Ω connection lines).

6.2 Future Work

This section briefly discusses methods to make a band-pass sharp filter. In order to make a band-pass filter with a fast roll-off at the band edges, using embedded filters inside the couplers has the advantage of providing frequency selectivity. It also offers more control over the feed-network behaviour out of the couplers narrow bandwidth.

Embedding filters, which works at 5 GHz in a PCB, is quite a challenging task. Using Yttrium Iron Garnet (YIG) filters is a suggestion for making further improvements in the filtering action. Yttrium Iron Garnet (YIG) is a crystal that has very high Q characteristics. This high Q provides very low phase noise in oscillators and multi-octave frequency tuning for both oscillators and filters.). The size of the YIG spheres range from 10-30 mm. (Cohn, 1968)

Fig. 6.1 represents a branch-line coupler using a YIG tuned band-pass filter, this make the coupler tuneable as well.

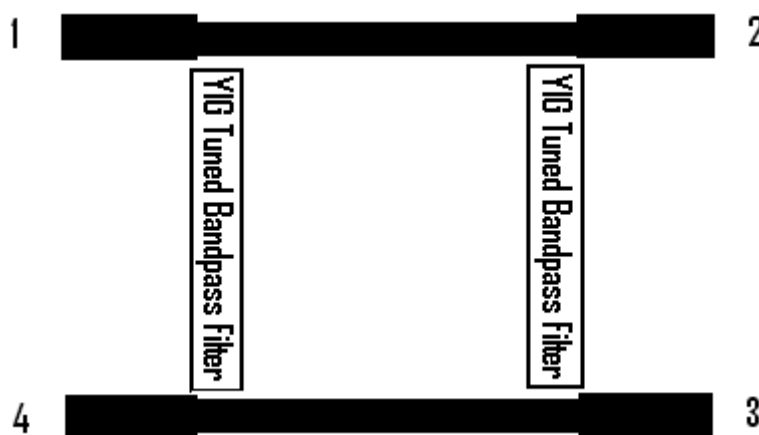


Figure 6.1: Branch-line coupler with an embedded YIG tuned filter.

Dielectric resonators could also be used in order to make high Q-factor band-pass filters at the 5.2 GHz. Their advantages are compactness, high temperature stability and ease of use. Dielectric resonators are designed to meet the demand of microwave applications for low-cost and high-performance devices. They could be used in several fields of circuit applications (filters / oscillators). Their frequency ranges from 800 MHz to 50 GHz. They can

be manufactured at different dielectric constants ranging from 24 to 78. Dielectric resonators are mainly designed to replace resonant cavities in microwave circuits (filters, oscillators, etc.). Like resonant cavities, their resonant modes of frequency are determined by dimensions. (Temex Ceramics, n.d.)

Chapter 7

References

Abbosh, A.M. (2007) Planar Ultra Wideband Antennas with Rejected Sub-bands. **IEEE Microwave Conference**. December, PP.1-4.

Akyildiz, Ian F. et al. (2006) **Next Generation/Dynamic Spectrum Access/Cognitive Radio Wireless Networks: A Survey** [Internet]. Available from: www.sciencedirect.com [Accessed: 28/10/10]

Andersen, J. B., Rasmussen, H. H. (1976) Decoupling and Descattering Networks for Antennas. **IEEE Transactions on Antennas and Propagation**, vol. AP-24, Nov. 1976, p. 841-846.

Andrews, M.R., Mitra, P. P. and de Carvalho, R. (2001) Tripling the capacity of wireless communications using electromagnetic polarization. **Nature**, vol. 409, no. 6818, January ,pp. 316–318.

Arslan, H., Chen, Z. N., Di Benedetto, M.-G.(2006) **Ultra Wideband Wireless Communication**, John Wiley & Sons, United States of America.

AWE Communications (2010) MIMO Antenna Systems in WinProp. [Internet] Available from:<http://www.awecomunications.com/Download/ApplicationNotes/NetworkPlanningMI MO.pdf> [Accessed: 28/09/11].

Balanis, C.A. (1997) **Antenna Theory: Analysis and design**. 2nd ed. New York, John Wiley & Sons, Inc.

Bennett, R. (2010) Technology and Policy Issues in the Mobile Internet. **Information Technology and Innovation Foundation, Going Mobile**, March, p.46.

Berlemann, L., Mangold, S. (2009) **Cognitive Radio and Dynamic Spectrum Access**. United Kingdom, JohnWiley & SonsWest.

Bhatti, R.A. et al. (2009) Compact Antenna Array With Port Decoupling for LTE-Standardized Mobile Phones. **IEEE Antennas and Wireless Propagation Letters**, Vol 8, PP: 1430 – 1433.

Chen, S.C. et al. (2008) A Decoupling Technique for Increasing the Port Isolation Between Two Strongly Coupled Antennas. **IEEE, Antennas and Propagation**. Volume 56, December, PP.3650-3658.

Chen, Y.M. et al. (2009) A Miniaturized Broadband Four-Port Antenna Located on a Cylindrical Conductor. **Microwave Conference, APMC 2009**, PP. 2637 – 2640.

Chim, K.C. et al. (2004) Investigating the impact of smart antennas on SAR. **IEEE Trans. Antennas Propagation**. vol. 52, May , pp.1370–1374.

Chiu, C. Y. et al. (2007) Reduction of mutual coupling between closely-packed antenna elements. **IEEE Trans. Antennas Propag.**, vol. 55, no. 6, , June, pp. 1732–1738.

Cohn, S.B. (1968) Microwave Band-pass filters containing high-Q Dielectric Resonators. **IEEE Transactions on Microwave Theory and Techniques**. vol. MTT-16, No.4 ,April, pp. 218-227.

Collin, R. E. (1992) **Foundations for Microwave Engineering**. 2nd ed. New York, McGraw Hill.

Diallo, A. , Luxey, C. ,Thuc, P.L. , Staraj, R. and Kossiavas, G. (2006) Study and reduction of the mutual coupling between two mobile phone PIFAs operating in the DCS 1800 and UMTS bands. **IEEE Trans. Antennas Propag.**, vol. 54, no. 11,November, pp. 3063–3073.

Ebrahimi, E., Kelly, J. Hall, P.S. (2009) A reconfigurable narrowband antenna integrated with wideband monopole for cognitive radio applications in **Proc. APS 2009.** , June, pp.1-4.

Esser, D., Solan, B., Chaloupka, H. (2006) Improved antenna isolation in transmit/receive applications. **German Microwave Conference - GeMiC.**

Federal Communications Commission (2003) **Facilitating Opportunities for Flexible, Efficient, and Reliable Spectrum Use Employing Cognitive Radio Technologies.** [Internet]. Available from :< <http://www.cs.ucdavis.edu/~liu/289I/Material/FCC-03-322A1.pdf> > [Accessed: 8/01/10]

Gardner, P. (2010) “**Microwave Engineering lecture notes.**” University of Birmingham.

Gardner, P. et al. (2008) Reconfigurable Antennas for Cognitive Radio: Requirements and Potential Design Approaches. **Wideband, Multiband Antennas and Arrays for Defence or Civil Applications, 2008 Institution of Engineering and Technology Seminar.** March, pp. 89-94.

Granelli, F., Zhang,H.(2005) Cognitive Ultra Wide Band Radio: A Research Vision and Its OpenChallenges **.IEEE Networking with Ultra Wide Band and Workshop on Ultra Wide Bandfor Sensor Networks.** 4-6 July, pp. 55 – 59.

Hall, P.S et al. (2008) Combined Wideband and Narrowband Antenna for Cognitive Radio Applications. **Cognitive Radio and Software Defined Radios: Technologies and Techniques.** September, pp. 1-4.

Harada, H. (2007) A Software Defined Cognitive Radio Prototype. **IEEE 18th International Symposium on Personal, Indoor and Mobile Radio Communications,** 3-7 September, pp. 1-5.

Hur, Y., Park, J. , Woo, W. , K. Lim, Lee, C.-H. , Kim, H.S. , Laskar, J. (2006) A wideband analog multi-resolution spectrum sensing (MRSS) technique for cognitive radio (CR) systems. **Proceedings. IEEE International Symposium on Circuits and Systems.** 21-24 May.

Jakobsen, K.B., Thaysen, J. (2007) **Checking capacity for MIMO configurations**. June [Internet] Available from: <
<http://www.mwrf.com/Articles/Index.cfm?ArticleID=15797&pg=1>> June

Jasteh, D.;Ebrahimi,E.;Hall, P.S.;Gardner,P.(2009) Feed network for antenna decoupling. **Loughborough Antennas & Propagation Conference**. 16-17 November, pp. 537-540.

Kandeepan, S. et al. (2009) Periodic Spectrum Sensing Performance and Requirements for Detecting Legacy Users with Temporal and Noise Statistics in Cognitive Radios. **IEEE GLOBECOM Workshops 2009**, PP. 1-6.

Kaneko, S. et al. (2008) Predicting Radio Resource Availability in Cognitive Radio - an Experimental Examination.**Cognitive Radio Oriented Wireless Networks and Communications, CrownCom 2008**, PP.1-6.

Karaboikis, C. Soras, G. Tsachtsiris and V. Makios (2004) Compact dual-printed inverted-f antenna diversity systems for portable wireless devices. **IEEE Antennas Wireless Propagat. Lett.** vol. 3, pp. 9-14.

Kildal, P.S. and Rosengren, K. (2004) Correlation and capacity of MIMO systems and mutual coupling, radiation efficiency, and diversity gain of their antennas: Simulations and measurements in a reverberation chamber. **IEEE Commun. Mag.**, vol. 42, December, pp. 104–112.

Kivekäs, O., Ollikainen, J., Lehtiniemi, T. and Vainikainen, P. (2003) Effect of the chassis length on the bandwidth, SAR, and efficiency of internal mobile phone antennas. **Microwave Opt. Technol. Lett.** vol. 36, no. 6, March, pp. 457–462.

Kokkinos, T., Liakou, E., Feresidis, A.P. (2008) Decoupling antenna elements of PIFA arrays on handheld devices. **Electron. Lett.**, vol. 44, no. 25, pp. 1442-1444.

Kramer, B.A. et al. (2006) Miniature UWB Antenna with Embedded Inductive Loading. **IEEE Antenna Technology Small Antennas and Novel Metamaterials**. 6-8 March, pp. 289 – 292.

Laskar, J., Mukhopadhyay, R. , Hur, Y. , Lee, C.-H. ,Lim, K. (2006) Reconfigurable RFICs and modules for cognitive radio. **Topical Meeting on Silicon Monolithic Integrated Circuits in RF Systems**, 18-20 Jan, pp. 283-286.

Lau, B. K. et al. (2006) Impact of Matching Network on Bandwidth of Compact Antenna Arrays. **IEEE Transactions on Antennas and Propagation**. vol. 54, No. 11, November, pp. 3225-3238.

Li, Z., Rahmat-Samii, Y. (2005) Optimization of PIFA-IFA combination in handset antenna designs. **IEEE Trans. Antennas Propag.** vol. 53, May, pp. 1770–1778.

Lihao, H. et al. (2010) Reduction of mutual coupling between closely-packed antenna elements with split ring resonator (SRR). **International Conference on Microwave and Millimeter Wave Technology (ICMMT)**. 8-11 May, pp. 1873 – 1875.

MacKenzie, A.B. et al. (2009) Cognitive Radio and Networking Research at Virginia- Tech. **Proceedings of the IEEE**. Vol. 97, No. 4, April, pp. 660 – 688.

Mitola, J. (1995) The software radio architecture. **IEEE Communications Magazine**. Vol. 33, No. 5, May, pp. 26-38.

Mitola, J. (2000) Cognitive radio: An integrated agent architecture for software defined radio. **Ph.D. Dissertation**, KTH

Mitola, J., III, Maguire, G.Q., Jr. (1999) **Cognitive Radio: Making Software Radios More Personal**. **IEEE Personal Communications**. Volume 6, August, pp. 13 – 18.

Mitola, J., III (1999) **Cognitive Radio for Flexible Mobile Multimedia Communications**. **IEEE Mobile Multimedia Communications**. 15-17 November, pp. 3 – 10.

Park, S., Jung, C. (2010) Compact MIMO antenna with high isolation performance. **Electron. Lett.** vol. 46, No. 6, pp. 390-391.

Pozar, D.M. (1998) **Microwave Engineering**. 2nd ed. New York, John Wiley & Sons, Inc.

Rau, B. (1998) **Brushing Up on VSWR**. [Internet]. Available from :<http://telephonyonline.com/wireless/mag/wireless_brushing_vswr/> [Accessed: 27/03/10]

Sarabandi, K. et al. (n.d.) **Antenna Miniaturization Techniques for Applications in Compact Wireless Transceivers**. [Internet]. Available from: <<http://www.ursi.org/Proceedings/ProcGA02/papers/p2037.pdf>> [Accessed: 10/02/10]

Shuai, Z. et al. (2009) Ultra wideband MIMO/diversity antennas with a tree-like structure to enhance wideband isolation. **IEEE Antennas Wireless Propag. Lett.**, vol. 8, pp. 1279 – 1282.

Temex Ceramics (n.d.) **Dielectric Materials: General Information**. [internet]. Available form: < <http://www.temex-ceramics.com/site/fichiers/dielectric.pdf>> [Accessed: 10/09/11]

Walker, John L.B. et al. (2006) **Classic Works in RF Engineering: Combiners, Couplers, Transformers, and Magnetic Materials**. Norwood, Artech House, Inc.

Wallace, J.W., Jensen, M.A. (2004) Mutual Coupling in MIMO Wireless Systems: A Rigorous Network Theory Analysis. **IEEE Transactions on Wireless Communications**. July, vol. 3, No. 4, pp. 1317-1325.

Wong, K.L. (2002) **Compact and Broadband Microstrip Antennas**. John Wiley & Sons, Inc., New York.

Wu, T.Y., Fang, S.T., Wong, K.L. (2002) Printed diversity monopole antenna for WLAN operation. **Electronic Letters**. December, vol. 38, No. 25, pp. 1625–1626.

Yazdanbakhsh, P., Solbach, K.(2009) Optimization of Monopole Four-Square Array Antenna Using a Decoupling Network and a Neural Network to Model Ground Plane Effects. **Antennas and Propagation Conference, EuCAP**. 23-27 March, pp. 3014 – 3018.

Appendix A The Scattering Matrix

The scattering matrix provides a complete description of the network as it seen at it's N ports. The scattering matrix relates the voltage waves incident on the ports to those reflected from the ports. For some components and circuits, the scattering parameters can be calculated using network analysis techniques. Otherwise, the Scattering parameters can be measured directly with a network analyzer; consider an N-port Network, where V_n is the amplitude of the voltage wave reflected from port n . The scattering matrix, or [S] matrix, is defined in relation to these incident and reflected voltage waves as (Pozar, 1998)

A specific element of [S] matrix can be determined as

—

Equation (2.2) says that S_{ij} is found by driving port j with an incident wave of voltage V_j , and measuring the reflected wave amplitude V_i coming out of port i , the incident waves on all ports except the j th port are set to zero, which means that all ports should be terminated in matched loads to avoid reflections. Thus, S_{ij} is the reflection coefficient seen looking into port i when all other ports are terminated in matched loads, and T_{ij} is the “Transmission Coefficient” from port j to port i when all other ports are terminated in matched loads. (Pozar, 1998)

Appendix B Touchstone Files

This is the Four port network's Touchstone file, imported to *Microwave Office* (AWR)

```
# GHZ S MA R 50
3      0      0      0      0      1      0      0      0
      0      0      0      0      0      0      1      0
      1      0      0      0      0      0      0      0
      0      0      1      0      0      0      0      0
4.8    0      0      0      0      1      0      0      0
      0      0      0      0      0      0      1      0
      1      0      0      0      0      0      0      0
      0      0      1      0      0      0      0      0
4.805  0      0      0.3  -90    0.95  -180  0      0
      0.3  -90    0      0      0      0      0.95  -180
      0.95 -180  0      0      0      0      0.3  -90
      0      0      0.95 -180  0.3  -90  0      0
5.4    0      0      0.3  -90    0.95  -180  0      0
      0.3  -90    0      0      0      0      0.95  -180
      0.95 -180  0      0      0      0      0.3  -90
      0      0      0.3  -180  0.3  -90  0      0
5.405  0      0      0      0      1      0      0      0
      0      0      0      0      0      0      1      0
      1      0      0      0      0      0      0      0
      0      0      1      0      0      0      0      0
11     0      0      0      0      1      0      0      0
      0      0      0      0      0      0      1      0
      1      0      0      0      0      0      0      0
      0      0      1      0      0      0      0      0
```

| Appendix B Touchstone Files

This is the Two port network's Touchstone file, imported to *Microwave Office* (AWR)

```
# GHZ S MA R 50
3      1      0      0      0      0      0      1      0
4.8    1      0      0      0      0      0      1      0
4.805  0.76  0      0.64  -90    0.64  -90    0.76  0
5.4    0.76  0      0.64  -90    0.64  -90    0.76  0
5.405  1      0      0      0      0      0      1      0
11     1      0      0      0      0      0      1      0
```